

A NUMERICAL APPROACH TO THE SOLUTION OF  
THE SUPERSONIC FLOW FIELD IN THE EXIT PLANE  
OF HIGH TURNING ANGLE TURBINE BLADES

by



SUBHASH CHANDRA SUTRADHAR, B.E., D.I.I.T.

Submitted to the Faculty of Graduate Studies  
in Partial Fulfilment of the Requirements  
for the Degree  
Master of Engineering

McMaster University

April 1982

A NUMERICAL APPROACH TO THE SOLUTION OF  
THE SUPERSONIC FLOW FIELD IN THE EXIT PLANE  
OF HIGH TURNING ANGLE TURBINE BLADES

MASTER OF ENGINEERING (1982)  
(Mechanical Engineering)

McMaster University  
Hamilton, Ontario

TITLE: A Numerical Approach to the Solution of the  
Supersonic Flow Field in the Exit Plane  
of High Turning Angle Turbine Blades

AUTHOR: SUBHASH CHANDRA SUTRADHAR, B.E., D.I.I.T.

SUPERVISOR: Dr. J. H. T. Wade

NUMBER OF PAGES: x, 154

## ABSTRACT

The power output from a high turning angle turbine blade passage depends on many factors and the most important of all is the appropriate pressure distribution along the pressure and suction surfaces of the blades. The operation of a fully choked passage requires the specification of the proper operating pressure ratio to avoid the formation of any compression waves after the geometric throat which would otherwise generate a total pressure loss for the system.

With the advancement of computational methods, the two-dimensional supersonic flow field existing after a choked passage is elaborately analysed to avoid the adverse effect of compression waves on the blade performance. For different pressure ratios the characteristic waves as well as the pressure distribution are presented which give a theoretical prediction for the presence of a possible shock wave after the geometric throat of the passage. The shock free operation of the passage definitely increases the power output of the cascade. The stream tube method of pressure distribution is extended for generating the characteristic waves covering the entire supersonic flow field existing near the trailing edge of the fully choked passage of a high turning angle turbine blade passage.

## ACKNOWLEDGEMENTS

The author wishes to express his sincere gratitude and appreciation to his supervisor, Dr. J. H. T. Wade, for his guidance and encouragement throughout the course of this study and other endeavours.

## TABLE OF CONTENTS

	Page
ABSTRACT	i
ACKNOWLEDGEMENTS	ii
TABLE OF CONTENTS	iii
LIST OF FIGURES	v
NOMENCLATURE	viii
CHAPTER 1: INTRODUCTION	1
CHAPTER 2: THEORETICAL ANALYSIS AND BLADE PROFILE CONSTRUCTION	5
2.1 Design Procedure	5
2.2 Design of Blade Shapes	9
2.2.1 Blade Layout	11
2.3 Stream-line Curvature Method	20
2.3.1 Stream-line and Quasi- orthogonal System	20
2.3.2 Derivation of Equations	22
2.4 Development of Computer Program	31
2.5 Alternative Choke Calculation	34
2.6 The Trailing Edge Region	36
2.7 Performance of a Transonic Passage	39
2.8 Shock-Boundary Layer Interaction	44
2.9 Flow Visualization Apparatus	45
2.10 Supercritical Blade Exit Conditions	48
CHAPTER 3: METHOD OF CHARACTERISTICS	53
3.1 General Flow Equations	53
3.2 Properties of Characteristics	55
3.3 Equations of Motion in Charac- teristic Form	55
3.3.1 Characteristic Equation	58
3.3.2 Compatibility Equations	61
3.4 Numerical Integration Procedure	62
3.4.1 Modified Euler Predictor- Corrector Method	63
3.4.2 Finite Difference Equations	66
3.4.3 The Solution for an Inte- rior Point	67

	Page
3.4.4 Equations Used for Computation	69
3.4.5 Solution for Wall Point	71
3.4.6 Free Pressure Boundary Point	73
3.5 Development of the Computer Program	74
3.5.1 Interior Points	75
3.5.2 Wall Point	76
3.5.3 The Free-Pressure Boundary Point	78
CHAPTER 4: METHOD OF CHARACTERISTICS (RIEMANN INVARIANTS)	80
4.1 General Considerations	80
4.2 Derivation of Equations	81
4.3 Computation Method	82
4.4 Lattice Point Method of Solution	85
CHAPTER 5: RESULTS AND DISCUSSIONS	89
CHAPTER 6: CONCLUSIONS	108
REFERENCES	110
APPENDIX A COMPUTER PROGRAM FOR PRESSURE AND MACH NUMBER DISTRIBUTION	113
APPENDIX B COMPUTER PROGRAM FOR METHOD OF CHARACTERISTICS	125

## LIST OF FIGURES

FIGURE	Title	Page
2.1	Blade Nomenclature	7
2.2	Regions of Interest in a Turbine Blade Passage	10
2.3	Pressure Distribution and Velocity Triangles	12
2.4	Variation of Flow Deviation with Exit Mach Number	14
2.5	Construction of Blade Profile (McMaster Blade)	16
2.6	Geometry of Suction Surface Curvature	17
2.7	Plot of $b/R_s$ vs. $x/b$	19
2.8	Approximate Channel Width for Curved Channels	21
2.9	Elementary Stream Tube System	23
2.10	Construction of an Orthogonal	25
2.11	Three-Dimensional Orthogonal Surface	26
2.12	Two-Dimensional Flow Field in a Natural Coordinate System	28
2.13(a)	Sonic Line in Convergent Blade Passage	30
2.13(b)	Stream Tube Approximation to Sonic Line	30
2.14	Pressure Distribution for McMaster Blade	37
2.15	Pressure Distribution around McMaster Blade used in the Present Study	41
2.16	Trailing Edge Pressure Distribution Using Wave System	43
2.17	Schematic of a Vertical Schlieren Arrangement	47



FIGURE	Title	Page
2.18	Semi-Expanded Blade Passage	49
2.19	Fully-Expanded Blade Passage	49
2.20	Effect of Outlet Pressure on Surface Pressure Distribution	51
3.1	Stream-line and Coordinate Axes	56
3.2	Characteristics as the Mach Lines at a Point in a Flow-Field	60
3.3	Finite Difference Network for Applying the Method of Characteristics	64
3.4	Solution for a Wall Point	72
3.5	Solution for a Free Jet Boundary	72
3.6	Initial Value Line and Characteristics	77
4.1	Characteristic Method using the Natural Coordinate System	83
4.2	Characteristic Network for the Two-Dimensional Method of Characteristics	87
5.1	Characteristic Lines (Riemann Invariants) for Straight-Back Turbine Blade ( $P_o/p = 2.486$ )	90
5.2	Characteristic Lines for Straight-Back Turbine Blade for Pressure Ratio, $P_o/p = 2.486$	91
5.3	Characteristic Lines for Straight-Back Turbine Blade for Pressure Ratio, $P_o/p = 2.752$	93
5.4	Characteristic Lines for Straight-Back Turbine Blade for Pressure Ratio, $P_o/p = 3.038$	94
5.5	Pressure Distribution on Suction Surface After Geometric Throat ( $P_o/p = 2.486$ )	95
5.6	Pressure Distribution on Suction Surface After Geometric Throat ( $P_o/p = 2.752$ )	96

FIGURE	Title	Page
5.7	Pressure Distribution on Suction Surface After Geometric Throat ( $P_o/p = 3.038$ )	97
5.8	Pressure Distribution on Suction Surface After Geometric Throat ( $P_o/p = 2.486$ ) (Riemann Invariants)	99
5.9	Blade Pressure Distribution ( $P_o/p = 2.486$ )	100
5.10	Blade Pressure Distribution ( $P_o/p = 2.752$ )	101
5.11	Blade Pressure Distribution ( $P_o/p = 3.038$ )	102
5.12	Characteristic Lines for Curved Back Turbine Blade for Pressure Ratio, ( $P_o/p = 2.486$ )	103
5.13	Characteristic Lines for Curved Back Turbine Blade for Pressure Ratio, ( $P_o/p = 2.752$ )	104
5.14	Characteristic Lines for Curved Back Turbine Blade for Pressure Ratio, ( $P_o/p = 3.038$ )	105
5.15	Proposed Schlieren System	106

## NOMENCLATURE

<u>Symbols</u>	<u>Description</u>
a	Speed of Sound
A	X-Sectional Area
b	Axial Chord
C	Curvature
$C_L$	Zweifel Lift Coefficient
$C_+$	Left Running Characteristics
$C_-$	Right Running Characteristics
$g_c$	Gravitational Constant
h	Step Size
M	Mach Number
$\dot{m}$	Mass Flow Rate
m	Slope of the Stream-lines
n	Distance along Orthogonal Lines
$n_0$	Length of Orthogonal
O	Throat Opening
p, P	Pressure
R	Radius of Curvature where $R = \frac{1}{C}$
$R_g$	Gas Constant
r	Radius
S	Distance along Stream-lines
s	Pitch

Symbols

T	Temperature
$r_T$	Trailing Edge Radius
u	Velocity Component in X-direction
v	Velocity Component in Y-direction
V	Resultant Velocity
$V_T$	Tangential Velocity
$\dot{w}$	Weight Flow Rate
X,Y	Rectangular Coordinate Axes
Z	Mass Flow Rate/Unit Area

Greek Symbols

$\alpha$	Flow Angle
$\beta$	Blade Angle
$\gamma$	Specific Heat Ratio
$\theta$	Angular Position of Stream-lines
$\nu$	Prandtl-Meyer Angle
$\mu$	Mach Angle
$\rho$	Density

Subscripts

x	Derivative in X-direction
y	Derivative in Y-direction
s	Suction Surface
p	Pressure Surface
mid	Midstream

Subscripts

0

Stagnation Condition

1,2,3,4

Points in Flow Stream-lines

i

Inlet Condition

e

Exit Condition



## CHAPTER 1

### INTRODUCTION

The performance of high turning turbine blades, neglecting the losses due to separation, exhibits the tendency to reach a limiting loading condition rapidly with the increase of operating total-to-static pressure ratios [1]. As the power output per blade may be augmented by increasing fluid deflection through the blading, the flow passage as well as the trailing edge portion of the blade should be thoroughly investigated for high power output associated with high operating pressure ratios. The Zweifel lift coefficient [3] in the power output equation may be increased by suitably varying the spacing of the blading as suggested by equation 2.1, but the variation of flow deflection needs further consideration. Once a blade row is choked for a certain pressure ratio, the reduction in downstream static pressure does not influence the flow upstream of the geometric throat of the passage except that further decreases in downstream pressure generate complications due to the effect of compressibility after the throat. The generation of any compression shock after the throat may lead to a loss of total pressure and thus adversely affecting the performance of the blade. While analysing the flow behaviour of a blade for certain loading

condition, it thus becomes inevitable on the designer's part to specify the range of operating pressure ratios so as to avoid the formation of such compression shock waves downstream of the geometric throat of the passage. The gradual increase of pressure ratios from the "just choked" condition definitely increases the overall area of the pressure plotting. However, the increase of pressure ratio after the fully expanded flow situation will not produce any increase in the power output at the expense of increased mass flow through the passage. The flow deflection caused by the presence of compression and expansion waves which may become excessive due to this high pressure ratio should be specified for the smooth operation of the flow through the passage. As the flow deflection influences the Zweifel lift coefficient, a proper assessment of the flow deflection becomes necessary to reduce any adverse effect on the power output of the blading.

The present thesis presents a method of determining the possible shock formation for different operating pressure ratios together with an outline of the procedure to obtain the pressure distribution inside the blade passage. The procedure used for designing any highly curved blade passage is the application of the streamline curvature method which is found to be more suitable than other methods not only because of its simplicity and rapidity discussed in Chapter 2 of this thesis. The pressure distribution for both the suction and

pressure surface is also obtained by this method as well as the Mach number distribution required to analyse the supersonic flow field, if, in fact, it exists. The parameters pertaining to the geometric throat are used to predict the presence of any compression waves downstream of the throat which may effect the flow near the blade trailing edge.


The method for analysing a supersonic flow system is discussed both in Chapter 3 and Chapter 4. The advantage of the method outlined in Chapter 3 is that the use of Cartesian coordinate system for the method of characteristics avoids the solution of the equation which expresses the Prandtl-Meyer expansion angle  $\nu$  in terms of the Mach number of the flow field. However, since the value of the Mach angle  $\mu$  is known the Mach number can easily be obtained and then  $\nu$  can be calculated using the Prandtl-Meyer expression. Also this method gives the coordinates of the points whereas the method described in Chapter 4 covers the entire flow field in the form of lattices with angles specified for each side of the lattice.

The aim of this thesis is to develop a suitable computer program for the analysis of a supersonic flow field including the location of compression shocks and expansion fans and the distribution of the static pressure on a suction surface downstream of the throat of a highly curved passage. Though it has been developed for a two dimensional case, the



method can be slightly modified to accommodate the problems of axi-symmetrical flow. In Chapter 4, the classical method (such as Riemann Invariants) for describing a supersonic flow field is briefly outlined and for a pressure ratio ( $P_0/P = 2.486$ ), this method is compared with that developed in Chapter 3 and as one would expect the methods tally with reasonable accuracy.

The numerical analysis technique utilizing the method of characteristics as developed in Chapter 3 is used for McMaster blade passage with three different total-to-static pressure ratios viz. 2.486, 2.752 and 3.038. For comparison purposes the analysis is also carried out on another blade shape in which the flat back section of the blade downstream of the throat, on the suction surface is given a small radius of curvature. This modification would be of considerable structural value to the blade.



CHAPTER 2  
THEORETICAL ANALYSIS AND  
BLADE PROFILE CONSTRUCTION

2.1 Design Procedure

In the early 1900's, compressor and turbine stage design was based on the pitch-line calculations using mean camber line as the reference for inlet and exit angles. But later, due to the introduction of higher rotational speeds, the flow was observed to gravitate towards the shroud area of the blades. This gave a non-uniform flow distribution through the blade passage. This difficulty was overcome by using the concept of radial equilibrium which assumed that no radial flow existed in the flowpath and therefore, there existed a uniform axial mass flow through the passages. The basic idea was simply to "under-expand" the flow near the tip and "over-expand" the flow near the hub. This differential expansion process along with the increasing pressure distribution in the radial direction gave a uniform mass flow in the axial direction and this uniform mass flow gave a better distribution of loads in all sections of the blading. The design of blading on the concept of radial equilibrium was a considerable step forward in turbine and compressor design and its use was confirmed by the improved performance of the

blading. Utilizing the concept of radial equilibrium, the resulting design provided high pressure ratios and high enthalpy drops by stage and also high flow deflection angles.

The present day method of cascade performance depends on the radial equilibrium free vortex design. Two assumptions are involved in this design [25]

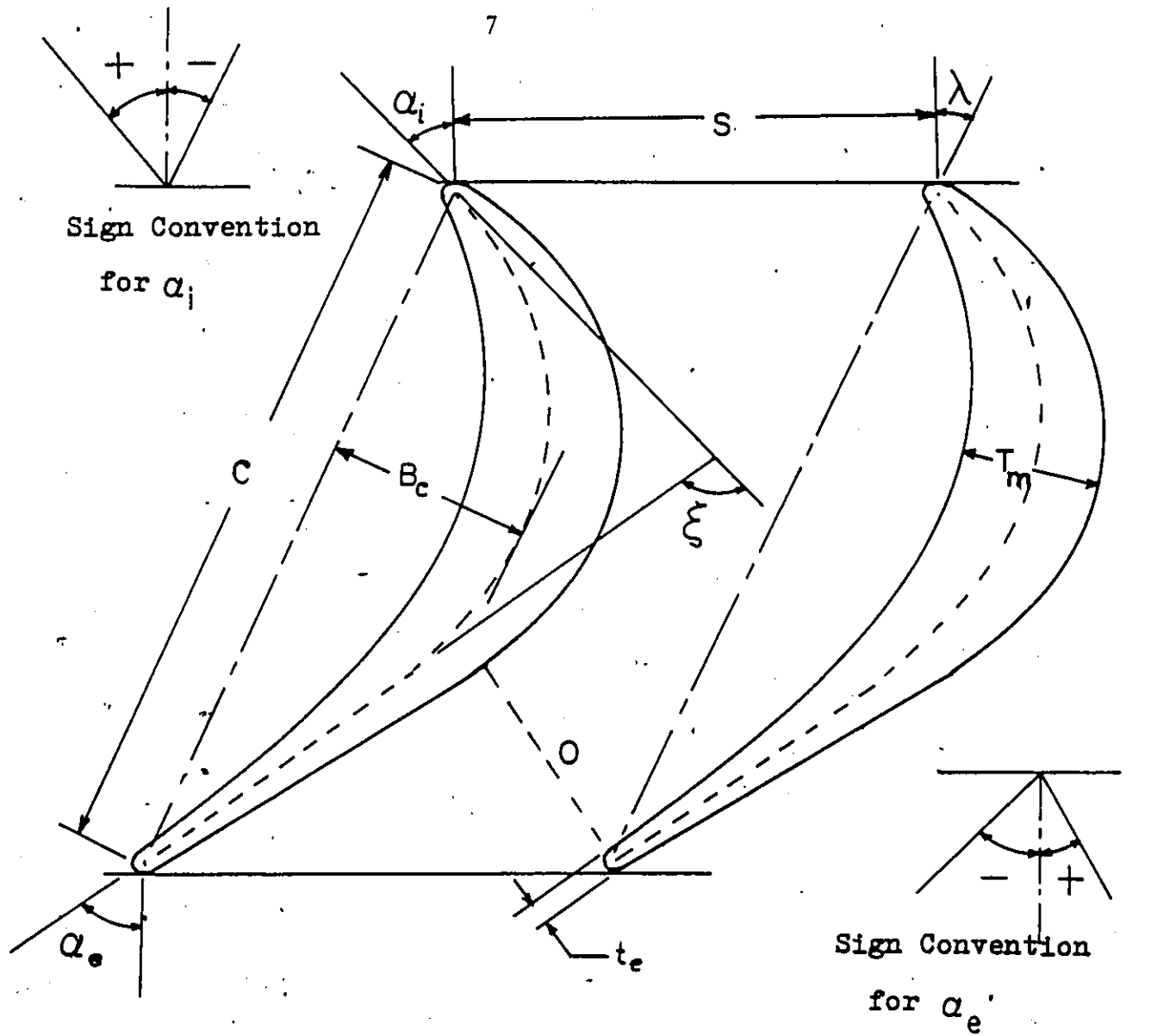
- i) The flow is assumed to be in radial equilibrium before and after all blade rows, such that

$$\frac{dp}{dr} = \frac{mv_T^2}{r}$$

- ii) The Tangential velocity distribution is idealized to be a free vortex in which the product of tangential velocity and radius is constant, that is,  $rv_T = \text{constant}$ .

The blades designed using this concept are generally known as free vortex blades. The free vortex design calls for a high degree of twist in the rotating blades and this results in a large change in the inlet and outlet angles across the span of the blades. Also, the manufacturing of twisted blades requires precise instrumentation and a high degree of technical expertise.

There are other types of design procedures used for compressor and turbine bladings. For example, the mapping techniques used in conjunction with potential flow theory may be used to establish the stream-lines through a cascade.



$\alpha_i$  - Blade Inlet Angle

$\alpha_e$  - Blade Exit Angle

$B_c$  - Maximum Camber

$C$  - Chord

$O$  - Throat

$\lambda$  - Stagger Angle

$\xi$  - Camber Angle

$t_e$  - Trailing Edge Thickness

$S$  - Blade Pitch

$T_m$  - Maximum Thickness

Figure 2.1 Blade Nomenclature

The flow turning is more realistically assessed with the air-foil thickness taken into consideration. These types of flow calculations are usually restricted to two-dimensional passages. The theoretical calculations are laborious however and it has been found easier and more direct to describe the profile shape over the required range of turning angles and then to design the channel by varying the curvature at points on the profile to obtain the most favourable pressure distribution around the blades.

The computation methods now available may break down when applied to a very high surface curvatures. The methods of Martensen (10) and Stanitz (9) have been used for many years in blade design. The method of Martensen is not an appropriate one to modern designs since it is essentially a method involving only incompressible flow. Stanitz's method involves laborious mathematical calculations for a relaxation solution of a potential function along a blade surface. The recent advancement of computer science made it possible to use finite difference or finite element solutions to the equations of motion, momentum, and energy. Examples of these methods are found in the work of McDonald [11] and Davies and Millar [4]. These later methods though very accurate in describing the flow through the blade passage, poses certain difficulties. A large number of nodal points are required to obtain a good engineering solution which again calls for

a computer with a large memory.

An easy and direct method of obtaining both the surface pressure and velocity distribution is the streamline curvature technique. This method is described in the works of Stannard (7), Kumar (5), Malhotra (6). The streamline curvature technique has two defects which may surface during the design. They can be briefly stated as follows:

(a) As the turning angle increases that portion of the blade covered by the method decreases (Region B, Figure 2.2).

(b) As the blade nears choking the basic assumptions used in the analysis break down.

## 2.2 Design of Blade Shape

As the gas passes through a blade row it experiences a change in momentum. Depending on the total turning of the gas through the blade passage, the rate of change of momentum will vary and a proportional force can be derived from the blade row. The main aim of the blade shape design is to achieve high turning, which provides greater lift (up to a maximum, of course) across the blade without any unfavourable development or separation within the blade passage. The blade lift coefficient has been defined by Zweifel [3] as follows:

$$C_L = 2(s/b) \cos^2 \alpha_e (\tan \alpha_i - \tan \alpha_e) \quad (2.1)$$

where  $C_L$  is so-called Zweifel lift coefficient (please refer

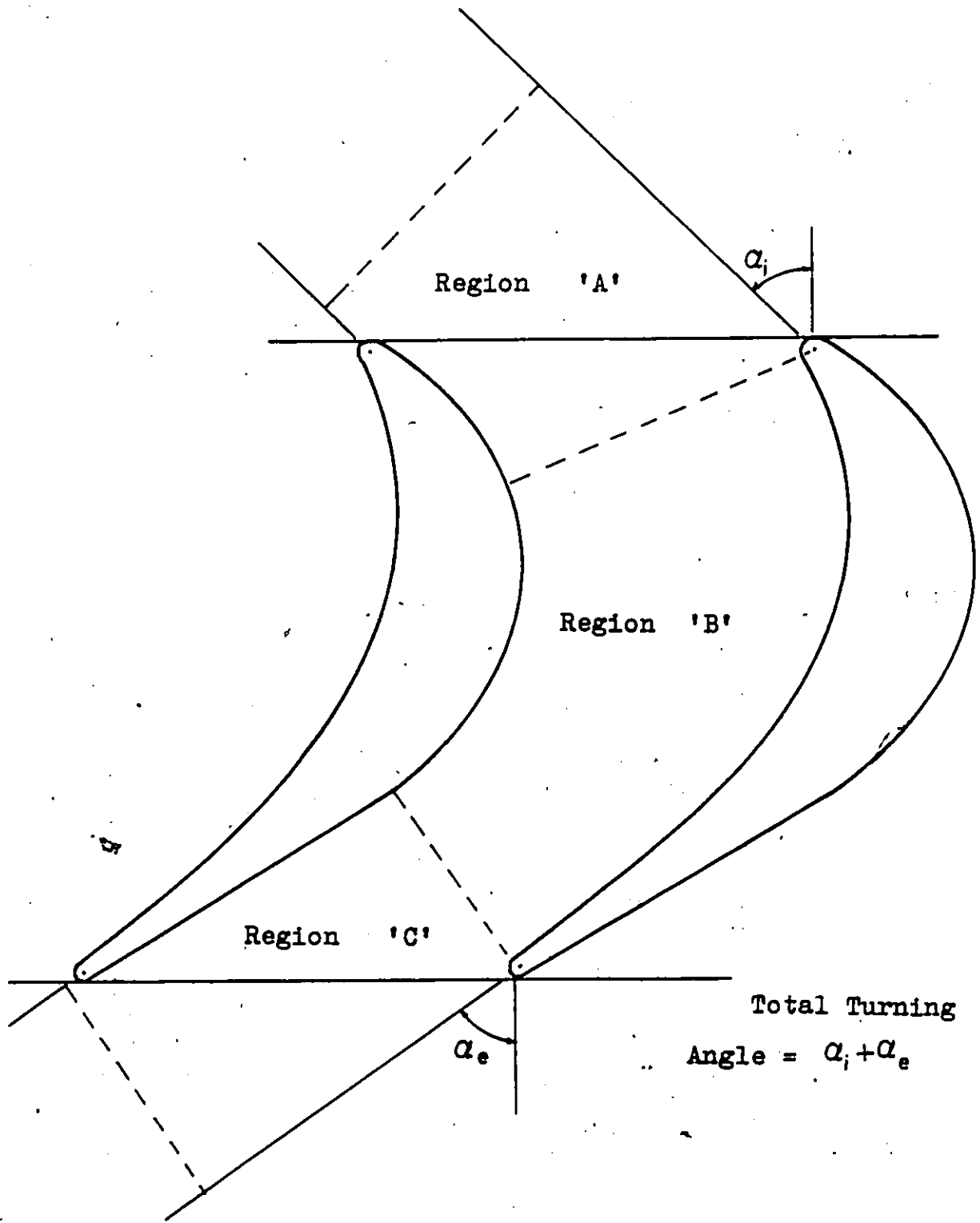


Figure 2.2 Regions of Interests in a Turbine Blade Passage

to Figure 2.1 and the nomenclature for further notations). In the design shown in this thesis lift coefficient is assumed to be 1.0 and hence for fixed inlet and outlet angles, the pitch-chord ratio ( $s/b$ ) is also defined.

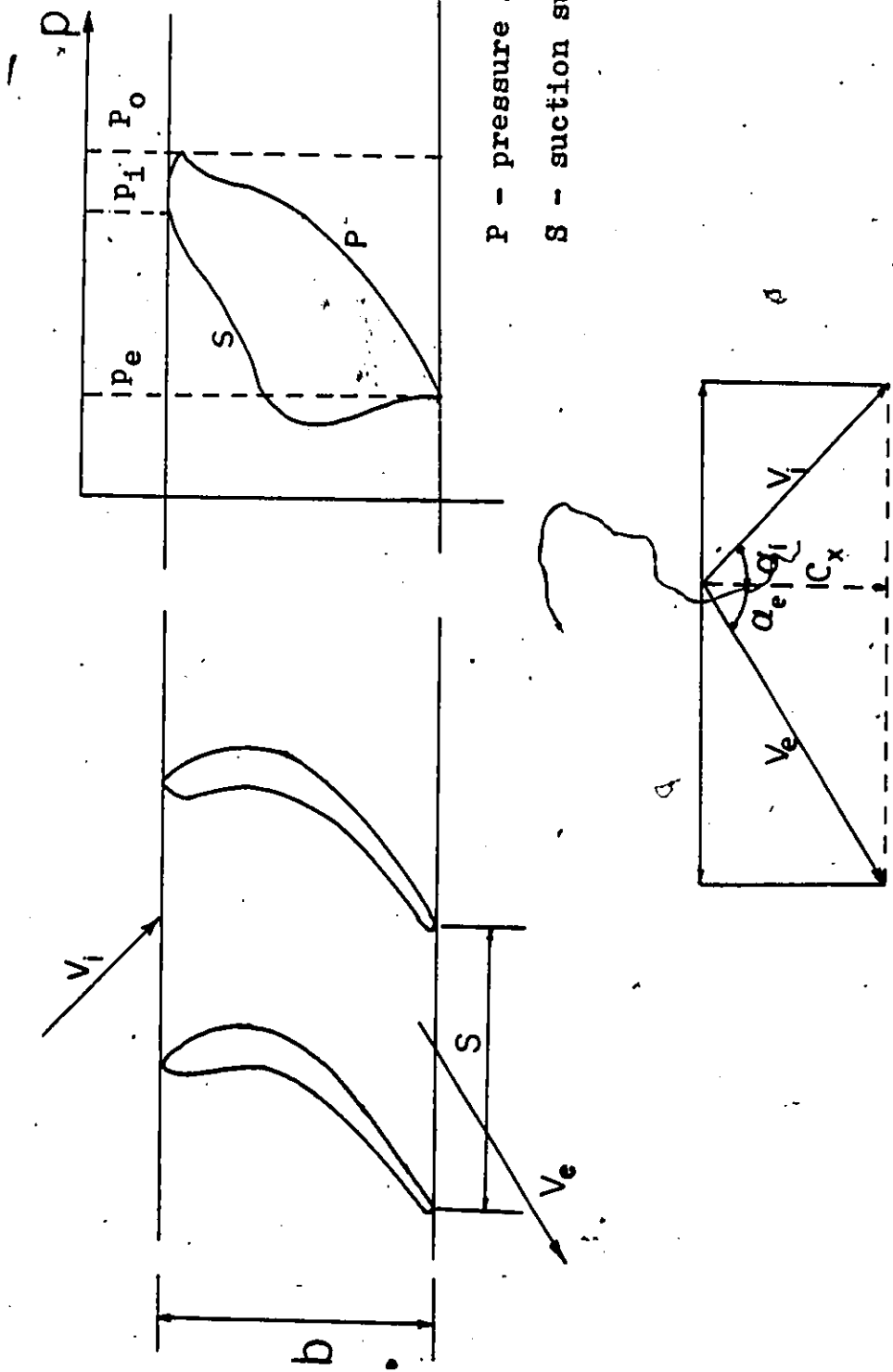
Thus, the design is simplified in defining the variation of surface curvature, particularly on the suction surface, to eliminate wherever possible adverse pressure gradients. From the design of any turbine blade, it is obvious that the velocity at the trailing edge region is very high (Figure 2.3), usually reaching sonic speed for blade pressure ratios slightly higher than the choking pressure ratio of 1.893:1. Once this stage is reached a slight change in curvature will give a very rapid increase in the velocity near the surface which induces patches of supersonic flow near the trailing edge region of the blade passage.

### 2.2.1 Blade Layout

The "flat-back" blade design is the easiest one to carry out since that portion of the blade downstream of throat is straight and no adverse pressure gradient is present in this region. The following steps are usually taken in the construction of the blade surface profile:

- (a) Two parallel lines are drawn at a distance  $b + r_T$  apart, representing the leading and trailing edges of





P - pressure surface  
S - suction surface

Figure 2.3 Pressure Distribution and Velocity Triangles

the cascade. A suitable scale may be chosen, say 1" = 10" for the proper sketching of the blade surface (see Figure 2.5).

(b) With the outlet angle known, for a flat-back blade, the throat dimension is effectively fixed by the blade spacing. The throat dimension ( $0$ ) is calculated from the following relation:

$$0/s = \cos \alpha_e$$

where  $\alpha_e$  = blade outlet angle.

(c) The pitch distance ( $s$ ) is marked on the trailing edge line and two trailing edge circles are drawn for the two blades ensuring that the trailing edge line is tangent to the circles. An arc of radius  $0 + r_T$  is now drawn with the centre located at the same point as the trailing edge circle. Depending on the blade rotational direction, either of the circles can be chosen as starting point.

(d) A tangent is drawn to the other circle at an angle  $\beta_{se} = \text{Arc cos } (0/s - \Delta \cos \beta)$  where  $\Delta \cos \beta$  depends on the exit plane Mach number ( $M_e$ ). The exit Mach number can be estimated from the velocity diagrams and from this the Mach number, and  $\Delta \cos \beta$  can be calculated from Figure 2.4 which shows the exit Mach number as a function of  $\Delta \cos \beta$ . A curve is then drawn from the trailing edge to the throat position. For flat-back blades, the curve can be replaced by a straight line. In practice of course, a small curva-

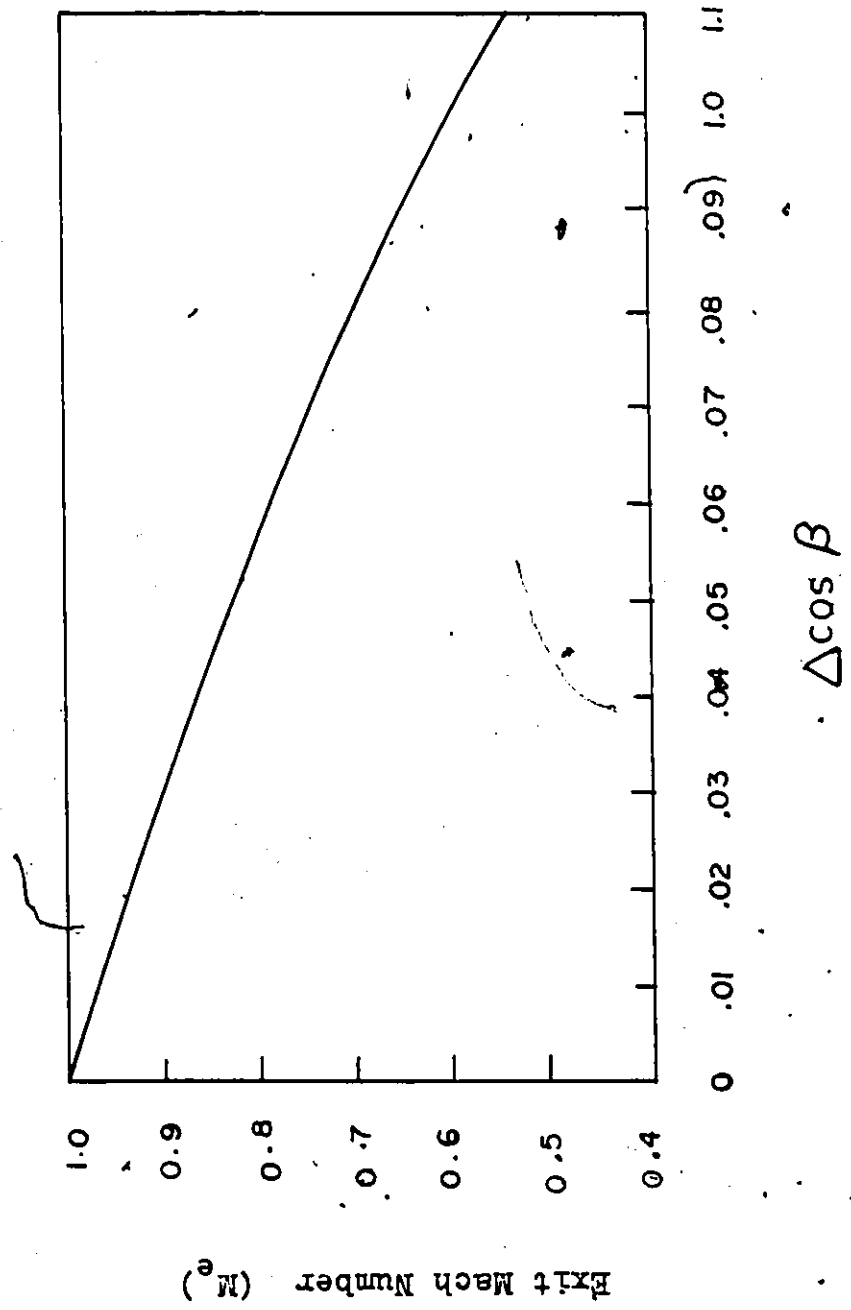


Figure 2.4 Variation of Flow Deviation with Exit Mach Number (Reference(4)).

ture is drawn at the throat position to complete the surface contour of the suction surface. A smooth continuous contour is required to avoid any undesirable flow separation near the trailing edge of the blades.

(e) The inlet blade angle  $\beta_{si}$  is determined at this stage which actually varies from  $\alpha_i + 20^\circ$  to  $\alpha_i + 15^\circ$  that is  $\alpha_i + \alpha_{ic} + \text{nose angle}/2.0$  where  $\alpha_i$  = flow angle at inlet;  $\alpha_{ic}$  = incidence angle which normally falls between  $0^\circ$  to  $5^\circ$ . Nose angle  $\approx 20^\circ$  (reaction blade, ref. 6). Once the blade inlet angle  $\beta_{si}$  is found, then  $\beta_{se}$ , the blade outlet angle may be calculated.  $\beta_{se}$  is the angle made by the suction surface at the point B as shown in Figure (2.5) and B is the point where the tangent from trailing edge circle touches the arc drawn from the other trailing edge point. The angle  $\beta_{se}$  usually varies from  $\alpha_e - 10^\circ$  to  $\alpha_e - 5^\circ$  where  $\alpha_e$  = flow angle at outlet of the cascade.

(f) The nose radius of the blade will effectively supply about  $15^\circ$  of the total turning. The remaining turning of the flow is obtained from the region of suction surface curvature between the tangent to the nose radius and throat. Hence, after calculating  $\beta_{si}$  and  $\beta_{se}$  it can be seen from a simple geometrical consideration, Figure (2.6) that

$$\left| \sin \beta_{si} \right| + \left| \sin \beta_{se} \right| = (x/b)/(R_s/b) = \frac{x}{b} \cdot \frac{b}{R_s} \quad (2.2)$$

where  $x/b$  is the non-dimensional chord.

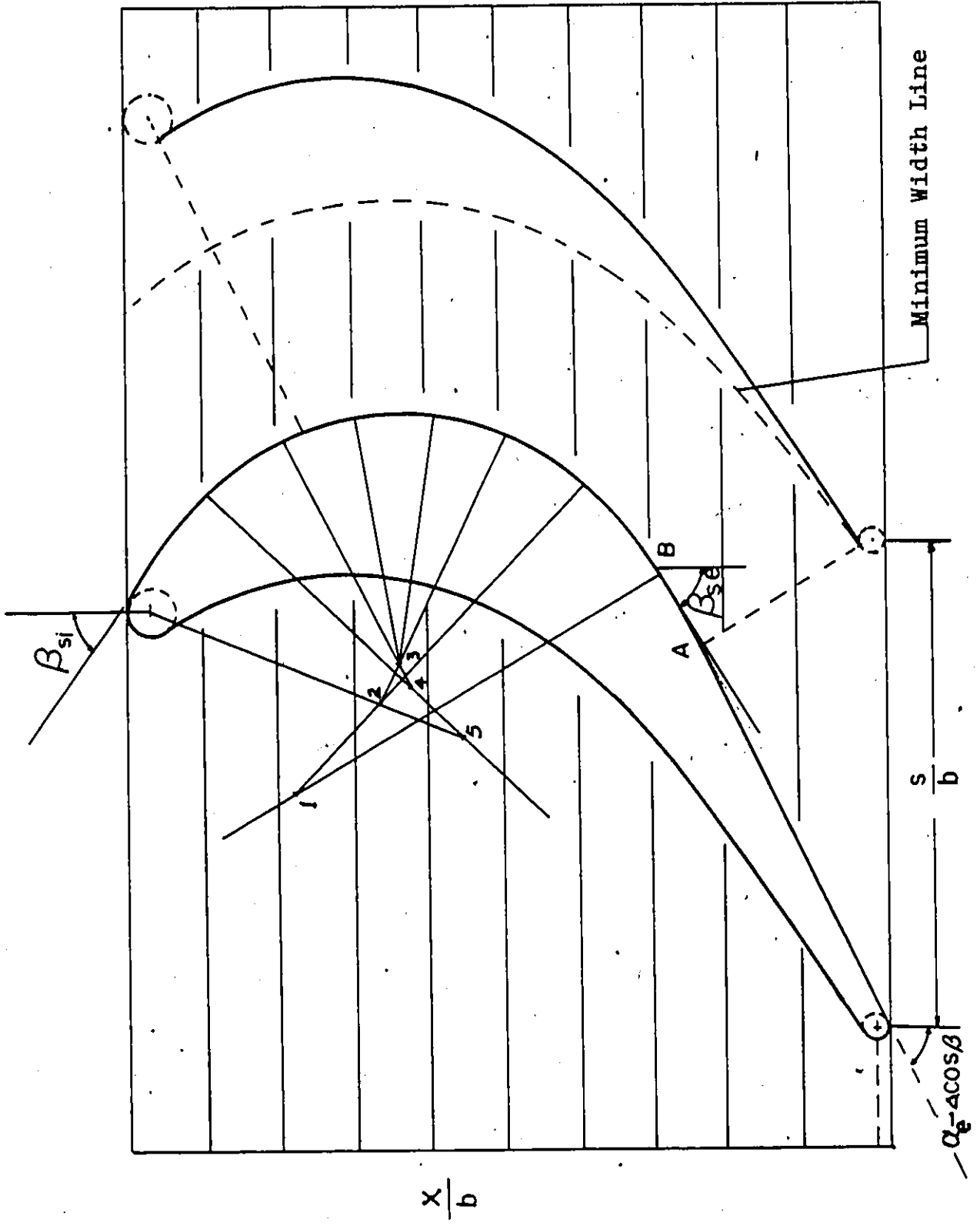
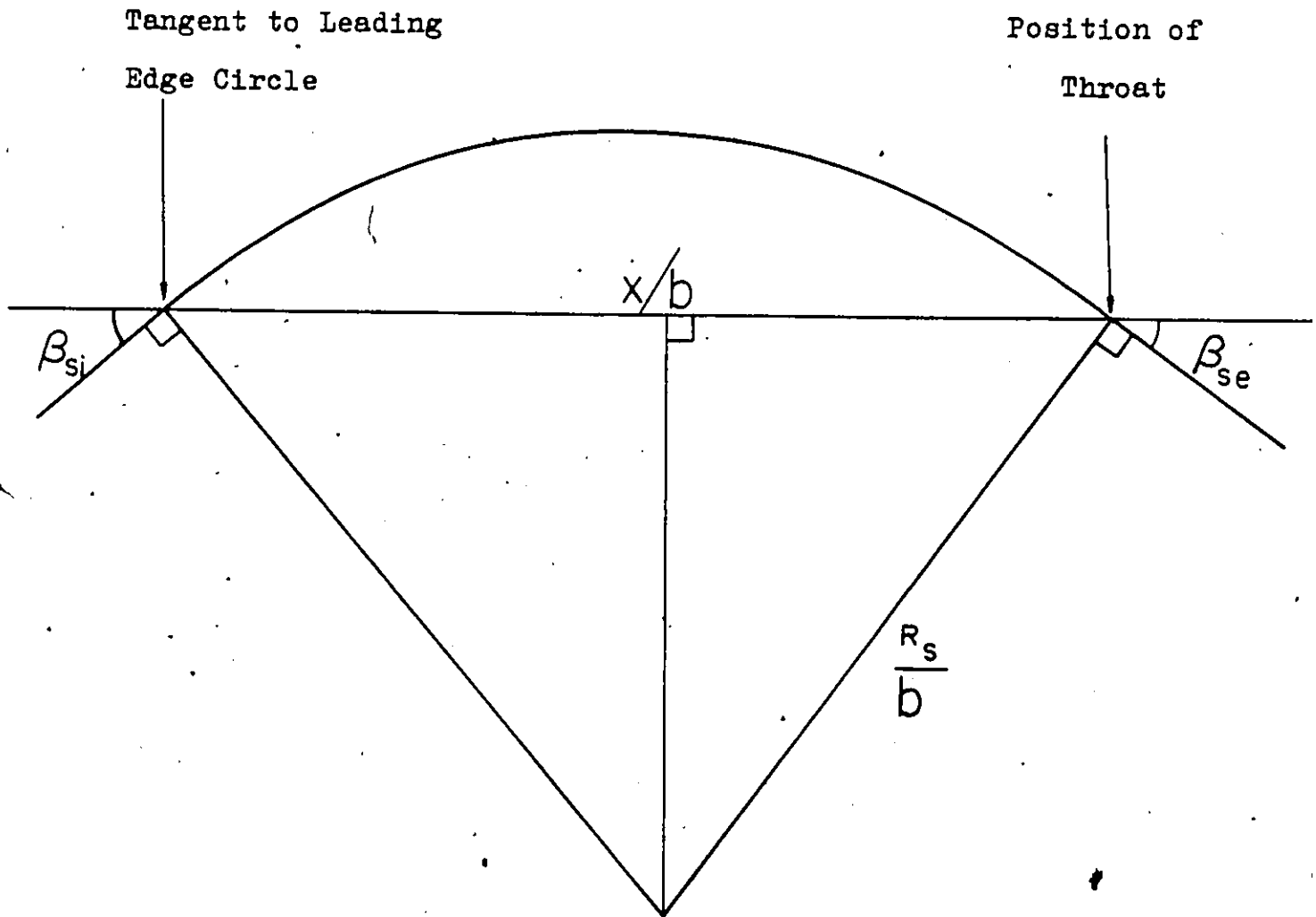


Figure 2.5 Construction of Blade Profile (McMaster Blade)



$$|\sin \beta_{sl}| + |\sin \beta_{se}| = x/b / R_s/b$$

$$= \left(\frac{x}{b}\right) \cdot \left(\frac{b}{R_s}\right)$$

$$= \text{Area of the Histogram}$$

Figure 2.6 Geometry of Suction Surface Curvature.

Equation (2.2) can be represented in the form of a rectangle of area  $|\sin \beta_{si}| + |\sin \beta_{se}|$  on a graph paper with coordinates  $x/b$  and  $b/R_s$ , Figure (2.7). The area of the rectangle now represents the blade suction surface curvature. The blade surface design entirely depends on the redistribution of this area in the form of histogram which ensures the desired pressure distribution over the suction surface without significant separation.

(g) A histogram is now superimposed on the rectangle drawn with the peak value of histogram lying somewhere  $0.2 < (x/b) < 0.55$ . The histogram is shown in Figure (2.7). Though the histogram is discontinuous, the actual blade curvature when drawn is necessarily continuous. The suction surface can next be drawn as continuous arcs equal to the radii taken from the histogram at proper  $x/b$  ratios which give the  $R_s/b$  for the curvatures. The entire process depends on good draftsmanship as the contours should be continuous.

(h) The pressure surface is drawn with monotonically decreasing channel width similar to the nozzle design. The work of Mr. Malhotra (6) can be referred to for obtaining further information on the process of the blade surface construction. (See also References 5 and 7.)

Using the above method and the original version of the pressure distribution program a series of such blades was designed by Malhotra (6) with lift coefficients varying

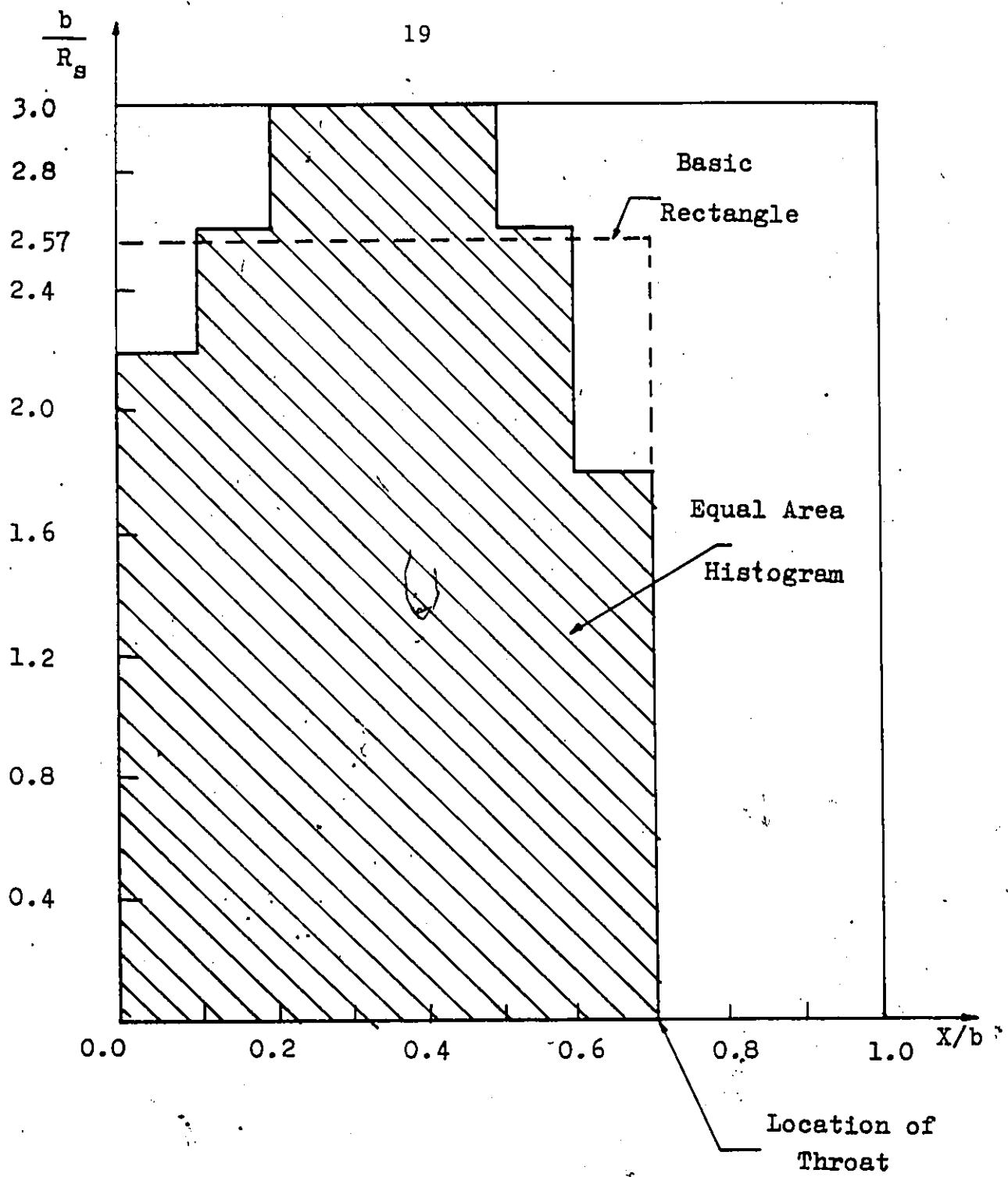


Figure 2.7 Plot of  $b/R_s$  versus  $x/b$



from 0.8 to 1.2 and total turning angles from  $115^{\circ}$  to  $140^{\circ}$ .

One particular blade which was chosen for further analysis is the McMaster blade with a lift coefficient of 1.0 and total turning angle  $128^{\circ}30'$ .

To establish the theoretical flow properties within a blade passage, the stream-line curvature method has been adapted as described in the next section.

### 2.3 Stream-line Curvature Method

This method is discussed elaborately in the work of Kumar (5) and Malhotra (6) and further details can be obtained from their works.

#### 2.3.1 Stream-line and Quasi-orthogonal System

In this method, the blade passage is divided into a number of stream tubes with the help of a good drafting machine. The number of stream tubes depends on the choice of the designer and in the case at hand nine stream tubes were chosen to cover the entire blade passage. The number of stream-lines chosen here gave good accuracy without overly complicating the computation method. The exact location of the generation of stream tubes may not be possible to determine at this stage.

Next a set of orthogonals are drawn which intersects every stream-line at 90 degrees exactly once. Figure (2.11)

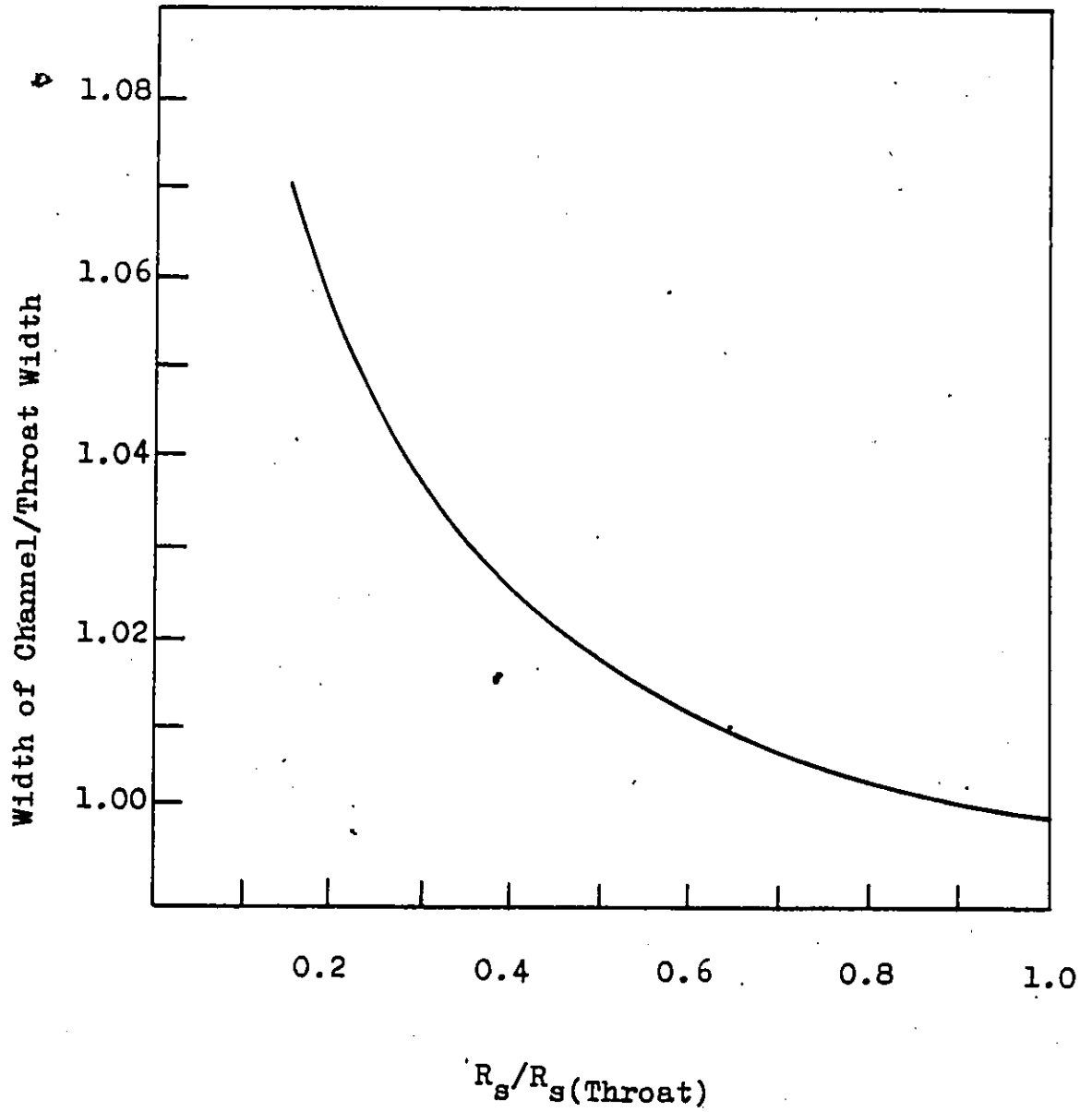


Figure 2.8 Approximate Channel Width for Curved Channels (Reference (4))

shows the three-dimensional orthogonal surface. The streamlines and their normals form a grid system for the flow solution. The system is drawn as accurately as possible with the aid of a drafting machine as shown in Figure (2.9). The general equations are developed below which are used in the solution of a computer program.

### 2.3.2 Derivation of Equations

The following assumptions are made in the derivation of the equations: -

- (a) the working fluid is inviscid, but compressible
- (b) the flow is steady
- (c) the flow is two-dimensional
- (d) the flow is isentropic, and
- (e) the mid-passage line is defined as a streamline.

Considering a unit depth of the field, the continuity equation for one stream tube is  $\rho V \Delta n$ , Figure (2.12).

For the whole passage the mass flow is

$$\dot{m} = \int_0^{n_0} \rho V dn \quad (2.3)$$

where  $n_0$  = total length of the orthogonal line between the two boundaries.

The Momentum equations along stream-lines and orthogonals respectively are:

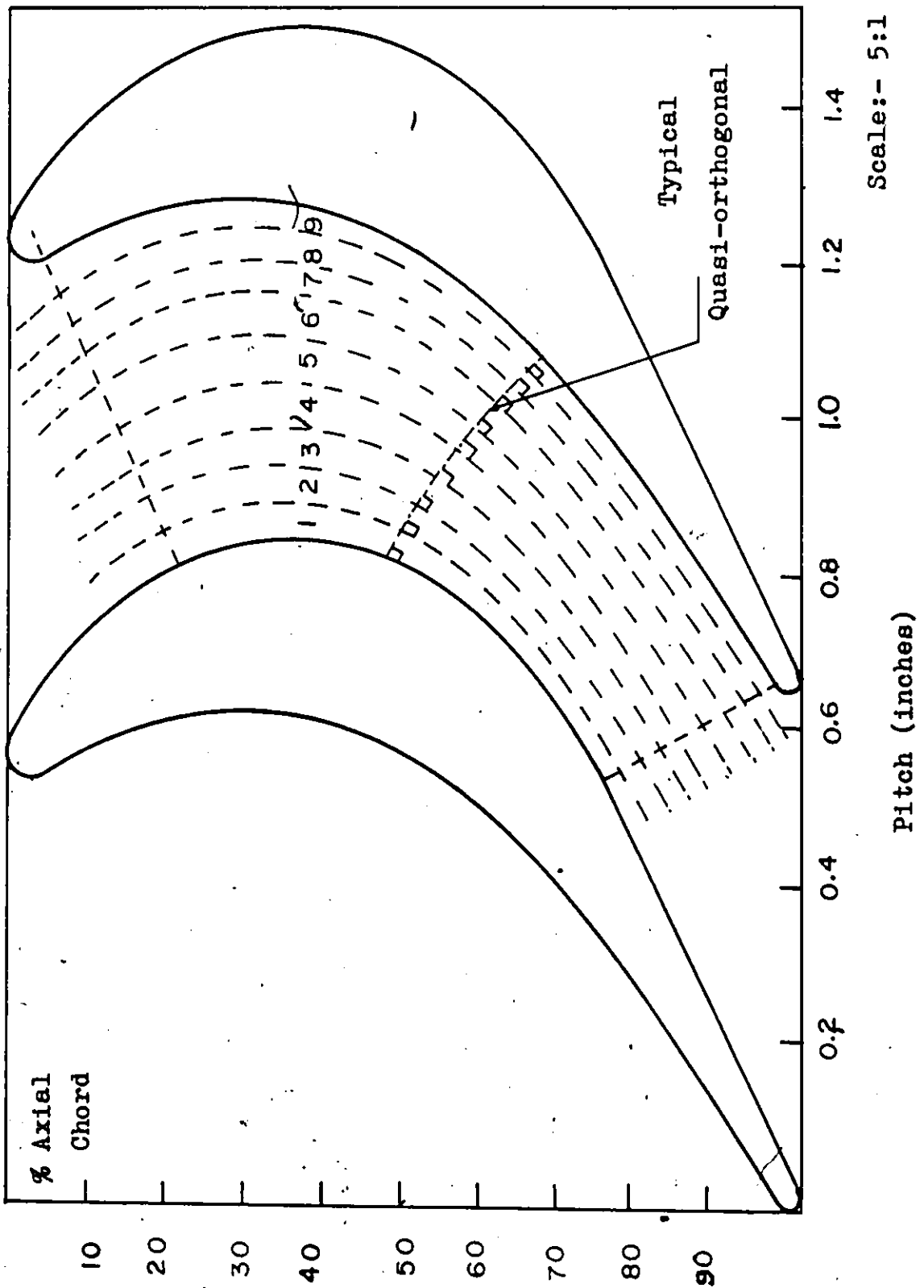


Figure 2.9 Elementary Stream Tube System

$$\rho V \frac{\partial V}{\partial s} = - \frac{\partial p}{\partial s} \quad \text{and} \quad (2.4)$$

$$\rho \frac{V^2}{R} = - \frac{\partial p}{\partial n} = \rho V^2 \frac{\partial \theta}{\partial s} \quad (2.5)$$

Equation 2.4 provides the balance between the acceleration and the pressure gradient along the stream-line whereas equation 2.5 is taken normal to the stream-line. For the latter case, the acceleration depends on the stream-line curvature,  $1/R$  or  $\partial\theta/\partial s$ .

Equations 2.3 and 2.5 can be numerically integrated along each orthogonal by assuming a certain velocity at either surface and then calculating the pressure, density and velocity at a neighbouring point with the help of the assumed velocity for the initial calculations and also considering the known value of radius of curvature at the point of consideration. Once the density and velocity at each point are known, the mass flow per unit height of the blade passage can be calculated and compared with the design mass flow rate. If there exists a difference in the calculated mass flows, the velocity is corrected to obtain the proper mass flow rate.

In the same fashion, the velocities and pressures can be calculated with the help of the known values of the radius of curvature at each point. A computer program has been provided for calculating the various flow parameters at each of the intersections of orthogonals and stream-lines.

From Equation 2.4, it can be conveniently shown that,

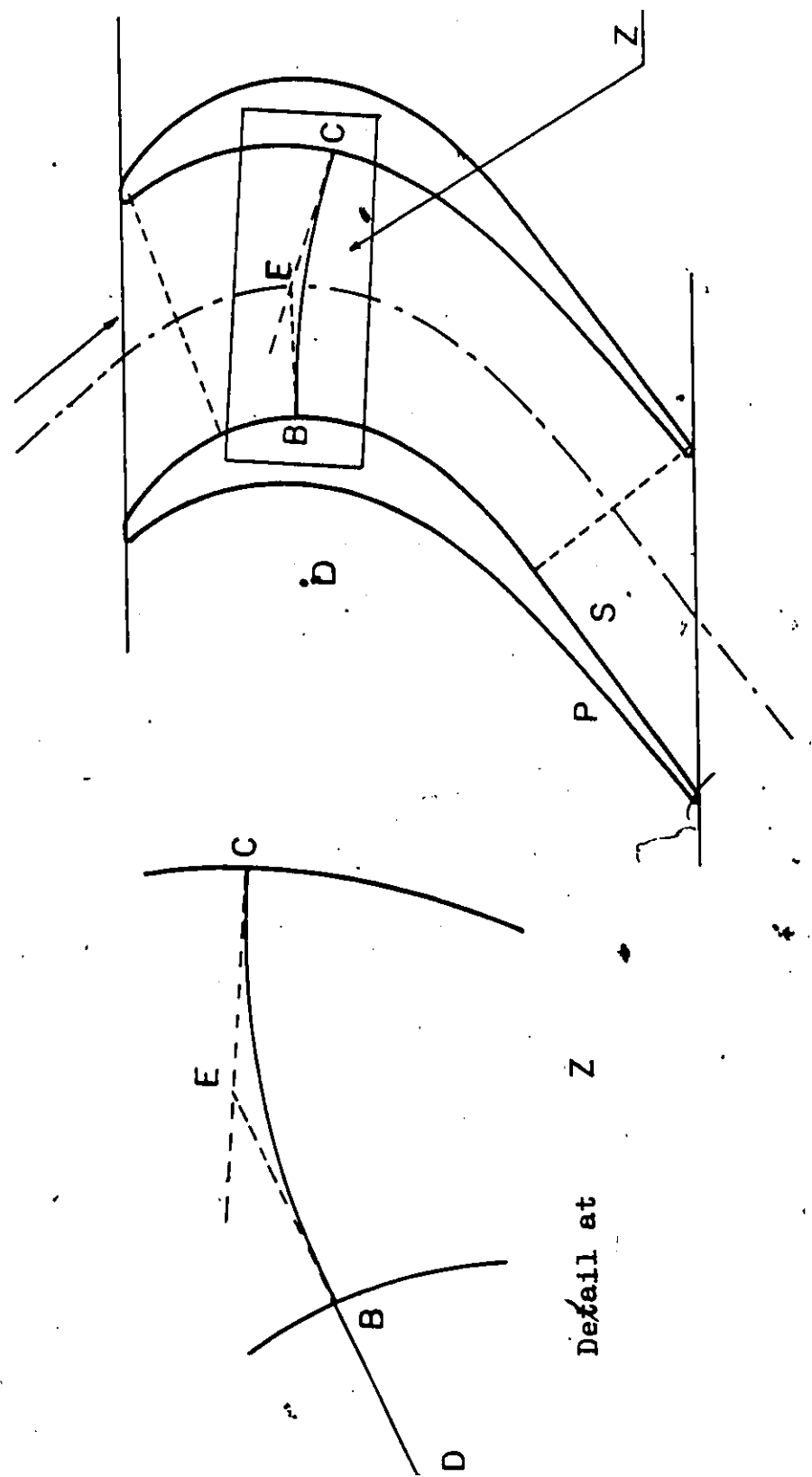


Figure 2.10 Construction of an Orthogonal Line

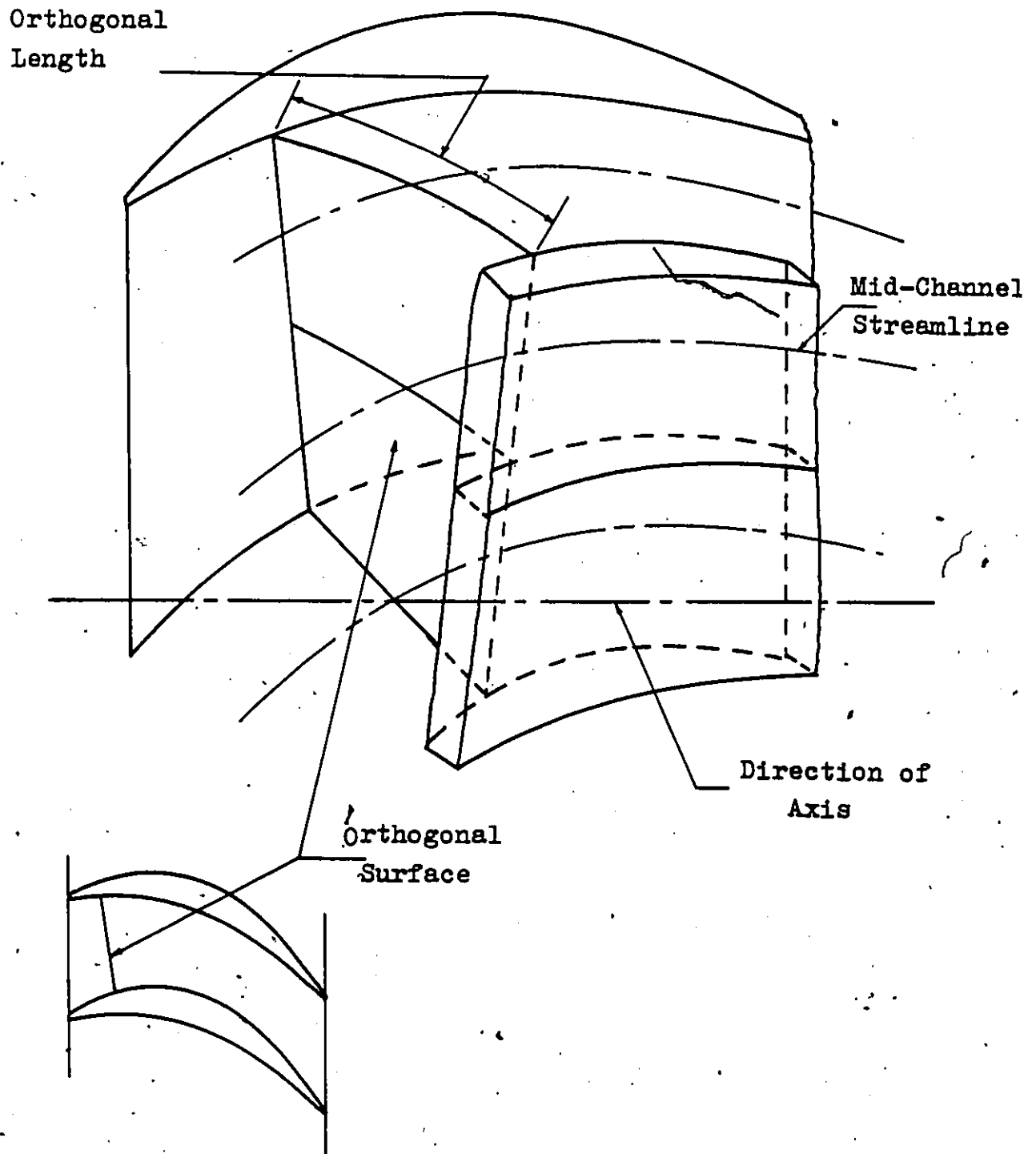


Figure 2.11 A Sketch Showing the Three-Dimensional Orthogonal Surface

$$VdV = -\frac{1}{\rho} dp \quad (2.6)$$

and from Equation 2.5

$$\frac{1}{\rho} dp = +\frac{V^2}{R} dn \quad (2.7)$$

(One should note that for the passage considered here,  $\frac{dp}{dn}$  is positive as  $dp$  increases with  $dn$ .)

From Equations 2.6 and 2.7

$$\begin{aligned} \frac{V^2}{R} dn &= -VdV \\ \text{or } \frac{dV}{V} &= -\frac{dn}{R} \end{aligned} \quad (2.8)$$

If  $C$  is the curvature, the Equation 2.8 may be re-written as:

$$\frac{dV}{V} = -C dn \quad (2.9)$$

The curvature  $C$  is assumed to vary linearly along the orthogonal and can be expressed in the form:

$$C = C_s + (C_p - C_s) \frac{n}{n_o} \quad (2.10)$$

where  $C_p$  and  $C_s$  are the curvatures at the pressure and suction surfaces respectively.

The differentiation of Equation 2.10 results in the following:

$$\begin{aligned} dC &= 0 + (C_p - C_s) \frac{dn}{n_o} \\ \text{or } dn &= \frac{n_o}{(C_p - C_s)} dC \end{aligned} \quad (2.11)$$

From Equations 2.9 and 2.11

$$\frac{dV}{V} = -\frac{n_o}{(C_p - C_s)} C \cdot dC$$



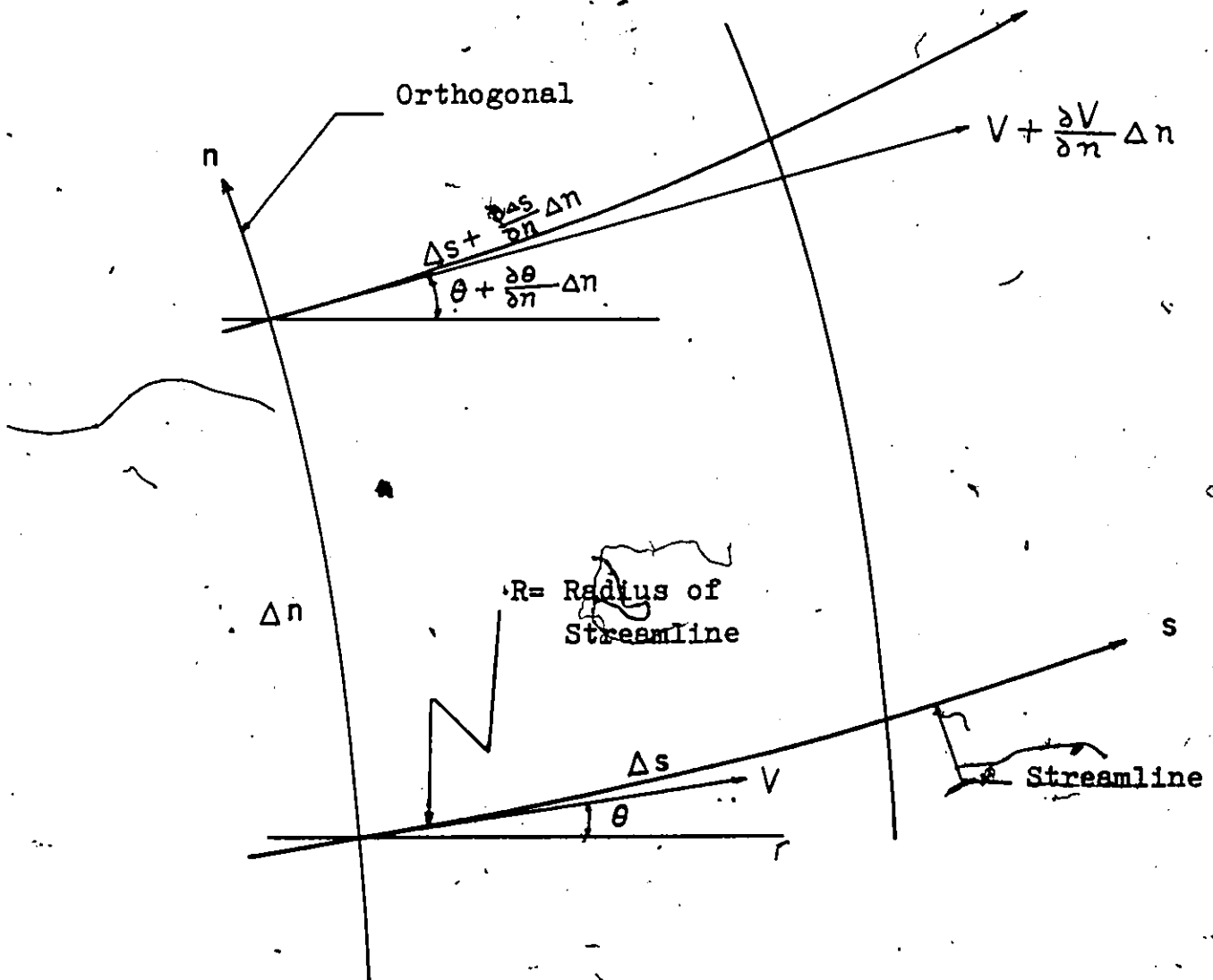


Figure 2.12 Two-Dimensional Flow Field in a Natural Coordinate System

$$\text{or } V = \exp\left\{-\frac{n_o}{2(C_p - C_s)} \cdot C^2\right\} \quad (2.12)$$

Equation 2.12 defines the velocity at any point on an orthogonal as a function of curvature. The velocity of the mid-channel can be obtained as follows:

$$C_{\text{mid}} = \frac{C_p + C_s}{2}$$

$$\therefore V_{\text{mid}} = \exp\left\{-\frac{n_o}{2(C_p - C_s)} \cdot C_{\text{mid}}^2\right\}$$

$$= \exp\left\{-\frac{n_o}{2(C_p - C_s)} \cdot \frac{(C_p + C_s)^2}{4}\right\}$$

$$\therefore \frac{V}{V_{\text{mid}}} = \exp\left\{-\frac{n_o}{2(C_p - C_s)} \cdot C^2 - \frac{(C_p + C_s)^2}{4}\right\} \quad (2.13)$$

Using the alternative simple assumption that radius of curvature varies linearly across the passage [6]:

$$\frac{V}{V_{\text{mid}}} = \left(2\left\{\frac{C_p + (C_s - C_p)\frac{n}{n_o}}{C_p + C_s}\right\}\right)^{\frac{n_o \cdot C_p \cdot C_s}{C_p - C_s}} \quad (2.14)$$

The above equation can be simplified to obtain an expression as follows:

$$\frac{V}{V_{\text{mid}}} = \exp\left\{n_o\left[C_s\left(\frac{3}{8} - \frac{n}{n_o}\right) + \frac{1}{8}C_p - \frac{1}{2}(C_p - C_s)\frac{n^2}{n_o}\right]\right\} \quad (2.15)$$

At the pressure surface  $C = C_p$  and Equation 2.12 can be written

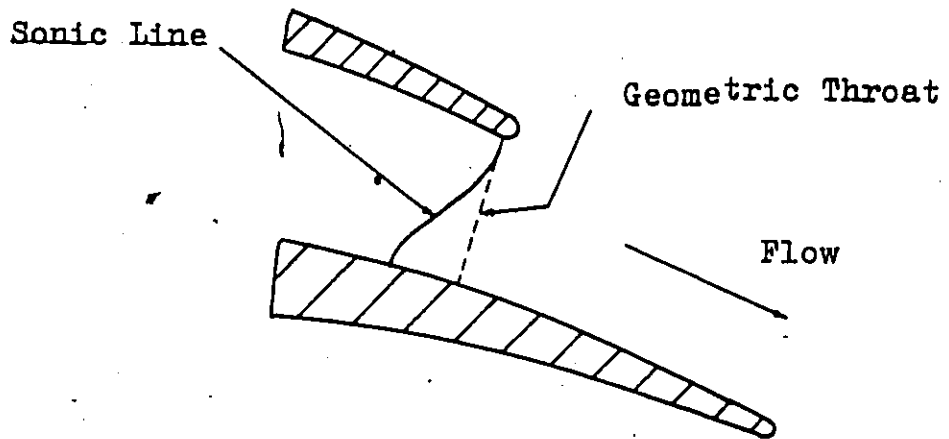


Figure 2.13(a) Sonic Line in Convergent Blade Passage

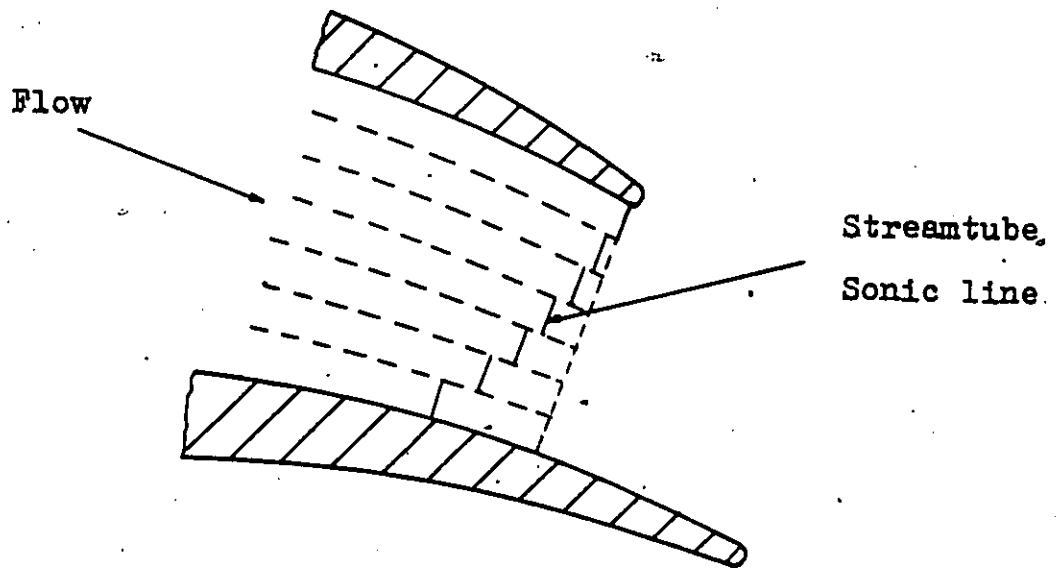


Figure 2.13(b) Stream tube Approximation to Sonic Line

$$V_{\text{pressure}} = \exp\left\{-\frac{n_o}{2(C_p - C_s)} \cdot C_p^2\right\}$$

$$\text{hence } \frac{V}{V_{\text{pressure}}} = \exp\left\{-\frac{n_o}{2(C_p - C_s)} (C^2 - C_p^2)\right\}$$

The above expression can also be simplified further to give

$$\frac{V}{V_{\text{pressure}}} = \exp\left\{\frac{n_o}{2}[(C_p + C_s) - 2C_s \frac{n}{n_o} - (C_p - C_s)\frac{n^2}{n_o^2}]\right\} \quad (2.16)$$

For the particular case when  $C_p = C_s$  which may occur near the blade trailing edge Equation 2.13 becomes:

$$\frac{V}{V_{\text{mid}}} = \exp\left\{n_o \left(\frac{1}{2} - \frac{n}{n_o}\right) C_s\right\} \quad (2.17)$$

With the help of the above equations, the mass flow per unit area can be calculated. From the known inlet flow conditions and the isentropic flow relations, the velocity distribution can also be estimated. For the mass flow calculation, iteration can be carried out using the mid-channel velocity as the variable until it converges to a total mass flow equal to that allowed by choking or to some other design inlet mass flow.

#### 2.4 Development of Computer Program

The computer program is used to find the Mach number distribution together with other flow parameters along the stream-lines. The Mach number distribution at the theoretical throat is utilized for analysing the trailing edge flow

behaviour of the McMaster blades for different pressure ratios. As the flow velocity at the theoretical throat exceeded the sonic velocity then the method of characteristics can be applied for analysing the downstream flow conditions. This technique allows one to show any expansion or compression waves that may exist in the downstream flow field of the blade passage. The actual flow pattern can be varied during model or full scale testing with the help of a Schlieren technique which can be used to observe the flow near the trailing edge region of the passage..

The complete program was initially developed and successfully used by earlier researchers, see references (5), (6), and (7). Further details can be obtained from these works.

The mass flow ( $\dot{m}$ ), can also be calculated using the relation

$$\dot{m} = \sqrt{\frac{\gamma g_c}{R_g T_{o_{rel}}}} * (0) * P_{o_{rel}} * 12.0 * \frac{M}{(1 + \frac{\gamma-1}{2} M^2)^{(\gamma+1)/2(\gamma-1)}}$$

For choking condition  $M = 1.0$  and for  $\gamma = 1.4$ , the above expression reduces to

$$\dot{m}_{choke} = \sqrt{\frac{1.4 * g_c}{R_g T_{o_{rel}}}} * (0) * P_{o_{rel}} * \frac{12.0}{1.728} \quad (2.18)$$

The static temperature ( $T$ ) at inlet is given by the isentropic flow relation in the form

$$T = \frac{T_{o\text{rel}}}{1 + \frac{\gamma - 1}{2} M_i^2} \quad (2.19)$$

where  $M_i$  = Mach number at inlet.

The static pressure (p), can be expressed as

$$p = P_{o\text{rel}}(\text{inlet}) * \left( \frac{T}{T_{o\text{rel}}} \right)^{\frac{\gamma}{\gamma-1}} \quad (2.20)$$

The density ( $\rho$ ) can be calculated from the Ideal Gas Law written in the form

$$\rho = \frac{p * 144.0}{R_g T} \quad (2.21)$$

While the sonic velocity (a) is given by the expression

$$a = \sqrt{\gamma g_c R_g T} \quad (2.22)$$

Hence the resultant velocity is

$$V = M * a \quad (2.23)$$

Also the design channel mass flow can be expressed as

$$\dot{m}(\text{design}) = \rho * V * \frac{C_i}{12.0} \quad (2.24)$$

where  $C_i$  = channel width at the inlet of the passage.

An iteration process is initiated by assuming a mid-channel stream-line velocity. The orthogonal is divided into eight equal parts and it is assumed that each part corresponds to a channel between two stream-lines. With the known values of pressure surface and suction surface curvatures and the length of the orthogonals, using Equations 2.15, 2.16,

and 2.17, the velocities at nine points along each orthogonal are obtained. Also from known values of relative total pressure, temperature and relative velocities, density at each stream-line is calculated using simple thermodynamic relationships.

Let  $Z(I) = (I) * W(I)$  where  $Z(I)$  is the mass flow per unit area. Then calculating  $Z(1), Z(2)...$  etc. at all the nine points along the orthogonal line, the total mass flow through the channel can be obtained using the following equation [12].

$$\begin{aligned} \dot{m} = & \{0.03489(Z(1) + Z(9)) + 0.20769(Z(2) + Z(8)) \\ & - 0.03273(Z(3) + Z(7)) + 0.37023(Z(4) + Z(6)) \\ & - 0.16014(Z(5))\} * \frac{\text{Gauge}}{12.0} \end{aligned} \quad (2.25)$$

Here the gauge refers to the orthogonal length.

The Mach number at each and every station is calculated based on the velocity as given above and the speed of sound based on the static temperature at the point in question.

## 2.5 Alternative Choke Calculation

The program discussed earlier may cause problems when applying it to calculate the flow parameters in the vicinity of a choked throat. As is obvious from the statement that for maximum mass flow, the derivative  $d\rho/dA$  changes its sign at the throat, the program diverges from the solution while hunting for the correct mass flow with the help of a simple algorithm. This difficulty is generally avoided by consider-

ing the blade surface to have a small curvature near the throat region. Though arbitrary and somewhat unsatisfactory, it does allow the computer program to proceed. Further, it has been observed that most turbine blades have a radius of curvature at the throat although it is difficult to numerically assess. In the final analysis it means that the actual location of the choked throat may be somewhat different than the theoretical location but close enough to it for all practical purposes.

With the method discussed earlier it is obvious that the flow will choke in the stream tube closest to the suction surface, the choking process will then progress towards the pressure surface. To make the computer program work under this condition, an alternative program statement is added. When the Mach number at the geometric throat reaches a critical value, the velocity distribution is calculated from the pressure surface towards the suction surface with the help of Equation 2.16. To start the calculation it is assumed that the flow has reached sonic condition on the pressure surface first. Though for a real viscous fluid, the throat may shift by a small percentage of axial chord (Figure 2.13), the assumption can be treated as first approximation for generating potential flow.

Certain shortcomings are inherent in this calculation as just described, because it is assumed that there is a



linear rate of change of curvature across the throat and also the mass flow as calculated is generally a little less than the design geometric throat value.

## 2.6 The Trailing Edge Region

The region of the blade passage downstream of the geometric throat has been termed the trailing edge region - this region constitutes a large portion of the suction surface of many highly loaded blades. The study of the trailing edge effect is important as the trailing edge region determines the flow pattern of the gases once they leave the blade passage. Depending on the working pressure ratio and trailing edge configuration, the flow pattern will be different for different conditions. Of the above two factors, the influence of operating pressure ratio plays an important role in shaping the flow pattern in the trailing edge region. The complete flow analysis in this region is important for the following vital reasons:

- (a) distribution of blade loading
- (b) aerodynamic moments about the neutral axis
- (c) blade vibration and flutter
- (d) boundary layer behaviour and wake thickness
- (e) flow deflection at exit plane, and
- (f) the estimation of the exit plane static pressure distribution for possible use in the design of

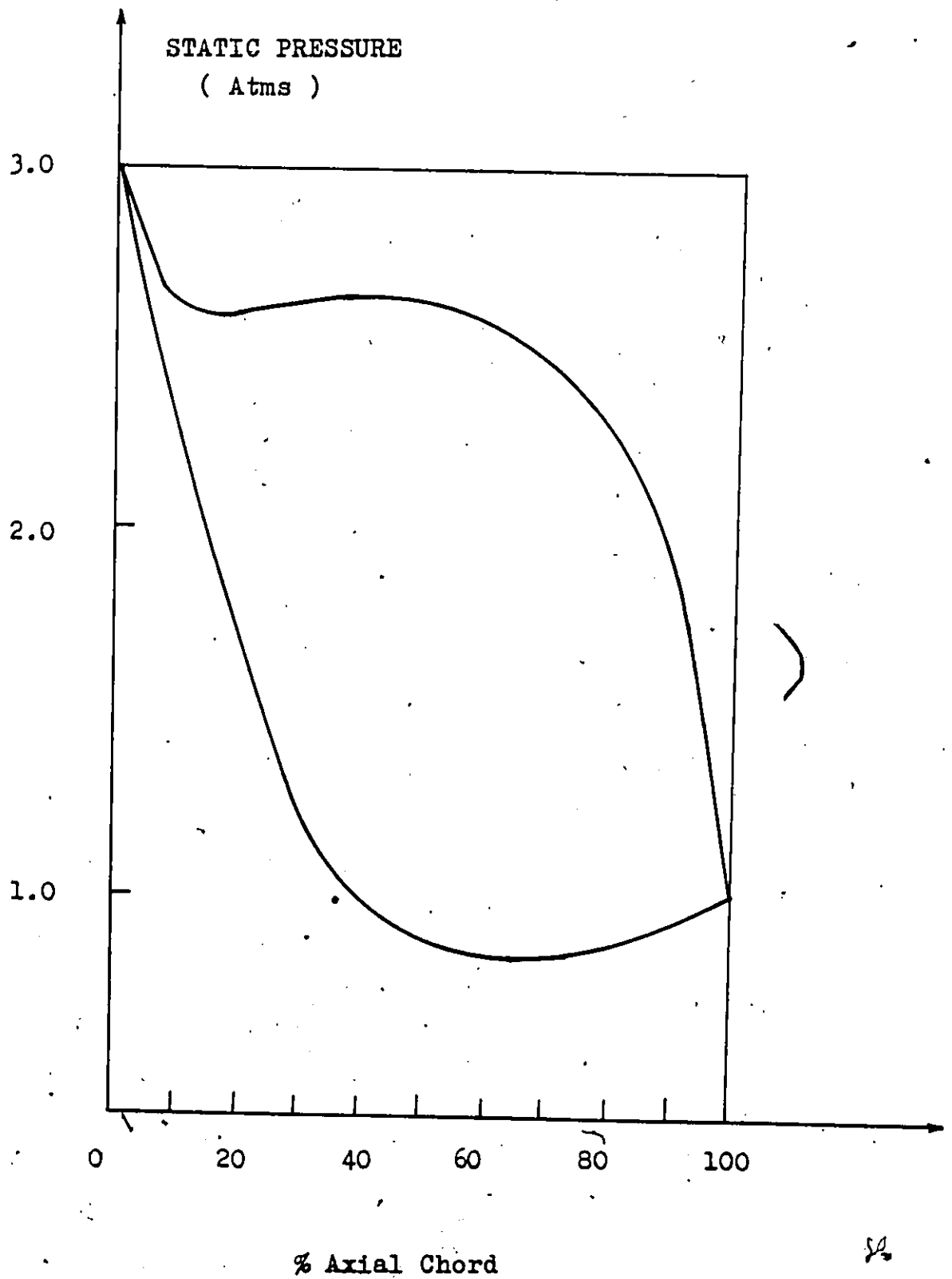


Figure 2.14 Pressure Distribution for McMaster Blade  
(Reference [6]).

blade cooling air passages.

For a converging passage the portion of the choke line and the fluid properties can be estimated for the critical operating condition of the passage. When the back pressure falls below the critical pressure at the throat, an expansion wave system exists around the trailing edge of the blade. Once the pressure ratio ( $p/P_0$ ) is below critical, the initial one-dimensional flow analysis will not give a proper solution of the problem. The expansion wave system generated at the trailing edge will modify the static pressure distribution as the flow passes through the expansion wave system. A variation of working pressure ratios will produce different expansion wave patterns around the blade trailing edge. The trailing edge thickness is neglected in the analysis and expansion waves, are considered to diverge from the centre of the trailing edge radius. The expansion fan so generated, interacts with a weak shock wave further downstream and this shock wave balances the pressure to the downstream back pressure. At a small distance downstream from the cascade the wave system cancels out leaving a net flow deviation and a reduced static pressure. The system can be represented for  $1^\circ$  or  $2^\circ$  waves depending on the accuracy required. For pressure ratios greater than 4:1, the wave pattern becomes more complicated and entropy changes along with the gradients of temperature and pressure may be noted.

For analysing the flow at the trailing edge region of a flat-back converging passage the method of characteristics is found to be more suitable. In the next chapter this method is developed as elaborately as possible and is applied to the flow analysis of the McMaster blade. The complete flow pattern inside the passage is of secondary importance here and the analysis is restricted only to the trailing edge region of the passage.

A computer program was developed for finding the pressure distribution over the McMaster blades. Though the general features of the distribution and changes with angle of attack awaiting experimental verification for this blade profile, a favourable pressure gradient is shown to exist on the suction surface for the under-expanded case. The computation method is adequate for design purposes. The Mach number distribution at the exit plane gives an approximation of the flow condition at the trailing edge or along the geometric throat of the blade passage. This Mach number distribution is utilized in finding the theoretical characteristic curves near the trailing edge of the passage as shown in a later section of this thesis.

## 2.7 Performance of a Transonic Passage

For isentropic flow through a convergent section the flow will choke for a critical ratio of stagnation pressure

TABLE 1LEADING PARTICULARS OF McMASTER BLADE

Total turning angle	128° 30'
Inlet air angle	64°
Outlet air angle (at Choking)	64° 30'
Lift coefficient (Zweifel)	1.0
Pitch	0.650 inches (16.51 mm)
Axial chord	1.00 inch (25.4 mm)
Uncovered turning	0°
Geometric throat	0.257 inches (6.53 mm)
Inlet choking Mach number	0.68

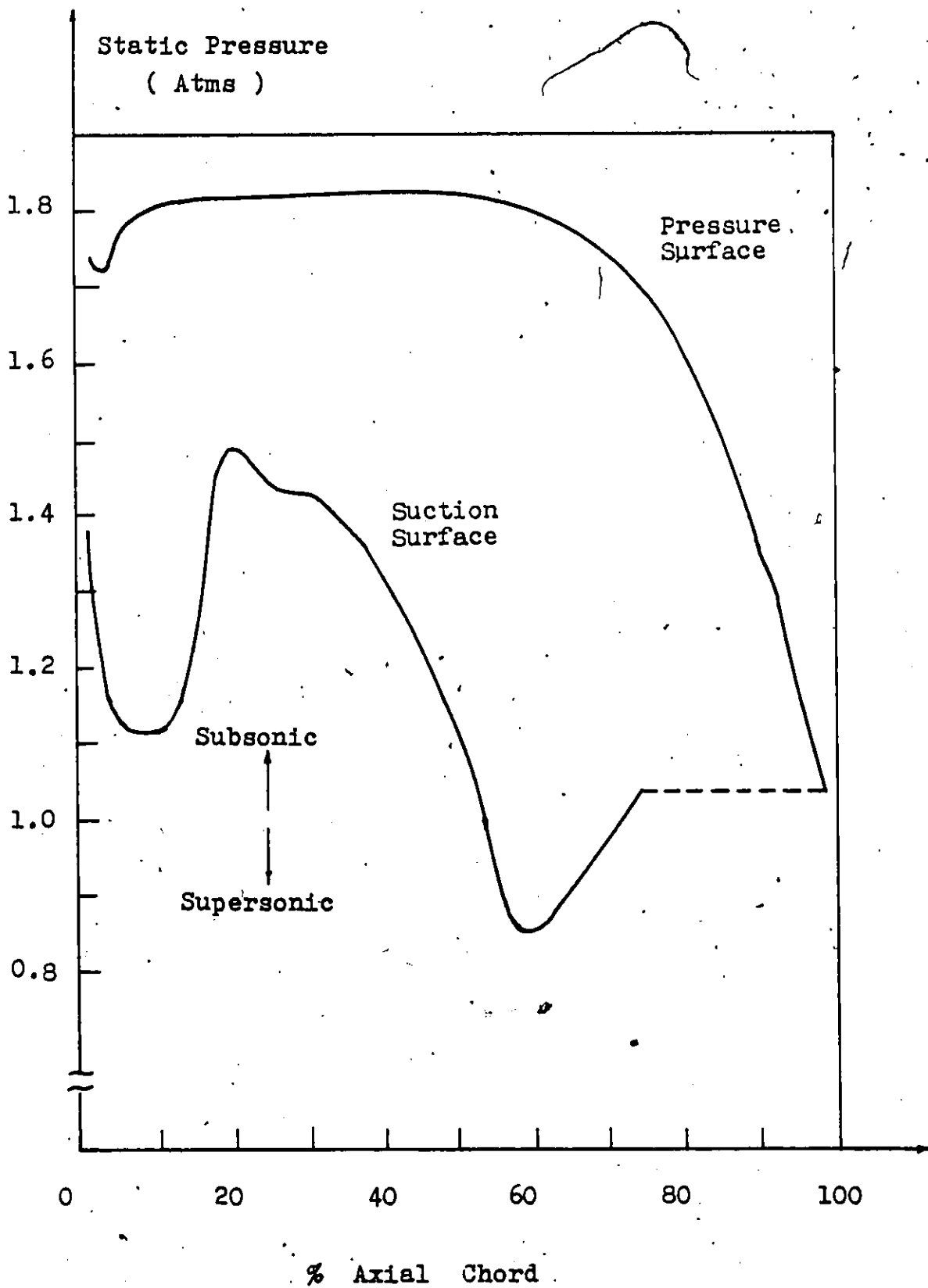


Figure 2.15 Pressure Distribution Around McMaster Blade  
● Used in the Present Study

( $P_0$ ) to back pressure ( $p_b = p^*$ ). The choking mass flow is then given by [25]

$$\frac{\dot{m} \sqrt{R_g T_0}}{A^* P_0} = 0.686$$

for  $M = 1.0$  and  $\gamma = 1.4$ .

For any back pressure higher than the critical pressure, the mass flow will decrease with the increase of back pressure. But if the back pressure is lower than the critical pressure, the flow will expand from the throat to the trailing edge of suction surface. If the section of the passage in this region is highly curved, under an over-expansion condition the efflux angle of the flow will deviate greatly from the normal operation without any expansion. The characteristic curves for a curved back surface will be of complicated nature denying any theoretical prediction of gas outlet angle from the cascade. For a straight or flatback blade surface this difficulty is reduced to some extent as the flow characteristics are much simpler on flatback blades. The only resort left to the designer in either case for estimating the exact gas outlet angle is to make use of a flow visualization technique.

In transonic passages there are supersonic flow patches in the flow field even with a subsonic inlet Mach number. The highly curved blades again worsen the situation for which a theoretical analysis will not give any adequate information of the flow condition inside the passage. Some researchers

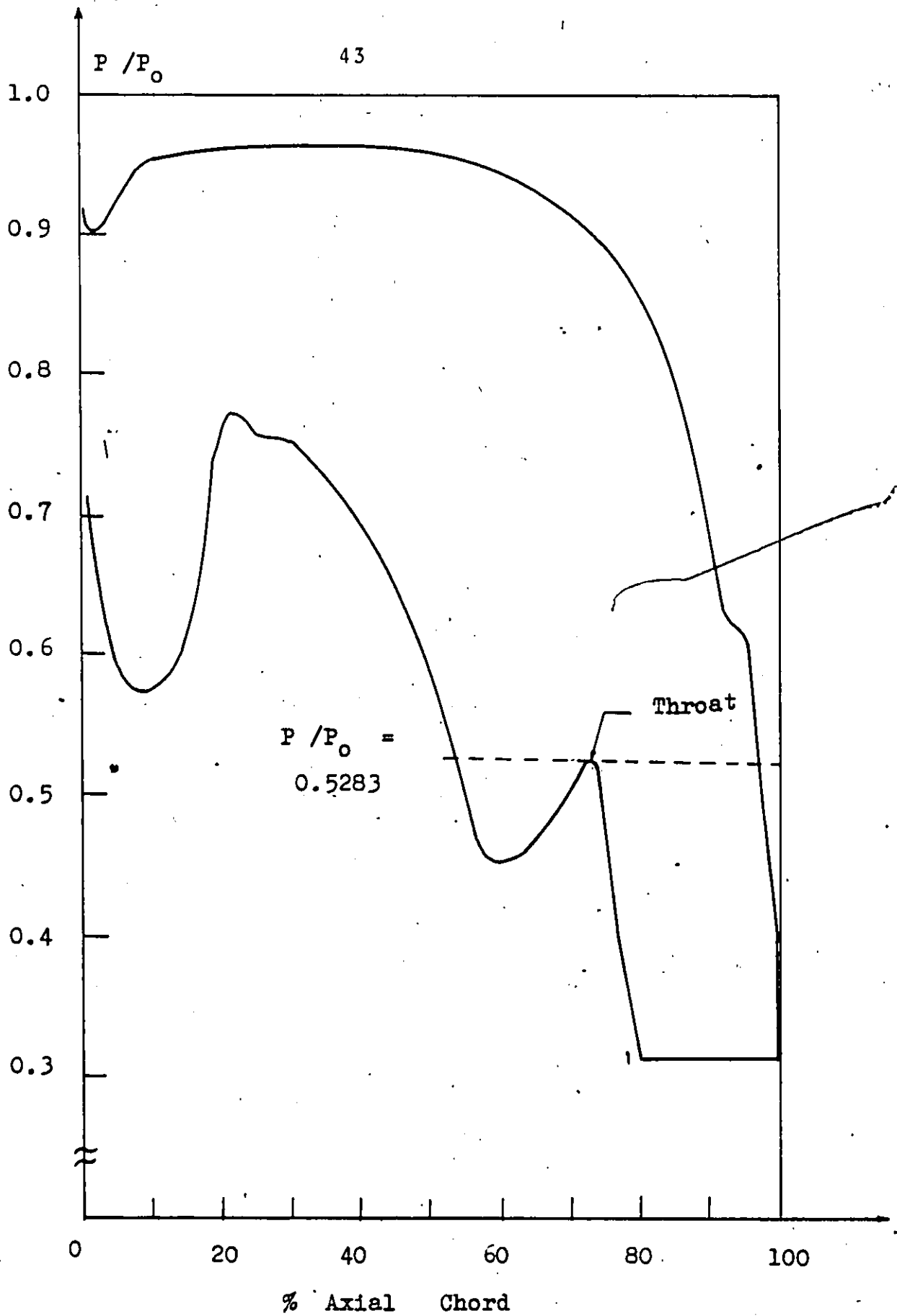


Figure 2.16 Trailing Edge Pressure Distribution Using Wave System (McMaster Blade)



[22] are of the opinion that shocks may even be generated near the suction surface leading edge. This occurrence of shock may drastically change the flow pattern and consequently the static pressure distribution in the blade passage.

## 2.8 Shock - Boundary Layer Interaction

The shock and boundary layer phenomena are complex by themselves, their interaction makes the problem more complicated. The analytic solution of the interaction is still not available, although the recent papers in the area show a combination of theoretical analysis and a flow visualization technique. The highly curved transonic blading are more readily effected by this phenomenon. So the study of the such blading with the help of a Schlieren or Shadowgraph apparatus becomes inevitable in the understanding of actual flow behaviour in such blades, particularly when considering a wide range of pressure ratios.

Consider the fact that a boundary layer is generated along a surface to maintain the no-slip condition between the fluid and the surface. The interaction of shock with the boundary layer produces adverse flow phenomenon which results in further losses in the blade passage. If the shock strength is enough to create a separation of the boundary layer from the surface there appears to be a gradual increase in the surface static pressure of the blading [30]. Though a weak

interaction may produce mild adverse effects, the prediction of a strong interaction is impossible using the present analytical procedure. These circumstances call for a flow visualization technique to be adopted in order to experimentally show the flow behaviour in transonic blading.

The experimental investigations [20] indicate that there is marked change in the pressure distribution due to the interaction. Though the interaction process was known to scientists, it is only recently that some numerical techniques are being applied to obtain a possible solution of the shock-boundary layer interaction.

All the above discussions call for a good visualization technique to be adopted to completely understand the flow behaviour. The Applied Dynamics Laboratory of McMaster University provides a very useful blow-down cascade type wind tunnel, but because of the horizontal construction of the test section a vertical Schlieren or Shadowgraph system is required. The information available for vertical Schlieren system is very limited, particularly applied to cascades, and because a vertical system is difficult to design to be very rigid researchers usually prefer a horizontal arrangement of the system.

## 2.9 Flow Visualization Apparatus

The proposed Schlieren/Shadowgraph system is shown in

Figure 2.17. The main light beam which traverses the test section is vertically oriented. A monochromatic light source S of high intensity generates sufficient light to illuminate the test section. The source may be either a circular or a rectangular type depending on the shape of the knife edge KE used in the system. Light from source S is reflected vertically downward with the help of a plane surface mirror  $M_1$  and then travels downward through the lens  $L_2$ , beam splitter BS and finally onto plane mirror  $M_2$ . The rays of light are then made incident on the parabolic mirror PM from there light rays travel through the test section onto the plane mirror  $M_3$ . The pencil of rays then travels back along the incident path and only at the beam splitter it is reflected to the camera  $\bar{C}$ . The parabolic mirror used is of f/8 size with a focal length of 48". The camera has a large focal length lens for obtaining the largest possible image of the test section. All the components are mounted on a portable structure which is normally independent of the test section structure of the wind tunnel.

The blades are to be fixed in the test section parallel to the light rays with the help of clear acrylic plastic which will give better fixing quality as well as maintaining the transparency for the light to pass through. The bottom and top sections are covered by two round glass plates which are designed to make the test section more rigid. All mirrors and lenses can be easily adjusted to suitable position for

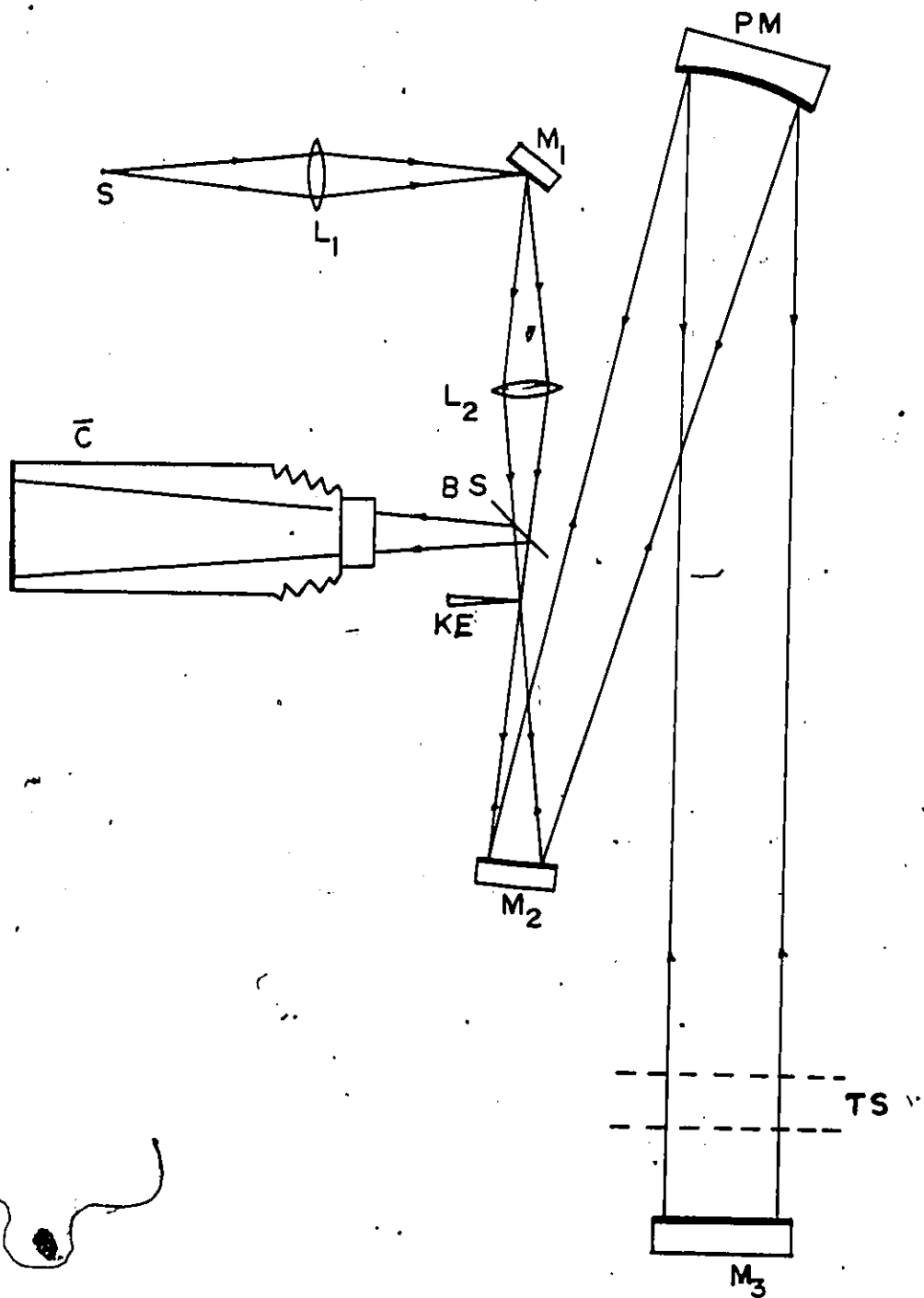


Figure 2:17 Schematic of a Vertical Schlieren Arrangement

obtaining the correct resolution and contrast of the image.

The arrangement of the Schlieren system is not commonly in practice. However, for the test section at hand the double traverse arrangement eliminates many practical difficulties [18, 19]. This arrangement of the Schlieren system has also been suggested in the discussion of reference 17, pp. 222.

#### 2.10 Supercritical Blade Exit Conditions

If the static pressure behind a turbine passage or blade row is progressively reduced, then a situation similar to the flow in a convergent-divergent nozzle with varying back pressure arises. The continual reduction in back pressure or increase in total pressure at the passage inlet will increase the exit velocity of the blade passage until at the geometric throat the velocity is sonic. If the passage is choked, that is Mach number relative to the blades at the throat is unity, then the condition upstream will be unaffected however, much the back pressure behind the throat is reduced.

The outlet flow condition after the throat has been studied by Hauser, Plohr and Sonder [27]. It was observed that, even at static-to-total pressure ratios considerably lower than that required to give critical velocity at the throat section, the flow was deflected in the tangential

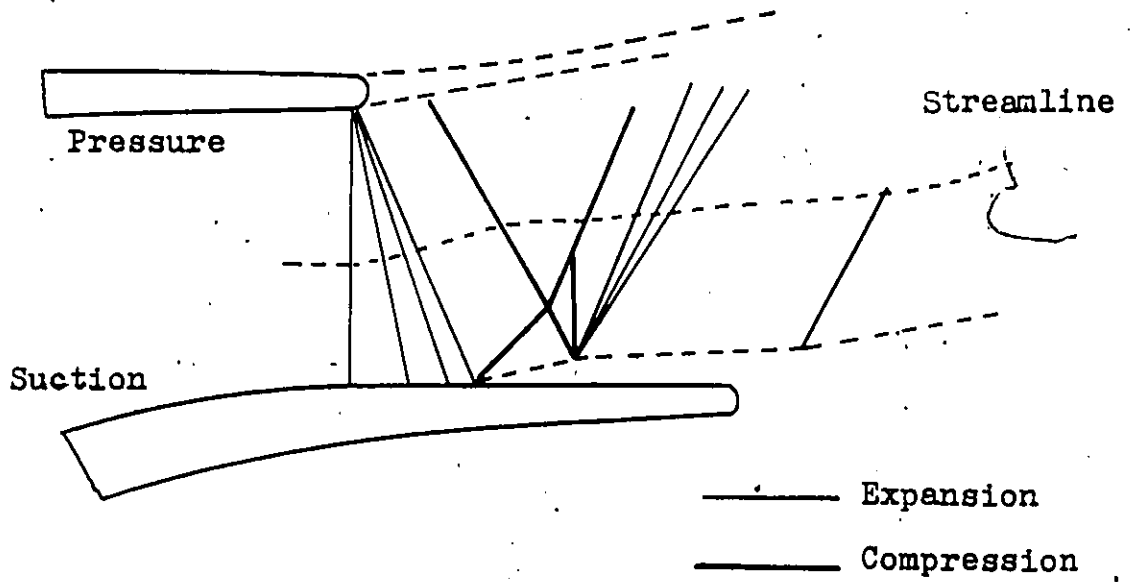


Figure 2.18 Semi-expanded Blade Passage (1)

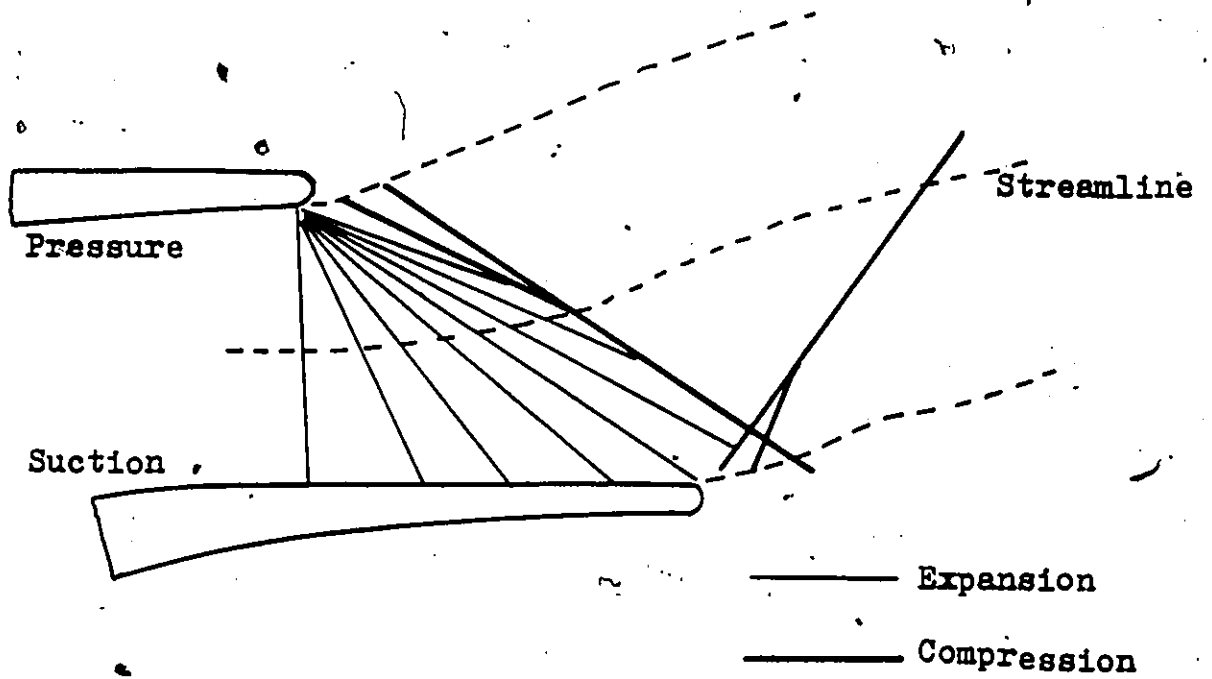


Figure 2.19 Fully-expanded Blade Passage (1)

direction. For further reductions in pressure ratio (static-to-total), the aerodynamic loading of the rear portion of the blade reached a maximum and remained constant. After this stage, the expansion downstream of the cascade took place with constant tangential velocity so that no further increase in the amount of turning across the blade row and no further increase in loading was available.

Figure 2.18 shows the flow picture when the supercritical flow conditions after the throat have been established. An expansion fan originates from the pressure surface extremity of the blade and the flow is slowly turned as it passes through the expansion wave system. As the flow proceeds further downstream a weak shock wave turns the flow in the opposite direction. As the pressure ratio (static-to-total) is reduced further, the expansion fan starts enlarging and the shocks are found to move towards the extremities of the blade (Figure 2.19). The flow also turns towards the tangential direction. Once the fully expanded flow is established the pressure distribution on the blade surface changes. A representative plot is shown in Figure 2.20 where the variation of pressure distribution after the throat is shown. For supercritical conditions an increased area and associated tangential force are produced by the decreased pressure on the suction surface. The "limiting loading" [1] condition is reached when the supersonic expansion fan after the blade throat first reaches

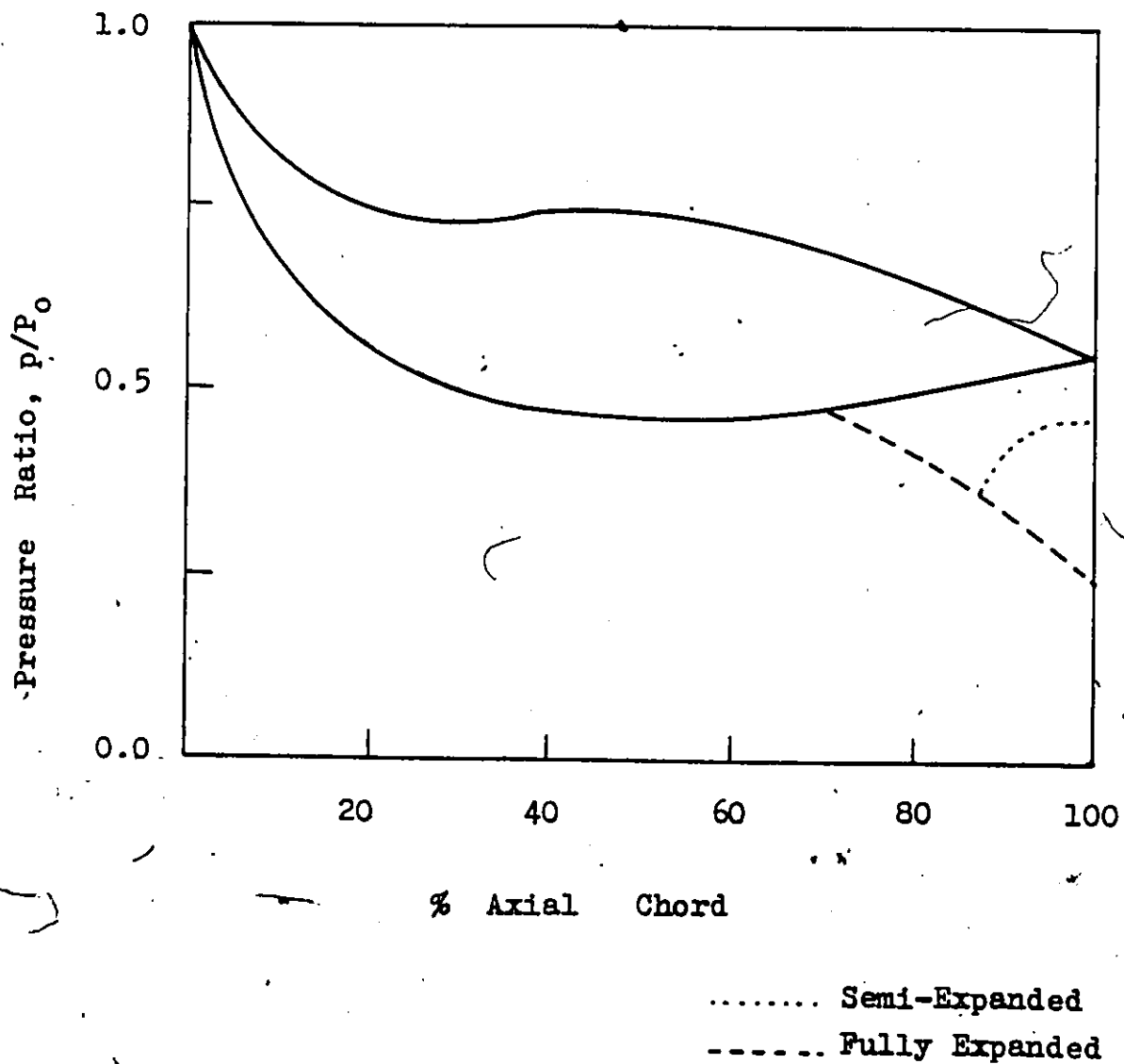


Figure 2.20 Effect of Outlet Pressure on Surface Pressure Distribution (1)



the extremity of its adjacent blade. This limiting loading condition is important because the pressure ratios below this condition will cause turbine efficiency to decrease as no increase in work per pound of gas is possible.

CHAPTER 3  
METHOD OF CHARACTERISTICS

3.1 General Flow Equations

The non-linear equations of motion for two dimensional, non-viscous irrotational plane flow are [8]

$$(u^2 - a^2) \frac{\partial u}{\partial x} + 2uv \frac{\partial u}{\partial y} + (v^2 - a^2) \frac{\partial v}{\partial y} = 0 \quad (3.1)$$

and  $\frac{\partial u}{\partial y} - \frac{\partial v}{\partial x} = 0 \quad (3.2)$

The above equations in general, are applicable to both subsonic and supersonic inviscid flows. Restricting the application to supersonic flows only that is, when  $(u^2 + v^2)/a^2 > 1$ , the equations are hyperbolic in nature and the numerical solutions may be obtained by method of characteristics. Hence, for the supersonic flow situation, the general flow properties at a particular point in the flow depends on the upstream flow conditions in a specified region of the flow, but are independent of the downstream flow conditions. Knowing the flow properties at some initial points, other points in the flow field may be calculated in a forward marching type numerical method. The method of characteristics may be applied in the solution of the above differential equations.

The method of characteristics of a supersonic flow

field governed by hyperbolic partial differential equations may be obtained by three possible procedures [13], namely:

- i) purely graphical
- ii) purely numerical, and
- iii) a combination of numerical and graphical methods.

Though the choice of the above methods depends on many factors, for a speedy accurate solution of the problem, a purely numerical method is indispensable. When of course, the numerical results are represented in a diagrammatic form, a complete picture of the pattern of the flow can be obtained.

Classical methods for the numerical solution of the method of characteristics follow the natural flow coordinate system [8]. However, with the advent of numerical analysis and digital computer the solution of method of characteristics may be obtained even using the cartesian coordinate system. For the present study emphasis is given to the numerical method using cartesian coordinates.

The computation method using the natural flow coordinate system faces the main difficulty of evaluating the value of Mach number for a particular value of Prandtl-Meyer expansion angle  $\nu$ . The values of Mach numbers corresponding to different values of  $\nu$  have to be supplied external to the computation system.

### 3.2 Properties of Characteristics

As mentioned previously, the solution of quasilinear partial differential hyperbolic equations can be obtained by method of characteristics. Some of the properties of the characteristics may be stated as follows [15]:

- i) a characteristic is a curve along which a physical disturbance should propagate and in supersonic flow disturbances propagate along the Mach lines, hence Mach lines are the characteristics for a supersonic flow.
- ii) across a characteristic the normal derivative of the dependent variables  $(u, v)$  may be discontinuous, while the property itself remains continuous.
- iii) on the characteristics, the dependent variables satisfy a certain relation known as the compatibility relation:

### 3.3 Equations of Motion in Characteristic Form

The change in any function  $f$  while going from point  $P$  to  $Q$  along the stream-line  $S$  (Figure 3.1) may be written as

$$df = \frac{\partial f}{\partial S} dS$$

In terms of coordinate system, this takes the following form

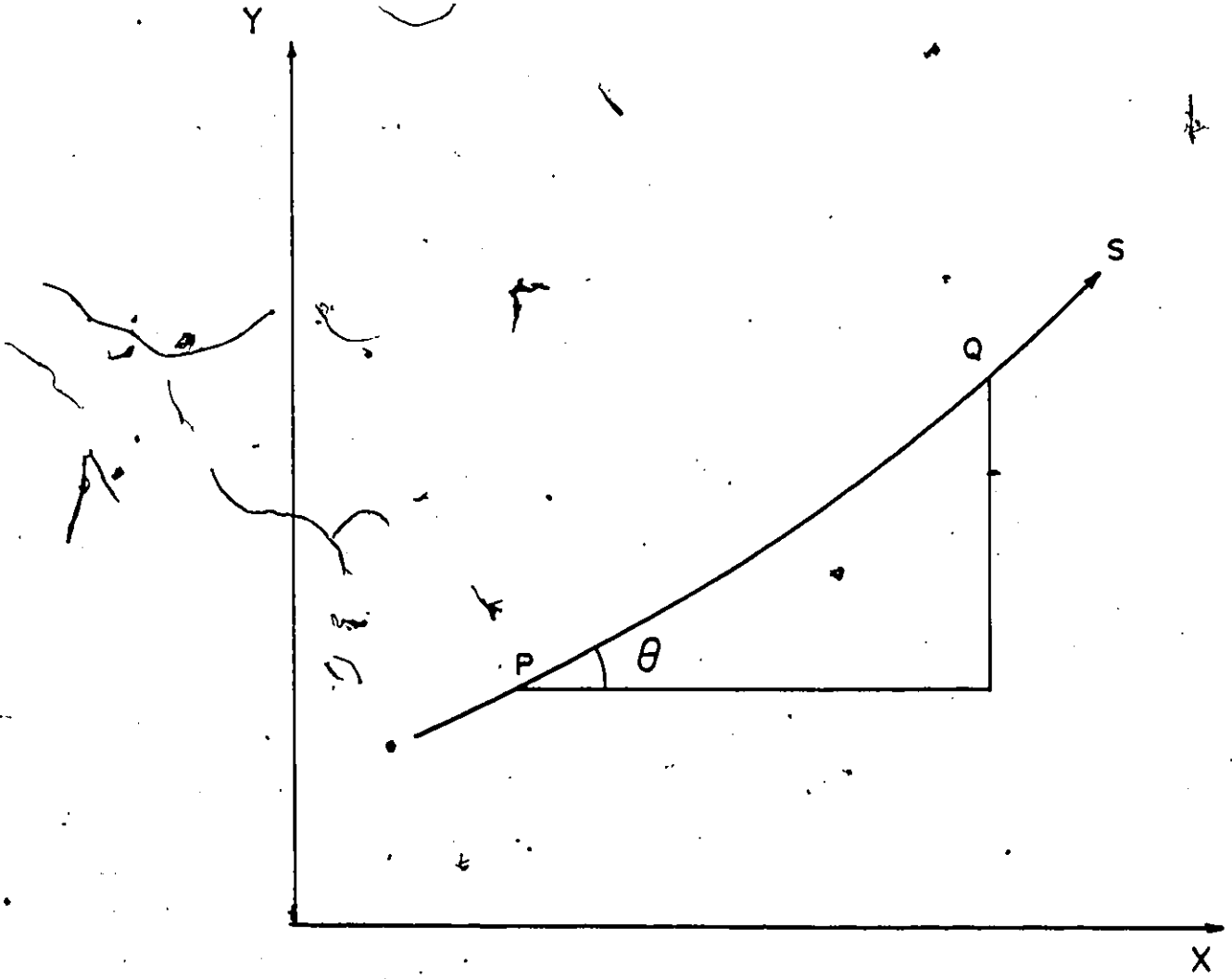


Figure 3.1 Streamline and Coordinate Axes

$$\frac{df}{dS} = \frac{\partial f}{\partial x} \cdot \frac{\partial x}{\partial S} + \frac{\partial f}{\partial y} \cdot \frac{\partial y}{\partial S} \quad (3.3)$$

or  $f_S = f_x \cdot x_S + f_y \cdot y_S$

In the same fashion, the change in variables  $u$  and  $v$  going from  $P$  to  $Q$  may be written as

$$u_S = u_x \cdot x_S + u_y \cdot y_S \quad (3.4)$$

$$v_S = v_x \cdot x_S + v_y \cdot y_S \quad (3.5)$$

The above two equations may be solved for  $u_x$ ,  $v_x$  on the line in terms of  $u_S$ ,  $v_S$ ,  $u_y$  and  $v_y$ .

From 3.4 and 3.5

$$u_x = \frac{u_S}{x_S} - m u_y$$

$$v_x = \frac{v_S}{x_S} - m v_y$$

where  $m = \frac{y_S}{x_S}$  is the average slope of the line between points  $P$  and  $Q$ .

Substituting the values of  $u_x$  and  $v_x$  in equations 3.1 and 3.2, the following form is obtained.

$$[-(u^2 - a^2)m + 2uv]u_y + (v^2 - a^2)v_y = -(u^2 - a^2) \frac{u_S}{x_S} \quad (3.6)$$

$$u_y + m v_y = \frac{v_S}{x_S} \quad (3.7)$$

Equations 3.6 and 3.7 are simultaneous algebraic equations which can be used to determine  $u_y$  and  $v_y$ . The matrix of the pair is [16]

$$\begin{vmatrix} 2uv - (u^2 - a^2)m & (v^2 - a^2) & -(u^2 - a^2) \frac{u_S}{x_S} \\ 1 & m & \frac{v_S}{x_S} \end{vmatrix}$$

Let the determinants  $D_1$  and  $D_2$  be

$$D_1 = \begin{vmatrix} [2uv - (u^2 - a^2)m] & (v^2 - a^2) \\ 1 & m \end{vmatrix} \quad (3.8)$$

$$D_2 = \begin{vmatrix} [2uv - (u^2 - a^2)m] & -(u^2 - a^2) \frac{u_S}{x_S} \\ 1 & \frac{v_S}{x_S} \end{vmatrix} \quad (3.9)$$

For  $u_y$  and  $v_y$  to have finite, but non-unique solutions, both  $D_1$  and  $D_2$  must be zero. The condition  $D_1 = 0$  determines the directions of given lines for which  $u_y$  and  $v_y$  are not uniquely determined, hence the characteristic equations of the characteristic curves. The condition  $D_2 = 0$  gives a relation that must be satisfied by the inner derivatives along such lines and hence the compatibility relations of the characteristic curves.

### 3.3.1 Characteristic Equation

Expanding  $D_1 = 0$  from Equation 3.8, the following quadratic equation may be written -

$$(u^2 - a^2) m^2 - 2uvm + (v^2 - a^2) = 0$$

Solving for m

$$m = m_1, m_2 = \frac{uv \pm a^2 \sqrt{\frac{u^2 + v^2}{a^2} - 1}}{u^2 - a^2}$$

$$m_1, m_2 = \frac{uv \pm a^2 \sqrt{M^2 - 1}}{u^2 - a^2} \quad (3.10)$$

Equation 3.10 defines two characteristic directions at each point which are real and distinct for  $M > 1$ . Consequently, the method of characteristics is applicable to steady two-dimensional supersonic flow, but is not applicable to a subsonic flow field.

Putting  $u = V \cos \theta$  ;  $v = V \sin \theta$

then  $a = V \sin \mu$  and  $\sqrt{M^2 - 1} = \cot \mu$

Equation 3.10 may be written as

$$m = \frac{\sin \theta \cos \theta \pm \sin \mu \cos \mu}{\cos^2 \theta - \sin^2 \mu}$$

With the help of trigonometric relations, this can be reduced to

$$m = \tan (\theta \pm \mu) \quad (3.11)$$

where  $\theta$  = flow angle

and  $\mu$  = Mach angle.

It is obvious from equation 3.11 that two characteristic directions are equally inclined to the stream-line



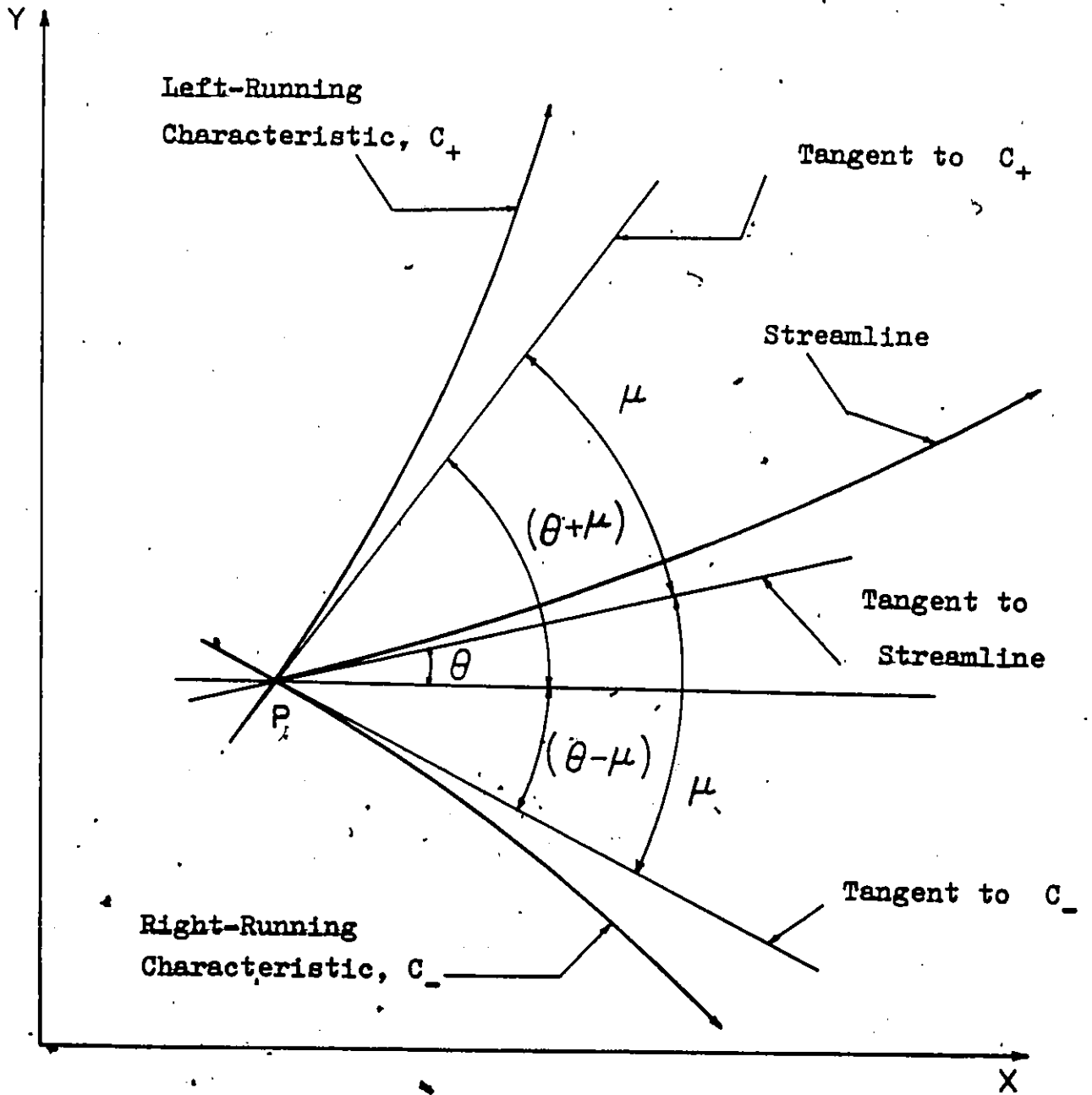


Figure 3.2 Characteristics as the Mach Lines at a Point in a Flow-Field

direction at the Mach angle  $\mu$  - these are the Mach line directions. In Figure 3.2 denoting the left and right running Mach lines at point P as  $C_+$  and  $C_-$  characteristics, Equation 3.11 then represents characteristic directions as:

$$\left(\frac{dy}{dx}\right)_+ = m_+ = \tan(\theta + \mu) \text{ along the } C_+ \text{ characteristics}$$

$$\left(\frac{dy}{dx}\right)_- = m_- = \tan(\theta - \mu) \text{ along the } C_- \text{ characteristics}$$

Hence, the characteristic equation may generally be presented as

$$\left(\frac{dy}{dx}\right)_\pm = m_\pm = \tan(\theta \pm \mu) \quad (3.12)$$

### 3.3.2 Compatibility Equations

Condition  $D_2 = 0$  of Equation 3.9 provides the equation of motion with respect to the characteristic coordinates. Expanding  $D_2 = 0$ , the following equation may be obtained:

$$[2uv - (u^2 - a^2) m] \frac{v_S}{x_S} + (u^2 - a^2) \frac{u_S}{x_S} = 0$$

Remembering  $u_S = \frac{du}{dS}$  and  $v_S = \frac{dv}{dS}$ , the above equation can be written in differential form along a characteristic curve as

$$(u^2 - a^2) du + [2uv - (u^2 - a^2) m] dv = 0$$

For  $C_+$  and  $C_-$  characteristics, the above equation can be put in the following form:

$$(u^2 - a^2) du_\pm + [2uv - (u^2 - a^2) m_\pm] dv_\pm = 0$$

The subscript  $\pm$  indicates that the differentials  $du$ ,  $dv$  are

to be evaluated along the  $C_+$  and  $C_-$  characteristics respectively, the corresponding slope is  $m_+$ .

Hence, the compatibility equation may generally be represented as

$$(u^2 - a^2) du_+ + [2uv - (u^2 - a^2) m_+] dv_+ = 0 \quad (3.13)$$

3.4

### Numerical Integration Procedure

The characteristic (3.12) and compatibility (3.13) equations are non-linear total differential equations and the solutions have been obtained by finite difference techniques. The characteristic equation (3.12) defines two characteristics passing through each point in the flow field whereas the compatibility equation (3.13) defines one relationship between the velocity components  $u$  and  $v$  on each of the two characteristics. Defining a network in which two characteristics intersect at a point, two independent relationships between  $u$  and  $v$  may be obtained at that point of intersection, so that on each of the intersecting characteristics one relation exists between  $u$  and  $v$ . In Figure 3.3, the common point 4 on  $c_+$  and  $c_-$  characteristics could be determined by simultaneous application of the compatibility equations. This gives the solution of the equations at a point interior to the flow stream.

For any point either on a solid wall or on a free

pressure boundary, minor change in the calculation procedure must be introduced. Also in applying the numerical technique, the characteristic curves are usually approximated by straight lines joining the solution points.

The numerical method employed here for the integration of characteristic and compatibility equations is the modified Euler predictor-corrector method [31]. This is a second order method for integrating total differential equations where coefficients are determined on the average property method where the numerical values of the coefficients of the differential equations are determined based on the average values of the properties at the initial points and final solution point [14].

#### 3.4.1 Modified Euler Predictor-Corrector Method:

For an ordinary differential equation in the form

$$\frac{dy}{dx} = f(x,y) \quad (3.14)$$

a predicted value of the solution of the above equation at a point  $x_{i+1} = x_i + h$ , denoted by  $y^0(x_i + h) = y_{i+1}^0$  may be obtained by a predictor algorithm in the following form:

$$y_{i+1}^0 = y_i + f(x_i, y_i)h \quad (3.15)$$

where  $h$  = the step size of the finite difference algorithm and  $y_i = y(x_i)$  where  $i$  is a known starting point.

The solution thus obtained by the predictor algorithm

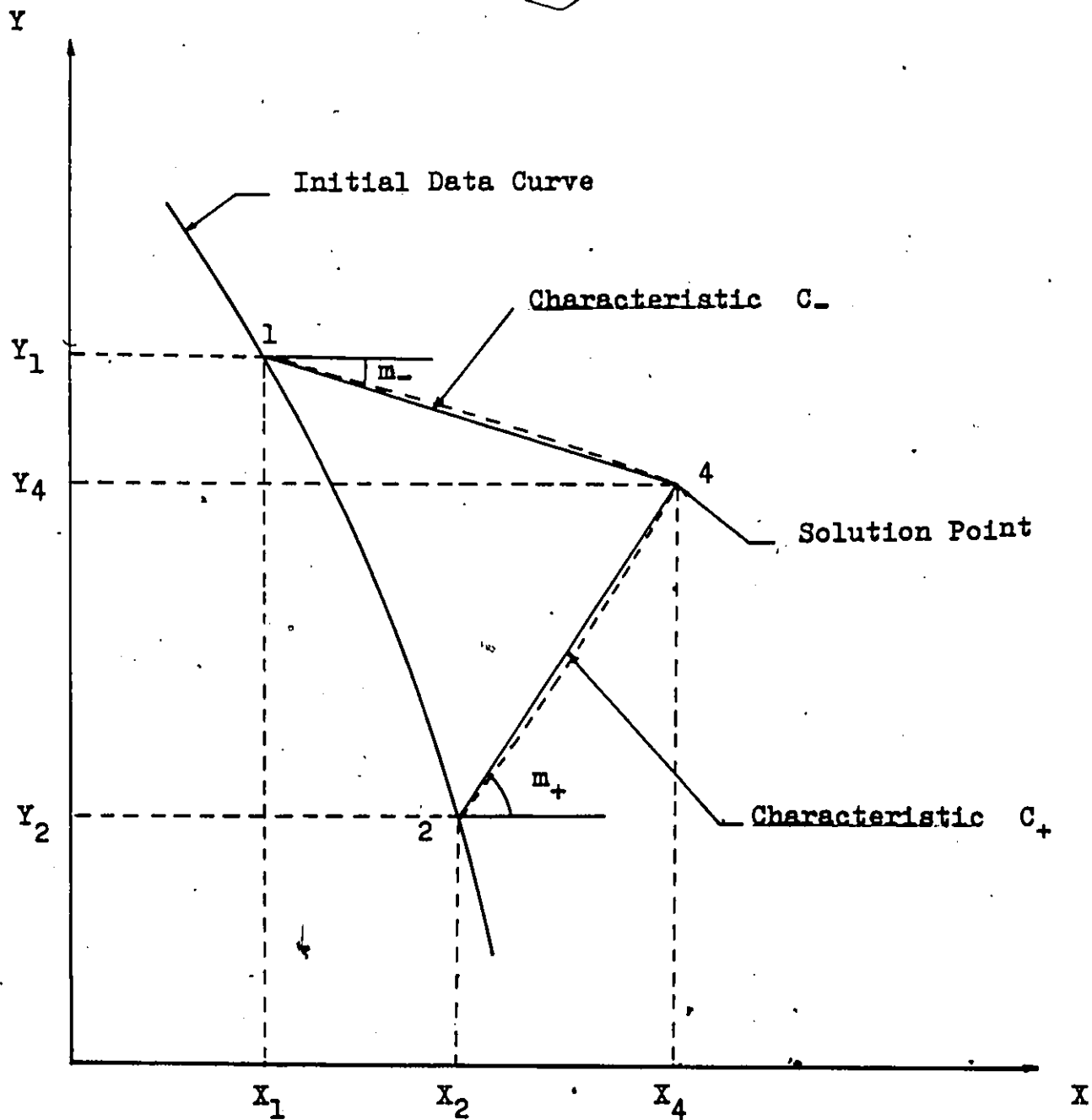


Figure 3.3 Finite Difference Networks for Applying the Method of Characteristics

may now be improved by employing the values  $y_i$  and  $y_{i+1}^0$  to find the value of  $y_{i+1/2} = y(x_i + h/2)$ . The value of  $f(x_i, y_i)$  in Equation 3.15 is then replaced by the value of  $f(x, y)$  determined at the mid-point of the interval. Hence

$$y_{i+1}^1 = y_i + f[(x_i + h/2), (y_i + y_{i+1}^0)/2]h \quad (3.16)$$

where  $y_{i+1}^1 = y^1(x_i + h)$  is the corrected value of the solution at  $x_{i+1}$ .

The predictor value  $y_{i+1}^0$  in the above equation may further be modified by the corrector value of  $y_{i+1}^1$  and repeating the use of Equation 3.16. Proceeding this way after  $n$  iterations, the corrector algorithm may be represented as follows:

$$y_{i+1}^n = y_i + f[(x_i + h/2), (y_i + y_{i+1}^{n-1})/2]h \quad (3.17)$$

where  $y_{i+1}^n$  = the value of  $y$  after  $n$  applications of the corrector.

Accuracy of the numerical values as obtained by the method presented depends on the step size and the number of applications of the corrector. Accuracy can also be controlled by assigning some value which controls the difference between values of the  $n^{\text{th}}$  and the  $(n - 1)^{\text{th}}$  iteration processes. Referring to the work of Hoffman [23] it has been observed that in most practical situations, the application of corrector algorithm about 3 times will provide a result accurate enough for all practical purposes. It has also

been found that the method is stable if  $h \frac{\partial f}{\partial y} < 2$ . Also to keep the error under control the stepsize should be small.

### 3.4.2 Finite Difference Equations

Replacing the differentials  $dx$ ,  $dy$ ,  $du$ , and  $dv$  in equations 3.12 and 3.13 with the help of  $\Delta x$ ,  $\Delta y$ ,  $\Delta u$  and  $\Delta v$  finite difference equations may be obtained as follows:

From Equation 3.12

$$\left(\frac{dy}{dx}\right)_+ = \left(\frac{\Delta y}{\Delta x}\right)_+ = m_+$$

$$\text{Hence, } \Delta y_+ = m_+ (\Delta x)_+ \quad (3.18)$$

From Equation 3.13

$$(u^2 - a^2) du_+ + [2uv - (u^2 - a^2) m_+] dv_+ = 0$$

$$\text{or } Q_+ \Delta u_+ + R_+ \Delta v_+ = 0 \quad (3.19)$$

$$\text{where } m_+ = \tan(\theta + \mu), \text{ from Equation 3.12} \quad (3.20)$$

$$Q = (u^2 - a^2) \quad (3.21)$$

$$\text{and } R = 2uv - (u^2 - a^2) m \quad (3.22)$$

The coefficients  $m$ ,  $Q$  and  $R$  are generally determined at the initial points for the predictor and in an average manner for the corrector. The above equations are used for finding the flow properties, mainly the flow deflection, in a supersonic flow field. This procedure may be used to find solutions at interior points as well as points on a solid wall or on free pressure boundary points.

### 3.4.3 The Solution for an Interior Point

Referring to Figure 3.3, the solution of point 4 may be obtained in terms of points 1 and 2 from Equations 3.18 - 3.22. Thus from Equation 3.18

$$(y_4 - y_2) = m_+ (x_4 - x_2)$$

$$(y_4 - y_1) = m_- (x_4 - x_1)$$

Hence, from above two equations

$$y_4 - m_+ x_4 = y_2 - m_+ x_2 \quad (3.23)$$

$$y_4 - m_- x_4 = y_1 - m_- x_1 \quad (3.24)$$

writing  $m$  in terms of  $\theta$  and  $\mu$

$$m_+ = \tan(\theta + \mu) \text{ and } m_- = \tan(\theta - \mu) \quad (3.24)$$

$$\text{where } \theta_+ = \tan^{-1} \left( \frac{v_+}{u_+} \right) \quad (3.25)$$

Also the resultant velocity-vector can be described by

$$V_+ = (u_+^2 + v_+^2)^{1/2} \quad (3.26)$$

The sonic velocity is determined from the stagnation conditions as follows:

$$\begin{aligned} a^2 &= a_0^2 - \frac{\gamma - 1}{2} V^2 \\ &= \gamma R T_0 - \frac{\gamma - 1}{2} V^2 \end{aligned} \quad (3.27)$$

If  $a$  is the sonic velocity, then

$$\mu_+ = \sin^{-1} \left( \frac{a_+}{V_+} \right) \quad (3.28)$$

Therefore,  $\theta_+$  and  $\mu_+$  can be evaluated for specified



values of  $u_+$  and  $v_+$  and thus  $m_+$  can be evaluated.

From the compatibility equations, using a similar procedure as above the following equations can be formed which are valid on  $C_+$  and  $C_-$  characteristics respectively.

$$Q_+ (u_4 - u_2) + R_+ (v_4 - v_2) = 0$$

$$Q_- (u_4 - u_1) + R_- (v_4 - v_1) = 0$$

$$\text{otherwise } Q_+ u_4 + R_+ v_4 = T_+ \quad (3.29)$$

$$Q_- u_4 + R_- v_4 = T_- \quad (3.30)$$

In the above equations

$$Q_+ = (u_+^2 - a_+^2) \quad (3.31a)$$

$$R_+ = (2u_+ v_+ - Q_+ m_+) \quad (3.32a)$$

$$T_+ = Q_+ u_2 + R_+ v_2 \quad (3.33)$$

$$Q_- = (u_-^2 - a_-^2) \quad (3.31b)$$

$$R_- = (2u_- v_- - Q_- m_-) \quad (3.32b)$$

$$T_- = Q_- u_1 + R_- v_1 \quad (3.34)$$

For the Euler predictor algorithm, the values of  $u_+$ ,  $v_+$  and  $y_+$  may be given the following initial conditions:

$$u_+ = u_2 \quad v_+ = v_2 \quad y_+ = y_2 \quad (3.35)$$

$$u_- = u_1 \quad v_- = v_1 \quad y_- = y_1 \quad (3.36)$$

For the Euler corrector algorithm, the values are

$$u_+ = (u_2 + u_4)/2 \quad v_+ = (v_2 + v_4)/2 \quad y_+ = (y_2 + y_4)/2 \quad (3.37)$$

$$u_- = (u_1 + u_4)/2 \quad v_- = (v_1 + v_4)/2 \quad y_- = (y_1 + y_4)/2 \quad (3.38)$$

3.4.4 Equations Used for ComputationSet (a)General Flow Equations

$$v_+ = (u_+^2 + v_+^2)^{1/2} \quad (3.26)$$

$$\theta_+ = \tan^{-1} \left( \frac{v_+}{u_+} \right) \quad (3.25)$$

$$a_+ = \left[ a_0^2 - \frac{\gamma - 1}{2} v_+^2 \right]^{1/2} \quad (3.27)$$

$$\mu_+ = \sin^{-1} \left( \frac{a_+}{v_+} \right) \quad (3.28)$$

Set (b)Determination of Coefficients

$$m_+ = \tan (\theta_+ + \mu_+) \quad (3.20)$$

$$Q_+ = u_+^2 - a_+^2 \quad (3.31)$$

$$R_+ = 2u_+ v_+ - Q_+ m_+ \quad (3.32)$$

Set (c)Computational Equations

$$y_4 - m_+ x_4 = y_2 - m_+ x_2 \quad (3.23)$$

$$y_4 - m_- x_4 = y_1 - m_- x_1 \quad (3.24)$$

$$T_+ = Q_+ u_2 + R_+ v_2 \quad (3.33)$$

$$T_- = Q_- u_1 + R_- v_1 \quad (3.34)$$

$$Q_+ u_4 + R_+ v_4 = T_+ \quad (3.29)$$

$$Q_- u_4 + R_- v_4 = T_- \quad (3.30)$$

Set (d)

Predictor Equations

$$u_+ = u_2 \quad v_+ = v_2 \quad y_+ = y_2 \quad (3.35)$$

$$u_- = u_1 \quad v_- = v_1 \quad y_- = y_1 \quad (3.36)$$

Set (e)

Corrector Equations

$$u_+ = 1/2(u_2 + u_4) \quad v_+ = 1/2(v_2 + v_4) \quad y_+ = 1/2(y_2 + y_4) \quad (3.37)$$

$$u_- = 1/2(u_1 + u_4) \quad v_- = 1/2(v_1 + v_4) \quad y_- = 1/2(y_1 + y_4) \quad (3.38)$$

In a supersonic flow field, knowing the values of  $u_+$  and  $v_+$  at two points 1( $x_1, y_1$ ) and 2( $x_2, y_2$ ), predictor equations provide the predicted values of  $u_+$  and  $v_+$  for a solution point which lies at the intersection of  $C_+$  and  $C_-$  characteristics. Next these values of  $u_+$  and  $v_+$  are then used in equations of Set (a) and (b) for determining the coefficients  $m_+$ ,  $Q_+$  and  $R_+$ . With the help of computational equations in Set (c)  $x_4, y_4, u_4,$  and  $v_4$  are determined. These values are then used in the corrector algorithm for correcting the predicted values. With the corrected values of  $u_+, v_+,$  and  $y_+,$  the above sets of equations are repeated. The iteration can be terminated either after use of certain number of corrector algorithms or comparing the difference

in values with a pre-assigned value. The determination for convergence after  $n$  applications of corrector are made as follows:

$$\left| S_T^n - S_T^{n-1} \right| \leq (\text{Specified Tolerance})$$

where  $S_T$  represents value of  $x_4$ ,  $y_4$ ,  $u_4$ , and  $v_4$  taken one parameter at a time. Typical tolerances for  $u_4$ ,  $v_4$ ,  $x_4$ , and  $y_4$  depend on the required accuracy of the problem.

### 3.4.5 Solution for Wall Point

For a solid wall, which can be specified by

$$y = y(x) \quad (3.39)$$

and  $\frac{dy}{dx} = \tan \theta = \frac{v}{u} \quad (3.40)$

the foregoing equations can be modified for the solution of a point on the wall. Along a solid wall, the flow velocity vector follows the contour of the wall, hence, the direction of this vector must be identical to the slope of the wall. If the wall lies on the right-hand side of the main flow direction, then as seen from Figure 3.4 a right running characteristic from an interior point meets the wall. Hence, for a right running or  $C_+$  characteristic Equations 3.24 and 3.30 may be solved along with Equations 3.39 and 3.40.

For any geometry of the wall a suitable equation may be generated, to represent the wall contour. This equation, when differentiated, will give the corresponding slope of the

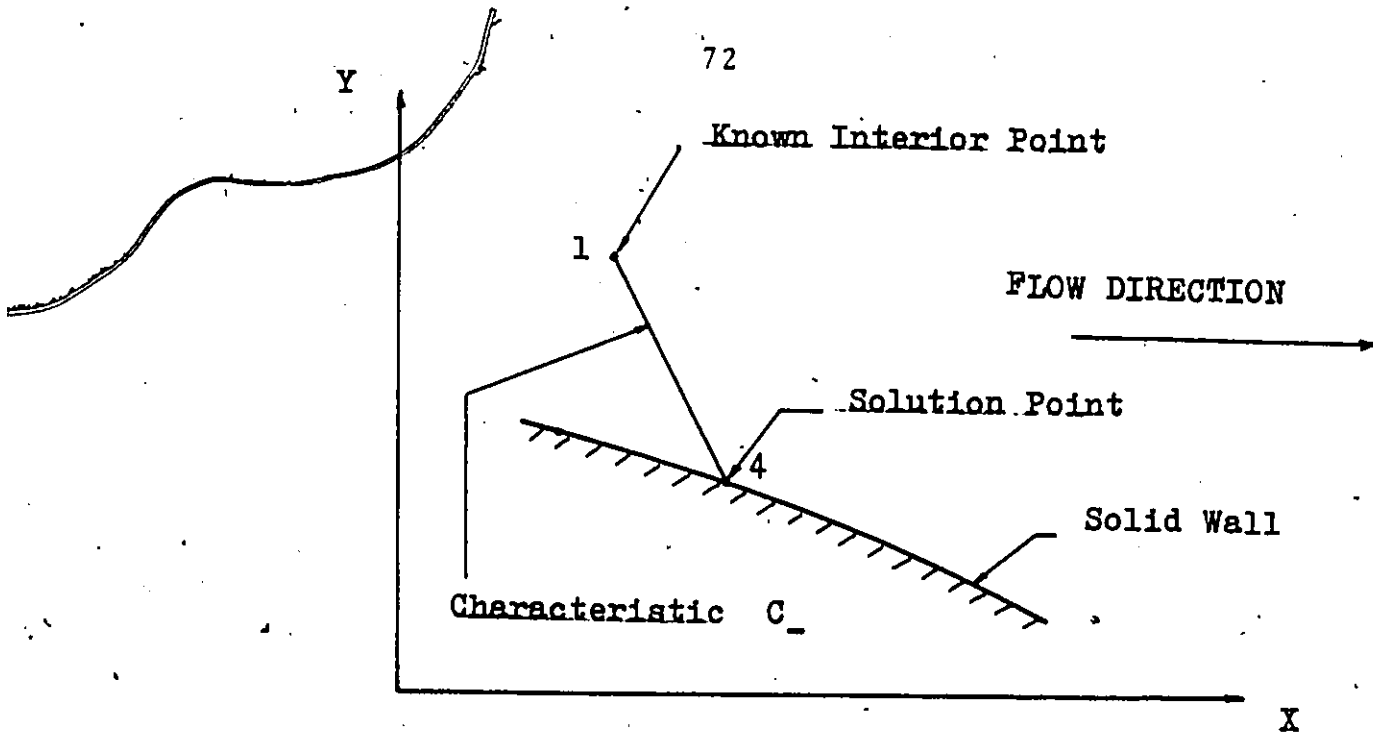


Figure 3.4 Solution for a Wall Point

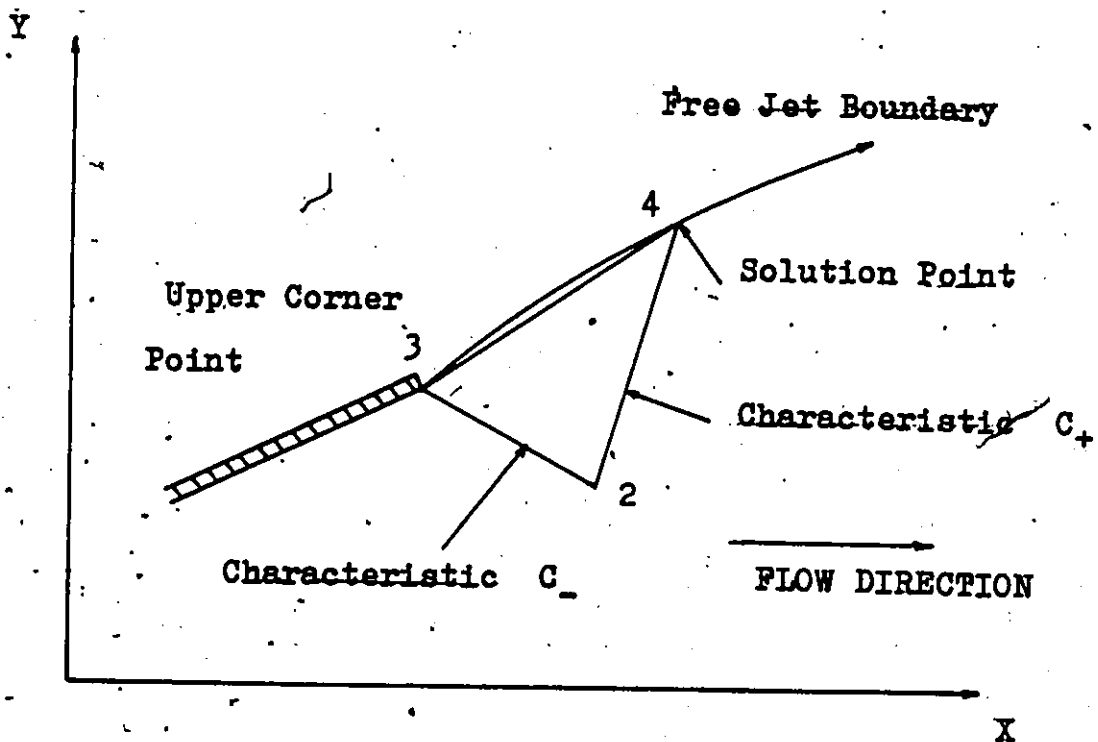


Figure 3.5 Solution for a Free Jet Boundary

flow velocity vector.

### 3.4.6 Free Pressure Boundary Point

On a free pressure boundary, the static pressure is equal to that of the ambient pressure. So for the solution of point 4 on the free pressure boundary the condition  $p_4 = p_a$  (where  $p_a$  is ambient pressure) is a known priori. The velocity  $V_4$  at the solution point is given as

$$V_4 = (u_4^2 + v_4^2)^{1/2} = f(p_a) = f(p_4) \quad (3.41)$$

Now from an interior point 2 a left running characteristic is extended to meet the free pressure boundary at the solution point. Hence, Equation 3.29 together with Equation 3.41 may be solved for  $u_4$  and  $v_4$ . The simultaneous solution of these two equations gives the following results:

$$u_4 = \frac{Q_+ T_+ - R_+ [V_4^2 (Q_+^2 + R_+^2) - T_+^2]^{1/2}}{Q_+^2 + R_+^2} \quad (3.42)$$

$$\text{and } v_4 = (V_4^2 - u_4^2)^{1/2} \quad (3.43)$$

The slope of the jet boundary from point 3 to point 4 may be obtained as

$$\frac{dy}{dx} = \frac{v}{u} = m_0 \quad (3.44)$$

where  $m_0$  = slope of line 3-4 (Figure 3.5).

In finite difference form, this yields

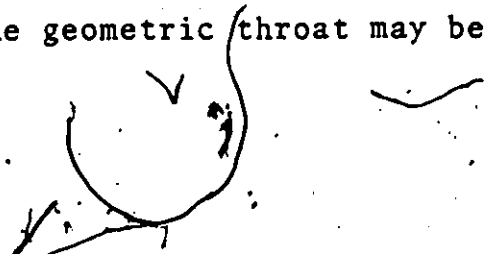
$$y_4 - m_0 x_4 = y_3 - m_0 x_3 \quad (3.45)$$

The computer program for the solution of an interior point may be modified to accommodate the above equations for solution of free pressure boundary points.

### 3.5. Development of the Computer Program

The solution for two-dimensional supersonic flow field by the method of characteristics requires an initial value line along which Mach number is greater than unity. This initial value line should not be a characteristic itself, but a line through which the characteristics may cross.

The Mach number distribution along the geometrical throat of McMaster blade as observed from the computer programming in Appendix A, is more than unity everywhere. The sonic line along which Mach number is unity at all points, exists slightly upstream of geometrical throat. Along the geometrical throat a few points (preferably equispaced) may be selected having known values of Mach number and coordinate position. The number of points selected depends entirely on the volume of information required for the flow field downstream of this geometrical throat. Knowing the working pressure ratio  $P_0/p$ , and from the isentropic gas table, the value of Prandtl-Meyer expansion angle  $\nu$  can be obtained. As at the exit plane of the geometric throat, the flow turns through a total angle of  $\nu$ , a linear distribution of  $\nu$  for each stream-line passing through the geometric throat may be



defined as the initial value line for the solution of the supersonic flow field that exists in the trailing region of a converging passage. The flow deflection along with the values of Mach number and coordinate axes for each point selected on the initial value line provides the  $u$  and  $v$  components of the resultant velocity at that point using the subroutine FLOW given in Appendix B. At each point on the initial value line, two characteristics will pass, a left-running or  $c_+$  and a right-running or  $c_-$  characteristic (Figure 3.2). The compatibility equation (equation 3.13) together with the characteristic equation (equation 3.12) may be integrated to obtain a solution point which lies at the intersection of a  $c_+$  and a  $c_-$  characteristics emanating from two specified, but adjacent points in the flow field. In equations 3.13 and 3.12, subscripts + (plus) and - (minus) refer to the  $c_+$  and  $c_-$  characteristic respectively.

### 3.5.1 Interior Points

To find the solution at a point interior to the flow field, subroutine INTPT in Appendix B has been developed according to para 3.4.3. To find the coordinate axes and velocity components at an interior point which is the point of intersection of the  $c_+$  and the  $c_-$  characteristic, one of each set of the characteristic and the compatibility equations may be used along the  $c_+$  and the  $c_-$  characteristic



respectively. Comparing Figure 3.3 and Figure 3.6, it should be observed that to solve for points E, F, and G (interior points) in Figure 3.6, the Figure 3.3 can be superimposed on each triangle so that the points E, F, and G correspond to point 4 of Figure 3.3 at each location. Therefore, to solve for point E, A and B with known values of  $x$ ,  $y$ ,  $u$  and  $v$  may be considered to correspond to points 1 and 2 of Figure 3.3 and by virtue of the similarity point E may correspond to point 4 of Figure 3.3. For point F, B and C may be set equivalent to points 1 and 2 of Figures 3.3 with F as point 4 and so on.

A necessary computer statement is incorporated in the main program as well as in subroutine INTPT in Appendix B to compute sufficient points inside the flow field and also to generate characteristic lines covering the entire flow field.

### 3.5.2 Wall Point

Subroutine WALPT in Appendix B is developed in accordance with the equations and specifications as stated in para 3.4.5. In this case, the wall is on the right-hand side of the mean flow direction, and therefore the compatibility and characteristic equations pertaining to the right running characteristic are utilized. Additional conditions required to specify the wall contour may be added in subroutine BOUNDARY

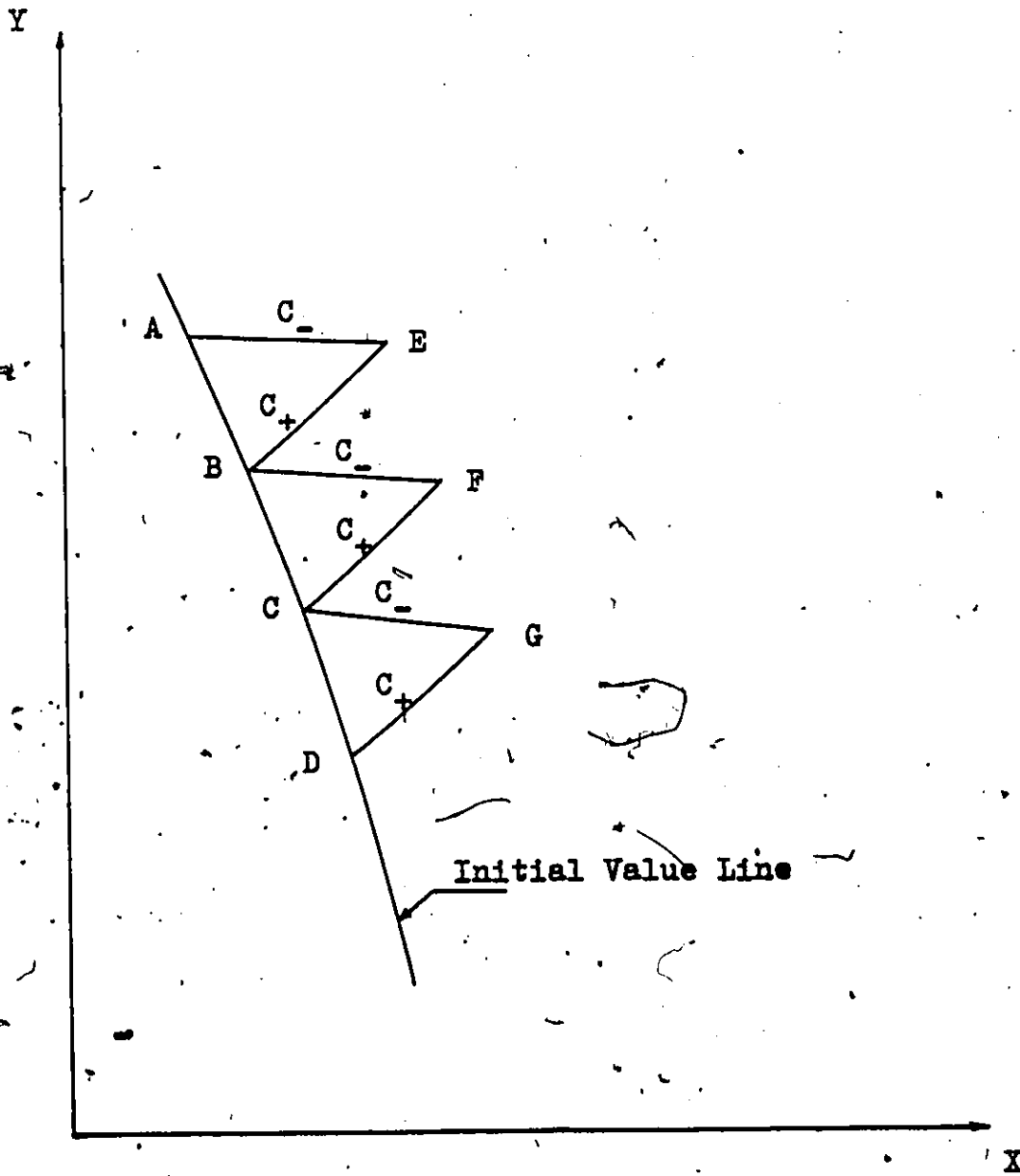


Figure 3.6 - Initial Value Line and Characteristics

in Appendix B. In general, any wall shape with known boundary conditions may be used in the solution of the characteristic curves.

Computer statements as in the previous case are added both in the main program GAS and the subroutine WALPT (see Appendix B) for generating sufficient wall points as the solution marches forward.

### 3.5.3 The Free-Pressure Boundary Point

As the free pressure boundary lies on left-hand side of the mean flow direction, only the left running characteristics intersect the boundary. From Figure 3.5, it is obvious that additional information is required (point 3) to obtain the values of the first point on the free pressure boundary. Designating this as the upper corner point, the required information is furnished external to the program for any particular case of blade position and spacing.

Subroutine BODPT in Appendix B has been developed keeping in mind the modifications specified in para 3.4.6. As the solution progresses forward, the computer statements for each solution point distribute the values of point 2 and point 3 in accordance to the Figure 3.5.

As each reflected wave crosses the free pressure boundary, it turns the boundary line towards the main flow

and as all the reflected waves or characteristics touch the boundary the boundary line finally becomes parallel to the mean flow direction. The design of a supersonic nozzle in which the exit plane flow direction is horizontal has a similar set of characteristics.

CHAPTER 4  
METHOD OF CHARACTERISTICS (RIEMANN INVARIANTS)

4.1 General Considerations

Many books on Gas Dynamics have described elaborately the classical method of characteristics (Riemann Invariants) and the method used to produce an excellent solution of many supersonic flow problems. The principal disadvantage of this method lies in the fact that the method is too laborious when a large number of points is required for describing the flow field.

The problem is amplified even when following what might be called good design office practice since one has to produce on a drawing the entire characteristic net using specific values of the Prandtl-Meyer expansion angles  $\nu$  and therefore Mach numbers.

$$\nu = f(M) = b_0 \arctan \frac{(M^2 - 1)^{1/2}}{b_0} = \arctan (M^2 - 1)^{1/2}$$

where  $b_0 = \left(\frac{\gamma+1}{\gamma-1}\right)^{1/2}$

and hence the solution of Mach number for a particular value of  $\nu$  is a tedious one which somewhat limits the accuracy of value of  $\nu = f(M)$  required for the purpose of drafting the characteristic lines.

#### 4.2 Derivation of Equations

From Equations 2.4 and 2.5, which describe the momentum change along the stream-lines and the orthogonals are, respectively (Figure 2.12).

$$\rho V \frac{\partial V}{\partial S} = - \frac{\partial p}{\partial S} \quad (2.4)$$

and 
$$\rho V^2 \frac{\partial \theta}{\partial S} = - \frac{\partial p}{\partial n} \quad (2.5)$$

The Continuity equation can be written as

$$\rho V \Delta n = \text{Constant} \quad (4.1)$$

The one-dimensional Momentum equation can be written in the form

$$\frac{\partial p}{\partial n} = - \rho V \frac{\partial V}{\partial n}$$

and introducing this value into Equation 2.5, the condition of irrotationality becomes as follows:

$$\frac{\partial V}{\partial n} - V \frac{\partial \theta}{\partial S} = 0 \quad (4.2)$$

The Continuity equation in more convenient form may be written

$$\frac{1}{\rho} \cdot \frac{\partial \rho}{\partial S} + \frac{1}{V} \cdot \frac{\partial V}{\partial S} + \frac{1}{\Delta n} \cdot \frac{\partial (\Delta n)}{\partial S} = 0$$

or 
$$\frac{1}{\rho} \cdot \frac{\partial \rho}{\partial S} + \frac{1}{V} \cdot \frac{\partial V}{\partial S} + \frac{\partial \theta}{\partial n} = 0 \quad (4.3)$$

From Equation 2.4, the elimination of the pressure term with the help of Equation  $a^2 = \partial p / \partial \rho$ , gives the following form

$$V \frac{\partial V}{\partial S} = - \frac{a^2}{\rho} \cdot \frac{\partial \rho}{\partial S} \quad (4.4)$$

which when combined with the Continuity equation has the

following form

$$\left(\frac{V^2}{a^2} - 1\right) \frac{1}{V} \cdot \frac{\partial V}{\partial S} - \frac{\partial \theta}{\partial n} = 0 \quad (4.5)$$

$$\frac{M^2 - 1}{V} \cdot \frac{\partial V}{\partial S} - \frac{\partial \theta}{\partial n} = 0 \quad (4.5a)$$

For supersonic flow, the Mach angle can be defined as  $\cot \mu = (M^2 - 1)^{1/2}$  and  $\sin \mu = 1/M$ .

The Prandtl-Meyer function  $v$  may be introduced as

$$v = \int \frac{\cot \mu}{V} dV$$

or  $dv = \cot \mu \frac{dV}{V} \quad (4.6)$

Combining 4.2, 4.5 and 4.6, a compatibility relation between  $v$  and  $\theta$  may be obtained, [8] and which according to the theory of hyperbolic equations must exist on the characteristics or Mach lines. The compatibility relations between  $v$  and  $\theta$  are

$$v - \theta = RI, \text{ constant along a } C_+ \text{ characteristic} \quad (4.7)$$

$$v + \theta = QI, \text{ constant along a } C_- \text{ characteristic} \quad (4.8)$$

Here RI and QI are the Riemann Invariants.

#### 4.3 Computation Method

Referring to Figure 4.1, it is observed that at point 4, there are two characteristics, one of type  $C_+$  and the other of type  $C_-$ . These two characteristic curves intersect the data curve at points 1 and 2, respectively. Knowing the

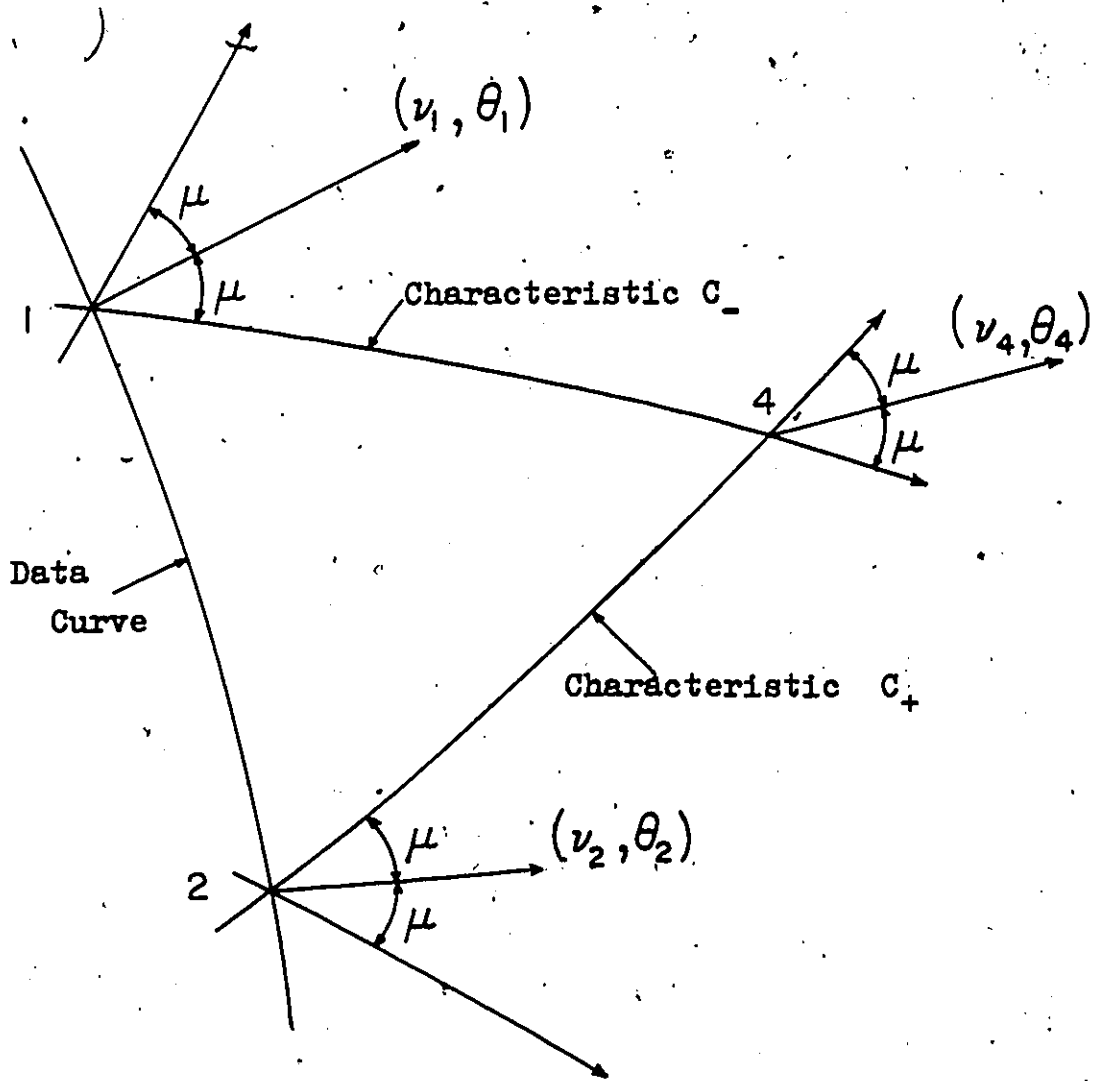


Figure 4.1 Characteristic Method Using the Natural Coordinate System



values of  $v$  and  $\theta$  at 1 and 2, the values of  $v$  and  $\theta$  at other points may easily be calculated.

As  $QI$  and  $RI$  are constants along  $C_-$  and  $C_+$  then

$$QI_4 = QI_1$$

and  $RI_4 = RI_2$

Replacing  $QI$  and  $RI$  with the help of Equations 4.8 and 4.7, the following relations may be obtained:

$$v_4 + \theta_4 = v_1 + \theta_1$$

and  $v_4 - \theta_4 = v_2 - \theta_2$

Solving for  $v_4$  and  $\theta_4$

$$v_4 = 1/2(v_1 + v_2) + 1/2(\theta_1 - \theta_2) \quad (4.9)$$

$$\theta_4 = 1/2(v_1 - v_2) + 1/2(\theta_1 + \theta_2) \quad (4.10)$$

Hence, in terms of the invariants, these may be expressed as

$$v = 1/2(QI + RI) \quad (4.11)$$

$$\theta = 1/2(QI - RI)$$

A complete solution of the flow field may be obtained by suitably subdividing the entire region into small "lattices" and the number of lattices directly controls the accuracy of the solution of the flow field.

To locate the characteristics, a step-by-step procedure is employed. The initial values are prescribed on a data curve and the solution proceeds outward from the known data curve. In calculating the characteristics in a flow

field, three different flow situations may arise as described earlier, namely, the solution at

- i) interior point
- ii) solid boundary point, and
- iii) free-pressure boundary point.

#### 4.4. Lattice Point Method of Solution

The general procedure for this method can be given by the following set of rules which are applied to flow in a straight-backed turbine blade (McMaster blade) with a known Mach number distribution along the geometric throat.

a) A scale drawing showing the flow boundaries is drawn. The deviation of the free pressure boundary surface is estimated from the operating pressure ratios and drawn along with the flow boundaries.

b) A suitable set of points (preferably equispaced) is selected on the geometric throat with known Mach numbers at each point (points 1, 2, 3 and 4).

c) A linear distribution of the flow angle  $\theta$  is assumed at each of the selected points.

d) From given initial conditions, the values for each of the points are determined from isentropic flow table.

e) The values of the Mach angle for each point on the geometric curve may also be estimated from the isentropic flow tables corresponding to the Mach number at each point.

f) Values of  $QI$  and  $RI$  are determined for each point using Equations 4.8 and 4.7, respectively.

g) Both the left-running and right-running characteristics (straight line segments) at each point are drawn extending downstream of the geometric throat. The inclinations of these lines are  $\theta + \mu$  and  $\theta - \mu$  respectively. Their intersections locate new lattice points on the characteristics.

h) Values of  $\theta$  and  $v$  for each new point are obtained by simultaneous solution of equations 4.7 and 4.8. For example, for point 6 in Figure 4.2

$$v_6 + \theta_6 = v_2 + \theta_2 = QI_2$$

since points 2 and 6 lie on a right-running characteristic.

Also

$$v_6 - \theta_6 = v_1 - \theta_1 = RI_1$$

since points 1 and 6 lie on a left-running characteristic.

Hence,

$$v_6 = 1/2(QI_2 + RI_1)$$

$$\theta_6 = 1/2(QI_2 - RI_1)$$

i) From the isentropic flow tables, corresponding to the value of  $v$ , the Mach angle  $\mu$  is determined. The left-running and right-running characteristics are drawn at the new point of intersection at inclinations of  $\theta + \mu$  and  $\theta - \mu$ , respectively.

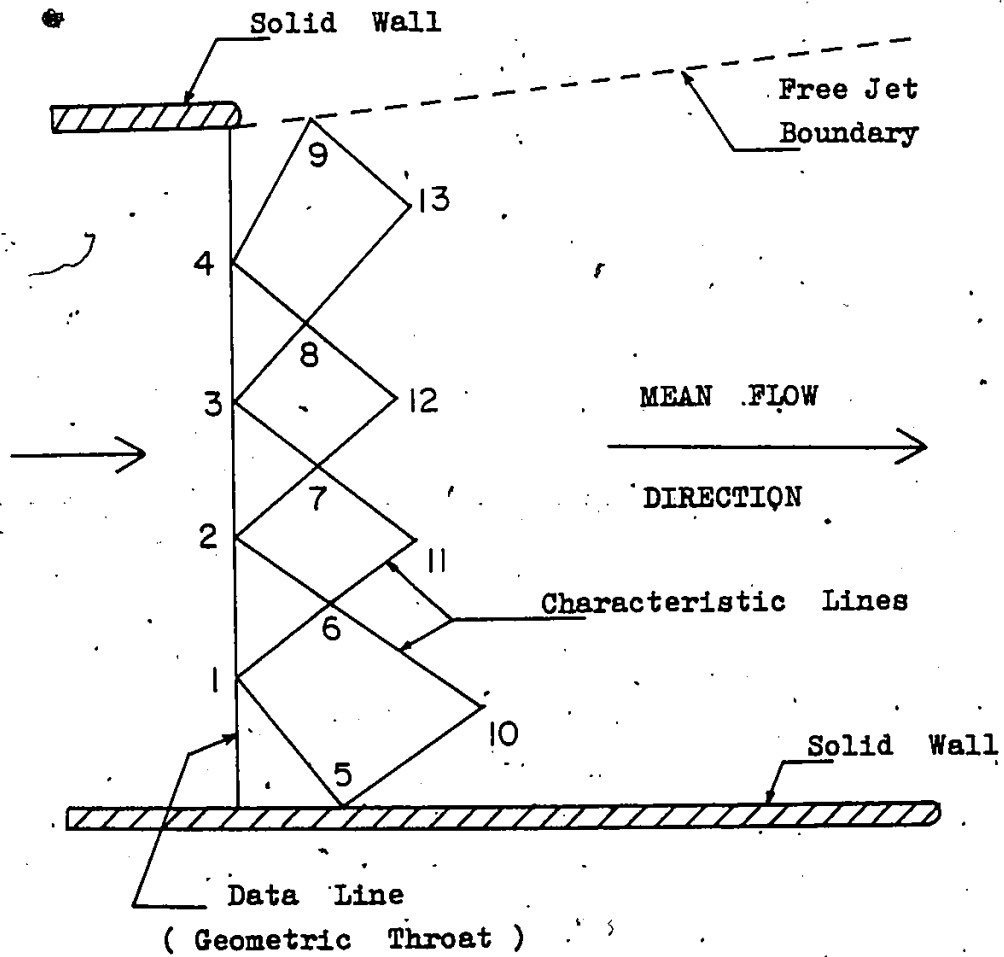


Figure 4.2 Characteristic Network for the  
2-D Method of Characteristics

j) The procedure is modified in case one of the new points lies on the solid boundary or a free pressure boundary point. In such cases the value of  $\theta$  is obtained from the geometry of the boundary of the flow field.

k) For each point covered by the characteristics, the Mach number corresponding to the value of  $v$  at that point may be determined. Once the Mach number at a point is known, other flow properties may be estimated from the Isentropic Flow Tables [29].

## CHAPTER 5

### RESULTS AND DISCUSSIONS

The numerical method developed for solving the supersonic flow with the help of the methods of characteristics conforms to the classical method of Riemann Invariants. The principal advantage of the numerical method is that the values of Mach number for different values of the Prandtl-Meyer expansion fan need not be calculated from the standard relation of  $M$  and  $v$ . As the numerical method works on the Cartesian system, the points of interest in the flow field are clearly defined. The corresponding values of static pressure, static temperature and flow deflection at any point in the flow field covered by method of characteristics are easily determined from the program set up.

Figure 5.1 shows the characteristic lines as drawn with the help of a drafting machine using calculation procedures as outlined in Chapter 4. This way of analysing a supersonic flow field is tedious. In this analysis, the conditions along the geometric throat are specified with the results obtained from the program outlined in Appendix A. In Figure 5.2 the characteristic lines are obtained by the method outlined in Chapter 3 and this method provides a very rapid analysis of the supersonic flow field covered by the charac-

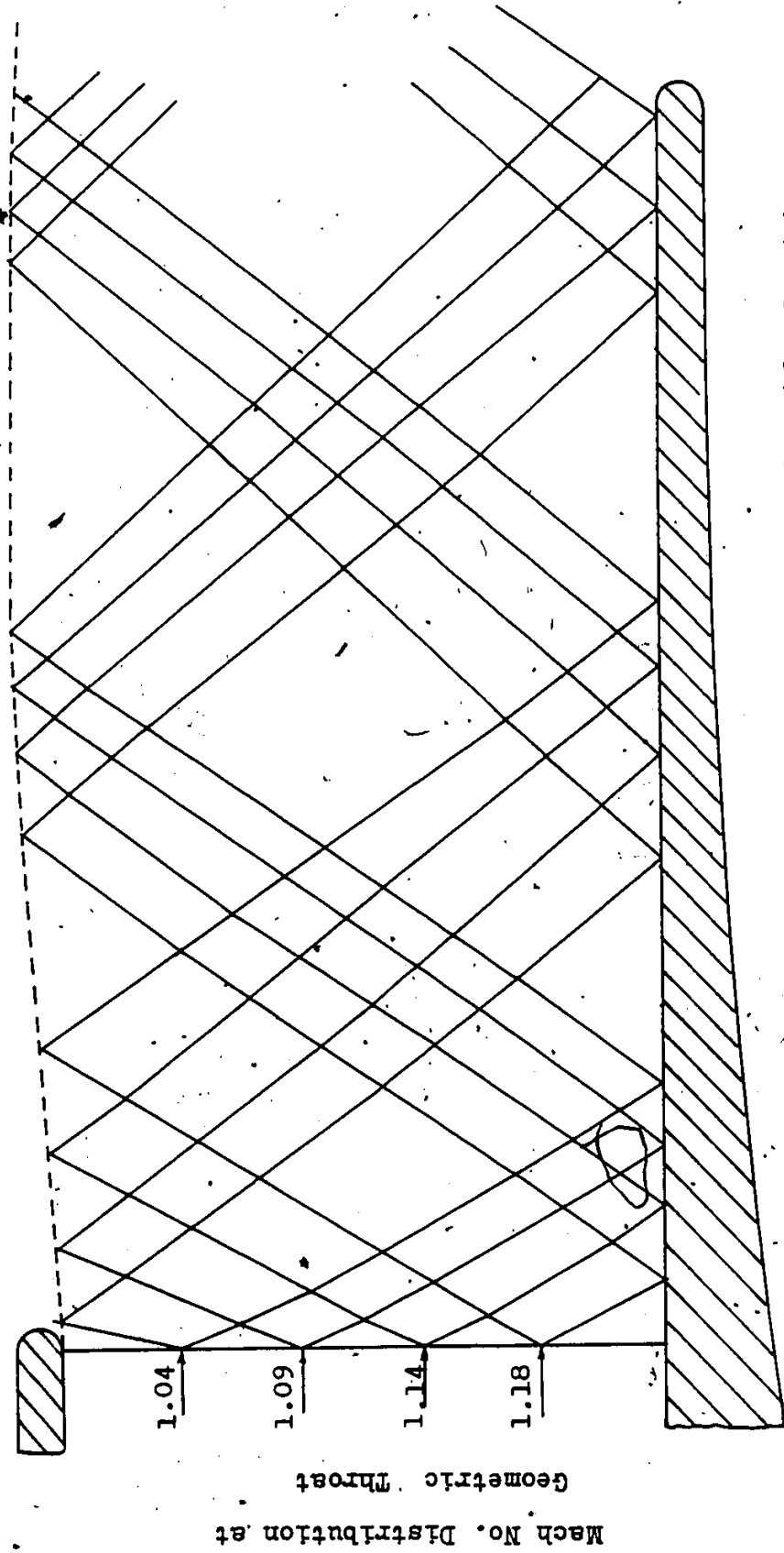


Figure 5.1 Characteristic Lines (Riemann Invariants) for Straight-Back Turbine Blade ( $P_0/p = 2.486$ )

Mach No. Distribution at

Geometric Throat

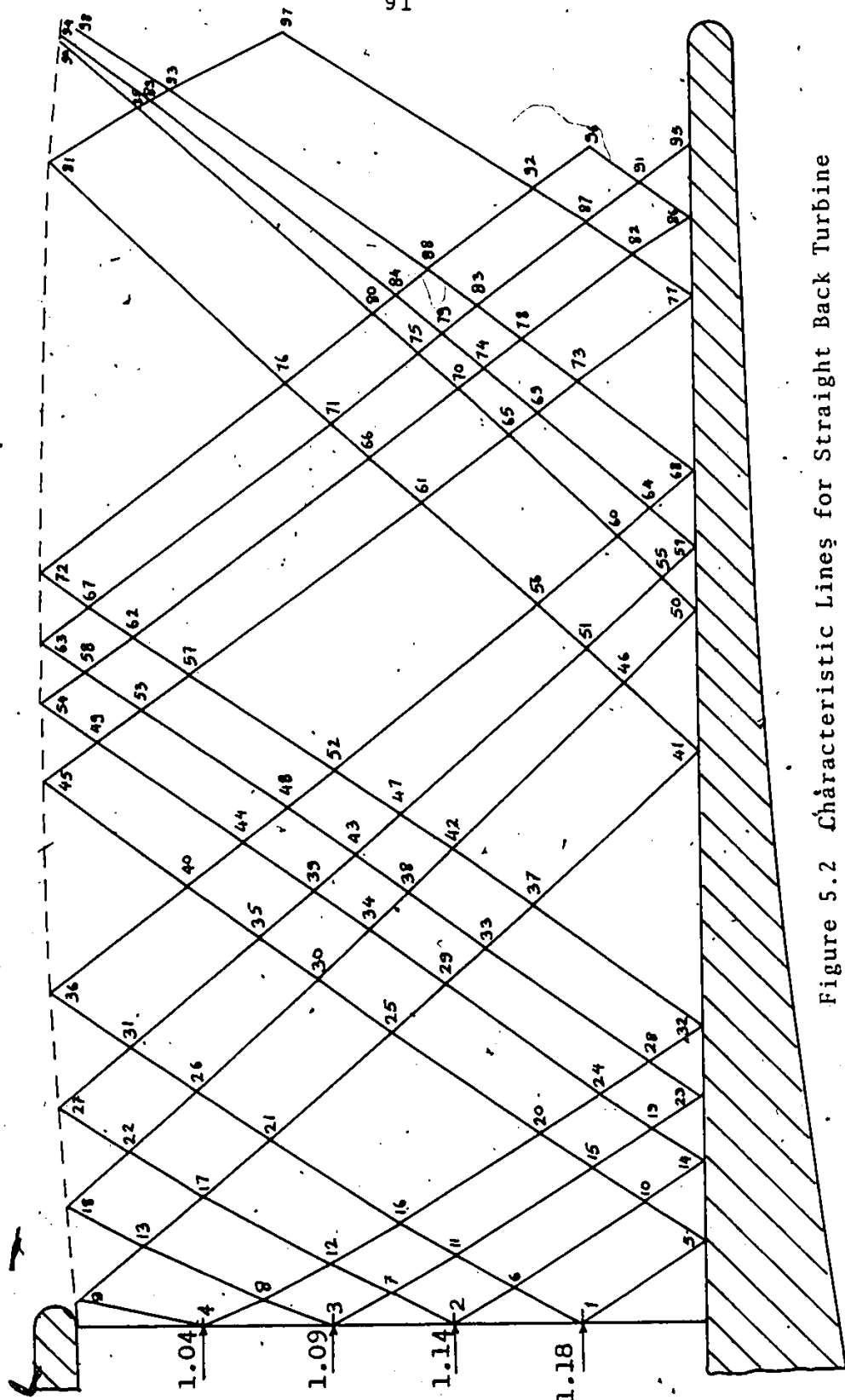


Figure 5.2 Characteristic Lines for Straight Back Turbine  
Blade for Pressure Ratio  $P_0/p = 2.486$



teristic lines. The position of the sonic line is first approximated and then for different pressure ratios the characteristic lines are drawn using the program developed in Appendix B based on the method described in Chapter 3. As seen from the Figures 5.3, 5.4, 5.5, 5.6 and 5.7 the position of the shock waves formed by the weak compression waves move steadily outward with the increase of total-to-static pressure of the system. The free pressure boundary surface is also found to move away from the horizontal reference lines with the increasing pressure ratio. The same discussion holds good for curved-back blade surfaces where with the increasing pressure ratio, the shock starts moving away from the geometric throat and the Prandtl-Meyer expansion fan increases with the pressure ratio.

From Figure 5.8 the approximate position of the compression shock is nearly 89% of the axial chord and from this point onward, the pressure ratio gradually starts increasing confirming the effect of the compression waves. Now for the same system pressure ratio of 2.486, when the method of Chapter 3 is used the position of shock is approximately 87.5% of the axial chord (Figure 5.5). This suggests that the computational method is better because the characteristic lines are drawn by computer system. As the working pressure is steadily increased the compression shock moves slowly away from the throat and for the under-expanded case, the

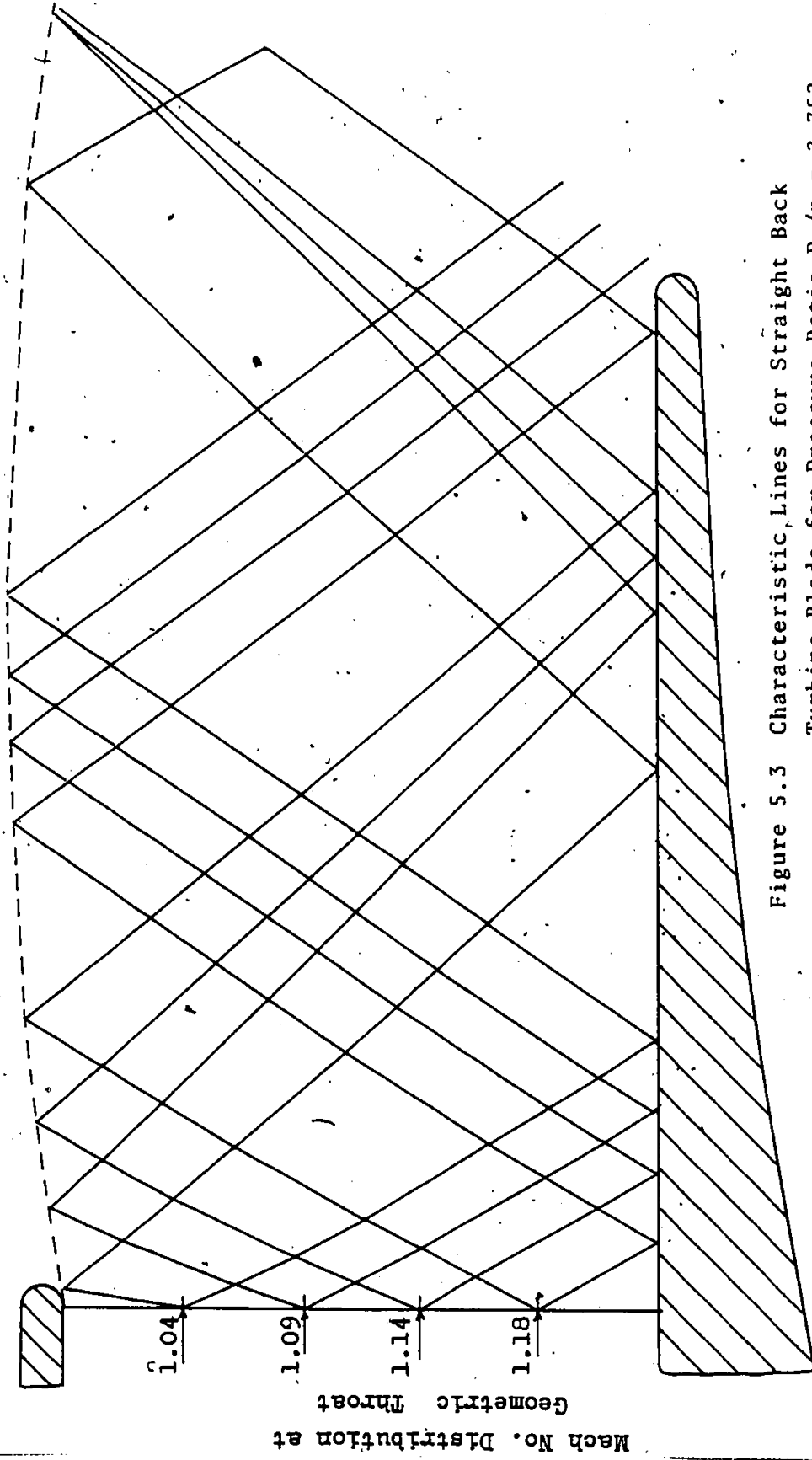


Figure 5.3 Characteristic Lines for Straight Back Turbine Blade for Pressure Ratio  $P_0/p_1 = 2.752$ .

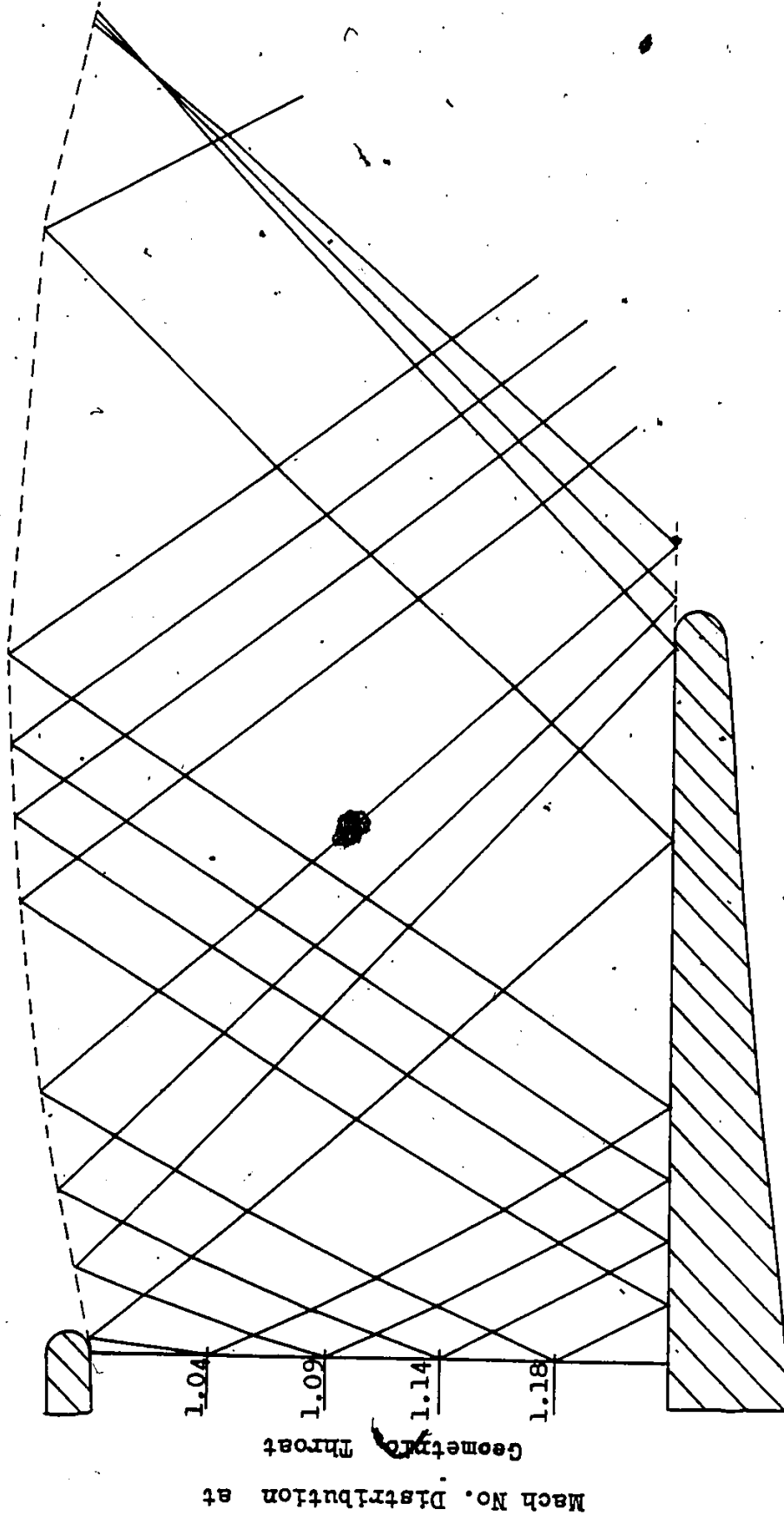


Figure 5.4 Characteristic Lines for Straight Back Turbine Blade for Pressure Ratio  $P_0/p = 3.038$

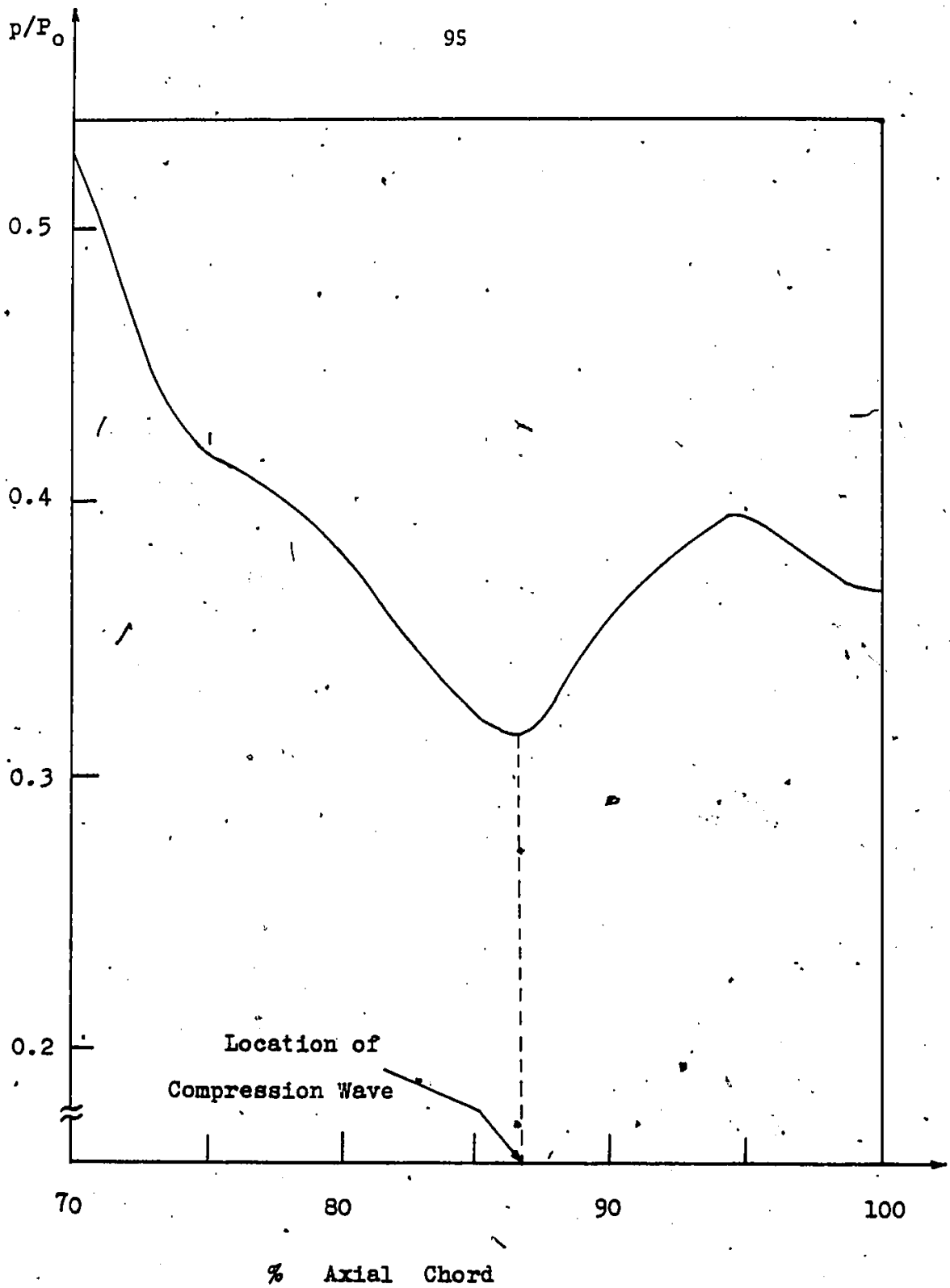


Figure 5.5 Pressure Distribution on Suction Surface After Geometric Throat ( $P_0/p = 2.486$ )

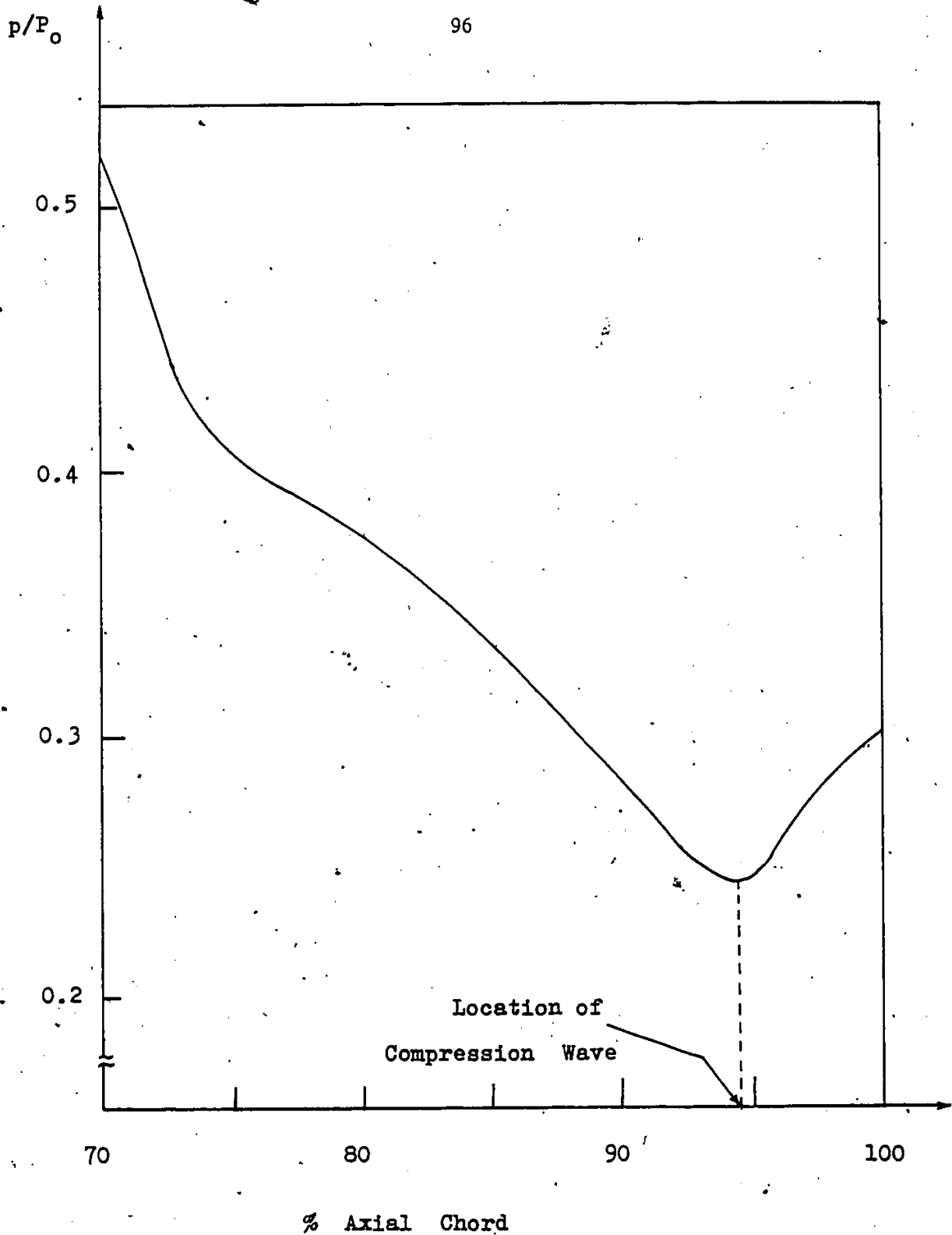


Figure 5.6. Pressure Distribution on Suction Surface After Geometric Throat ( $P_0/p = 2.752$ )

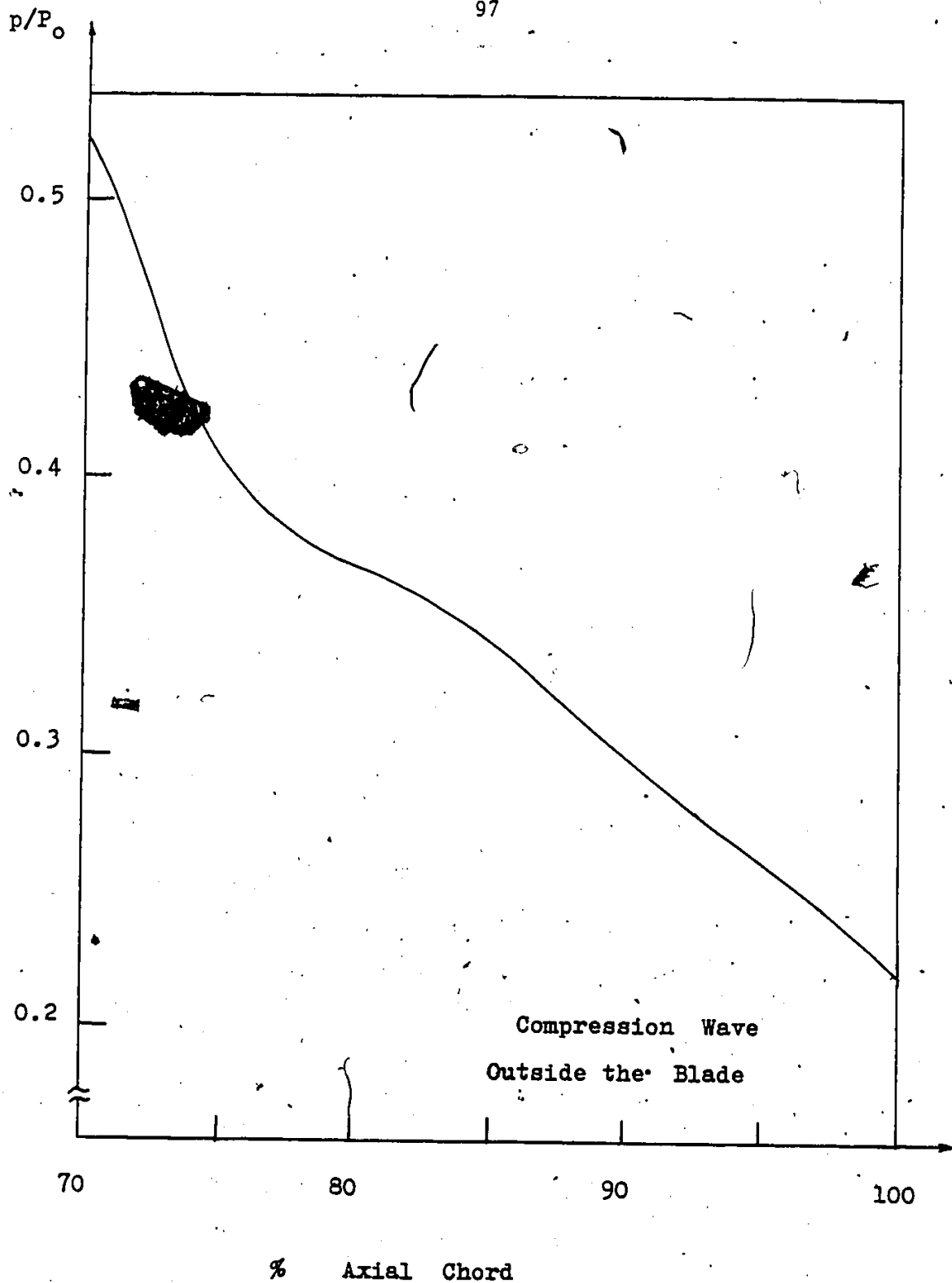


Figure 5.7 Pressure-Distribution on Suction Surface After Geometric Throat ( $P_0/p = 3.038$ )

shock is no longer in the blade passage, so there is no rise of static pressure as observed in the previous figures.

Scope for future studies:

The method of analysis for supersonic flow fields can be verified by carrying out experimental flow visualization studies in the cascade tunnel with the help of a suitable Schlieren system. The experimental method together with the method developed in this study will enable the researchers to analyse the supersonic flow field prevailing in the exit-plane of a highly curved turbine blade passage. A possible design scheme for the Schlieren system suitable for the blowdown cascade wind tunnel in the Applied Dynamics Laboratory of McMaster University is outlined in Figure 2.17, and discussed in Section 2.9 of this report.

Figure 5.15 shows the proposed Schlieren system to be used for the flow visualization of the flow passages of the turbine blade passages in the blowdown cascade wind tunnel in the Applied Dynamics Laboratory of McMaster University. Due to the inherent design of the test section of the wind tunnel, the proposed Schlieren system would prove to be one of the most suitable one. The structure is made of steel channels and mounted on four swivel wheels for the ease of mobility. All the major optical components have enough freedom of movements so that the desirable results

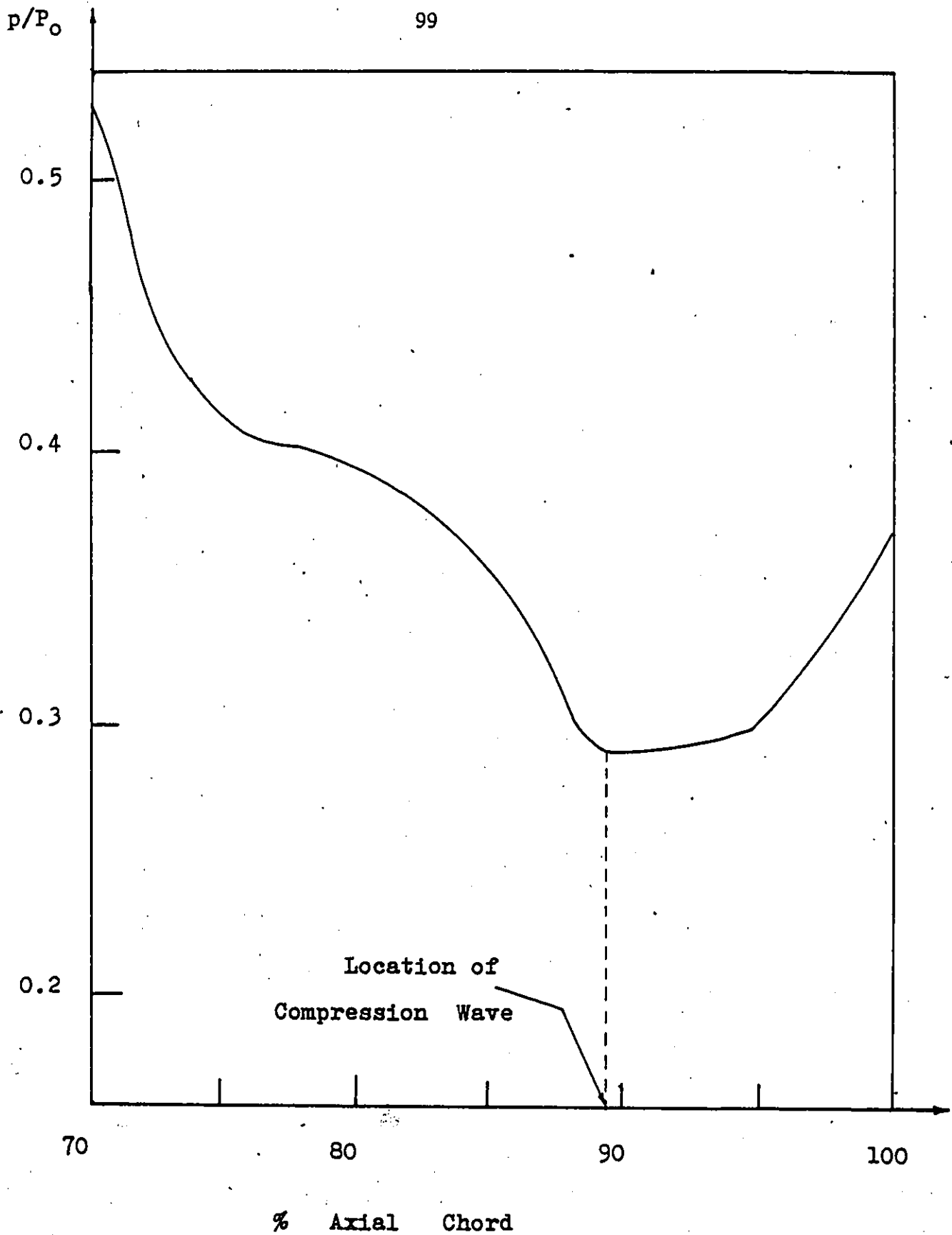


Figure 5.8 Pressure Distribution on Suction Surface After Geometric Throat ( $P_0/p = 2.486$ ) (Riemann Invariants)



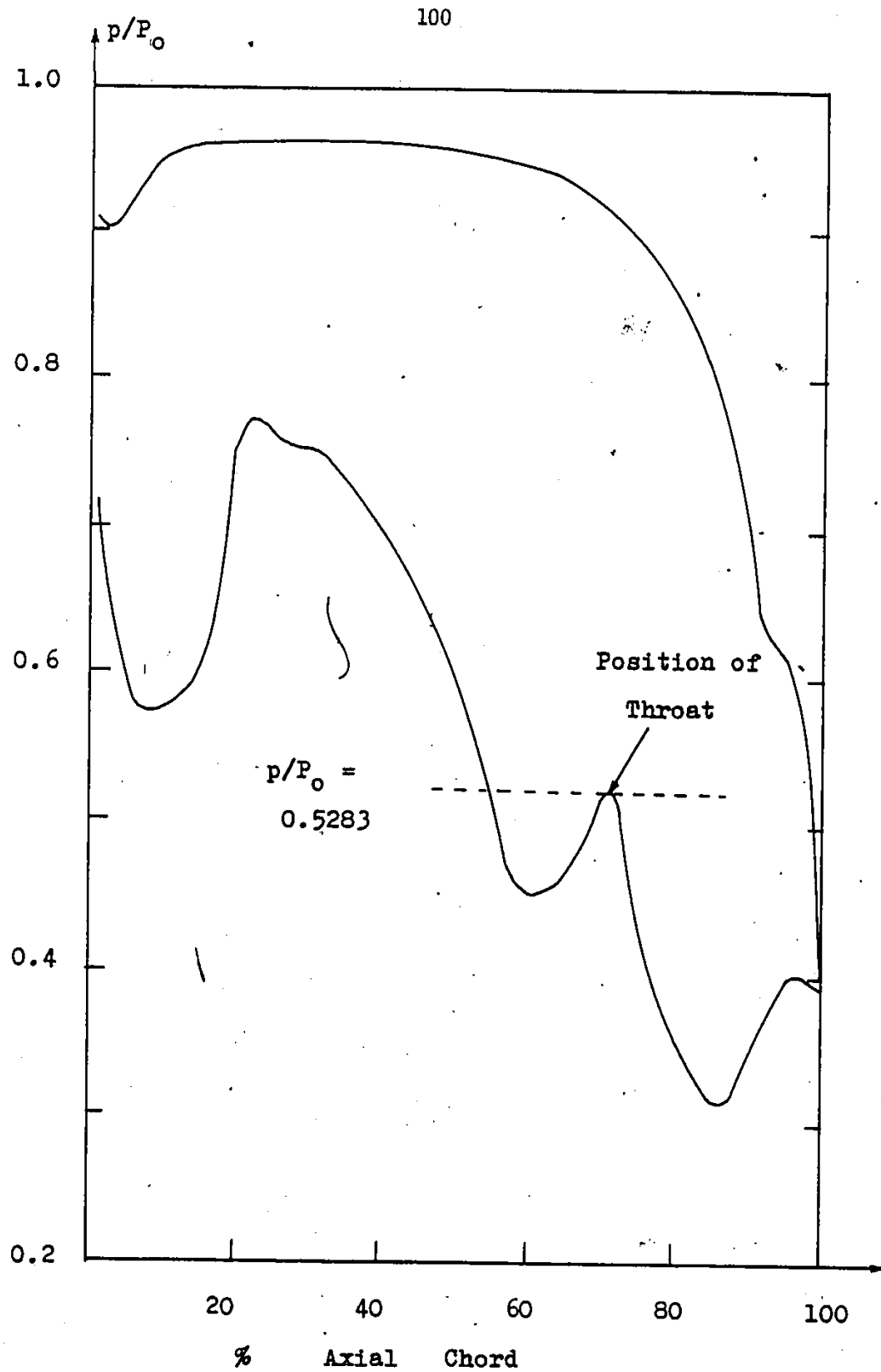


Figure 5.9. Blade Pressure Distribution ( $P_0/p = 2.486$ )

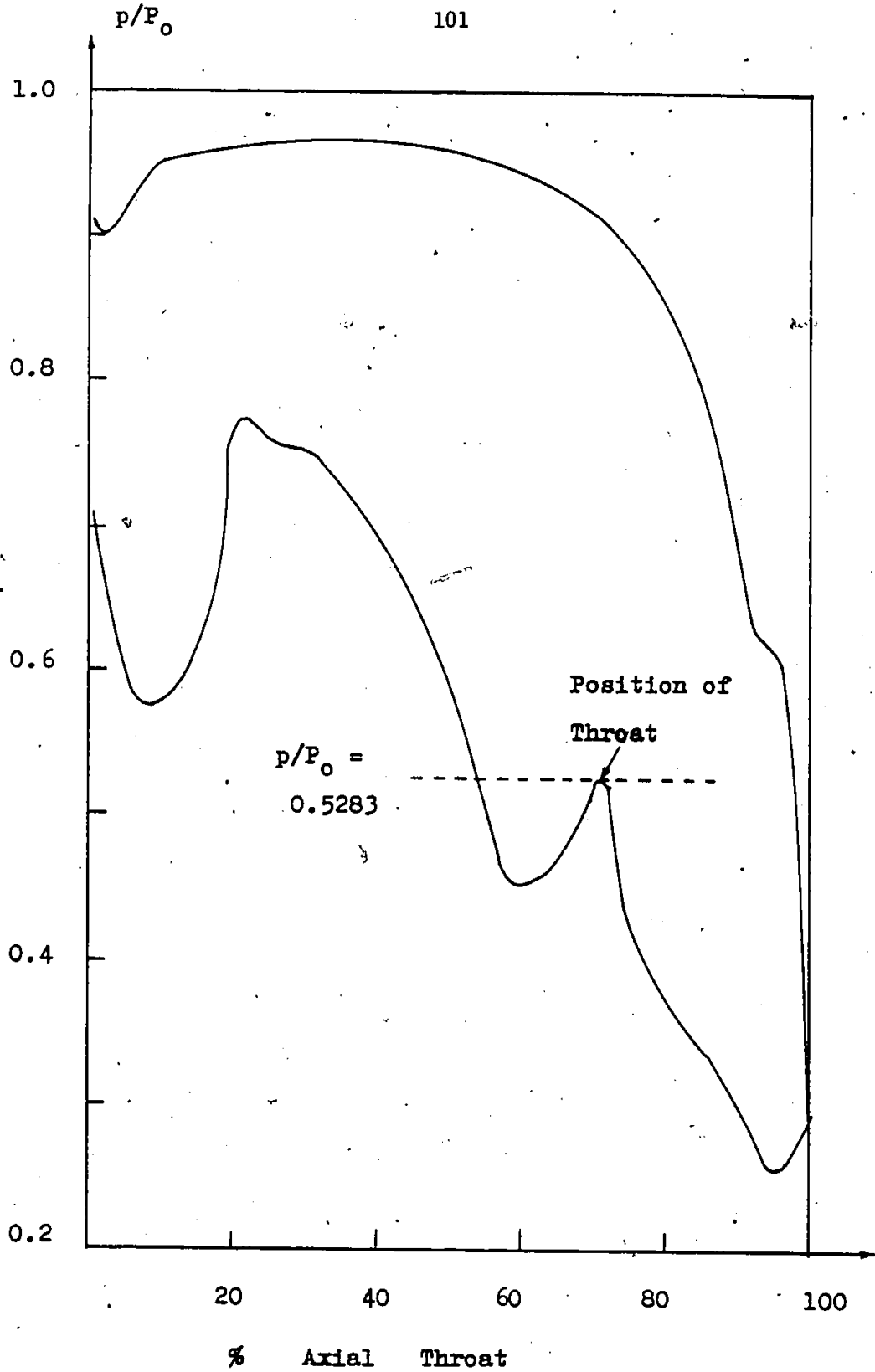


Figure 5.10 Blade Pressure Distribution ( $P_0/p = 2.752$ )

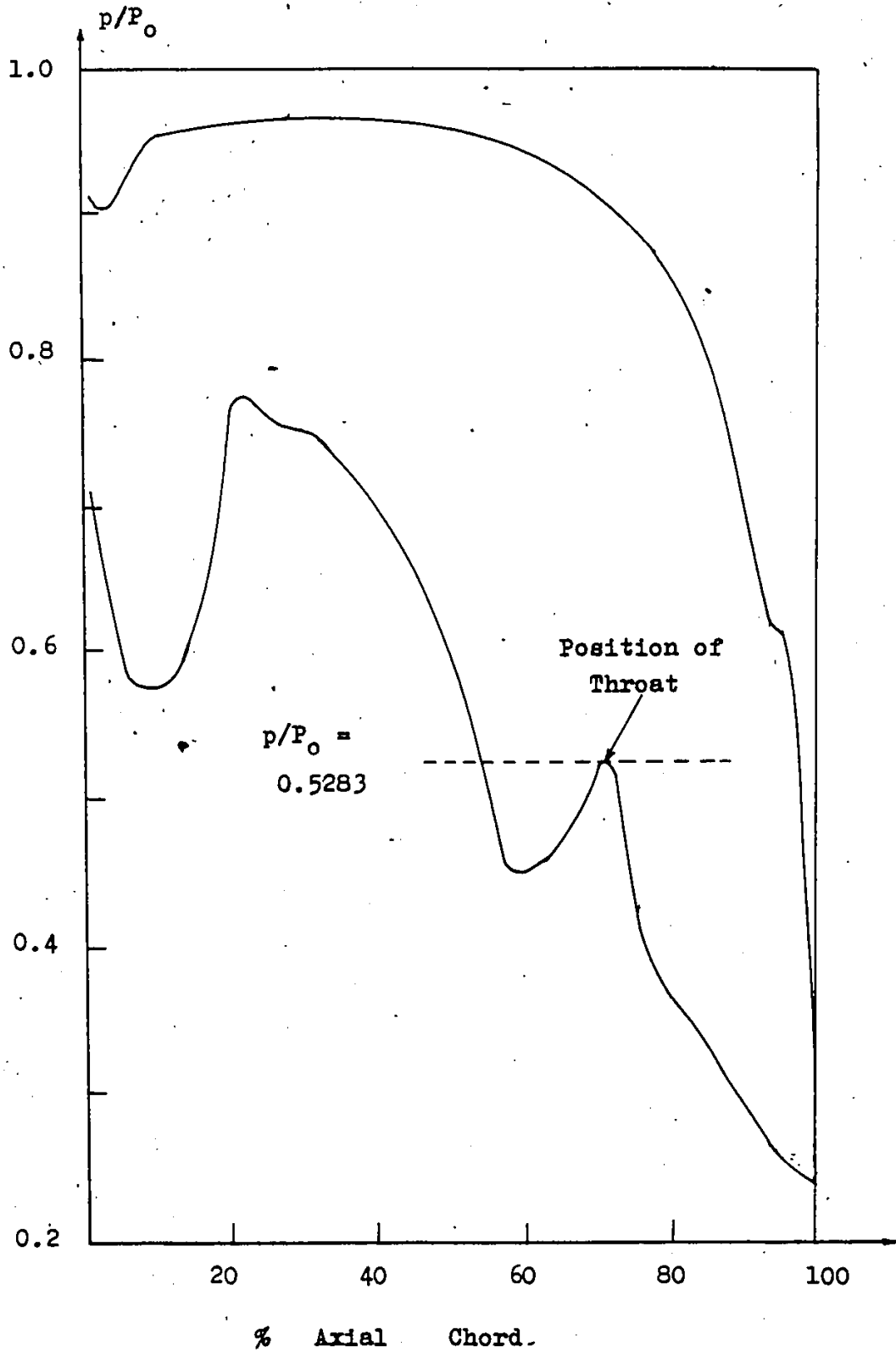


Figure 5.11 Blade Pressure Distribution ( $P_0/p = 3.038$ )

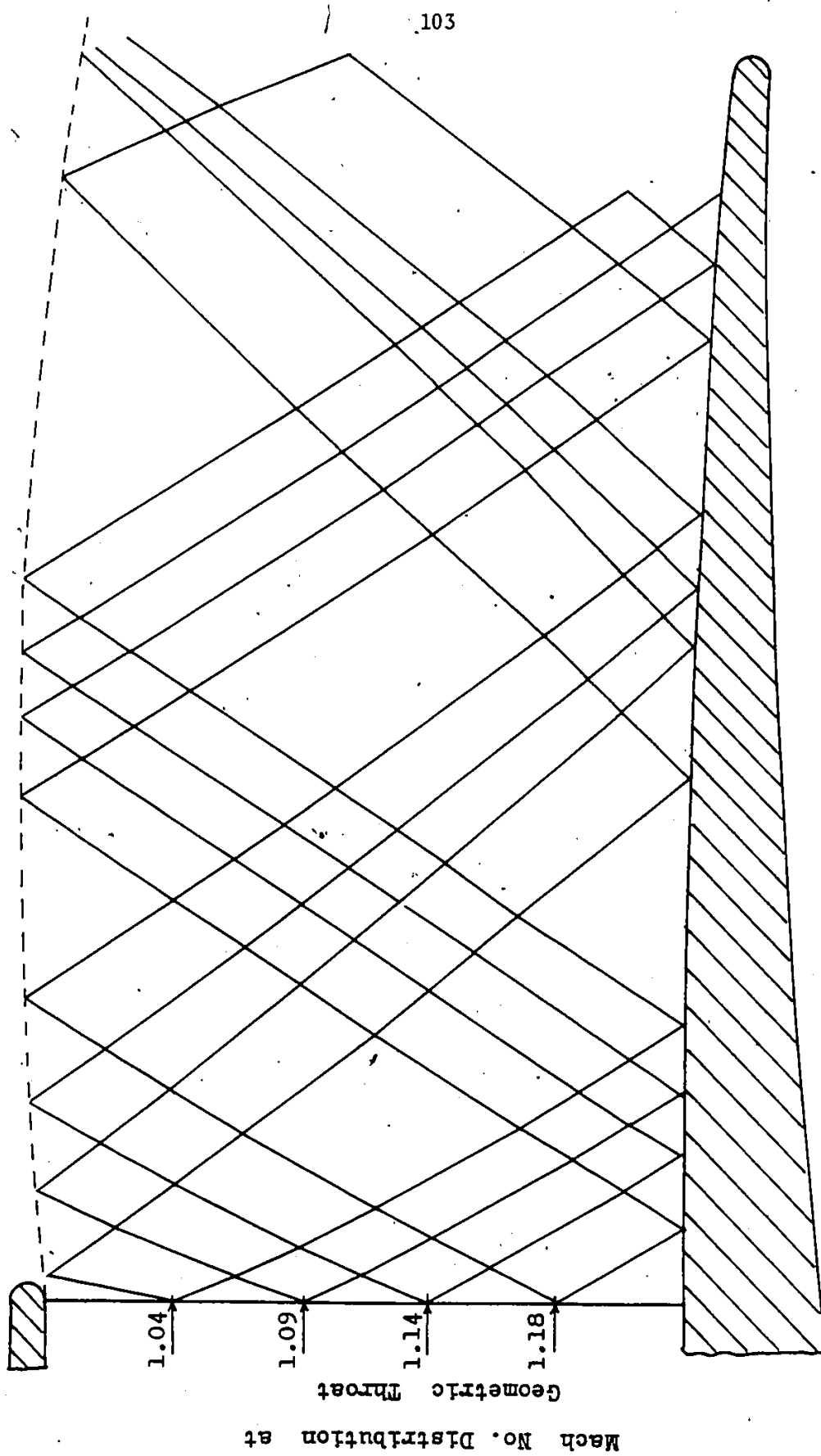


Figure 5.12 Characteristic Lines for Curved Back Turbine Blade  
for Pressure Ratio  $P_0/p = 2.486$

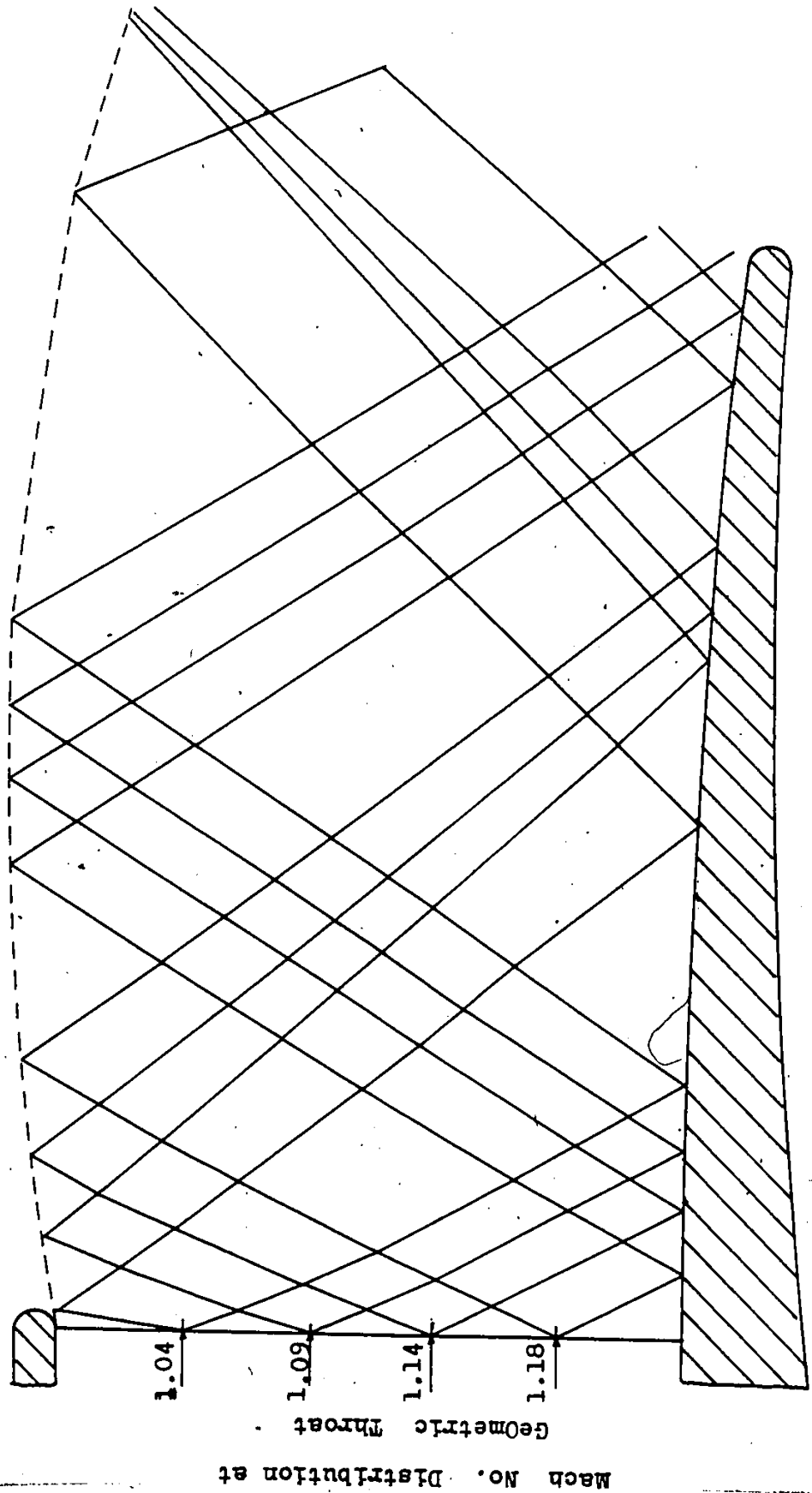


Figure 5.13 Characteristic Lines for Curved Back Turbine Blade  
for Pressure Ratio  $P_0/p = 2.752$

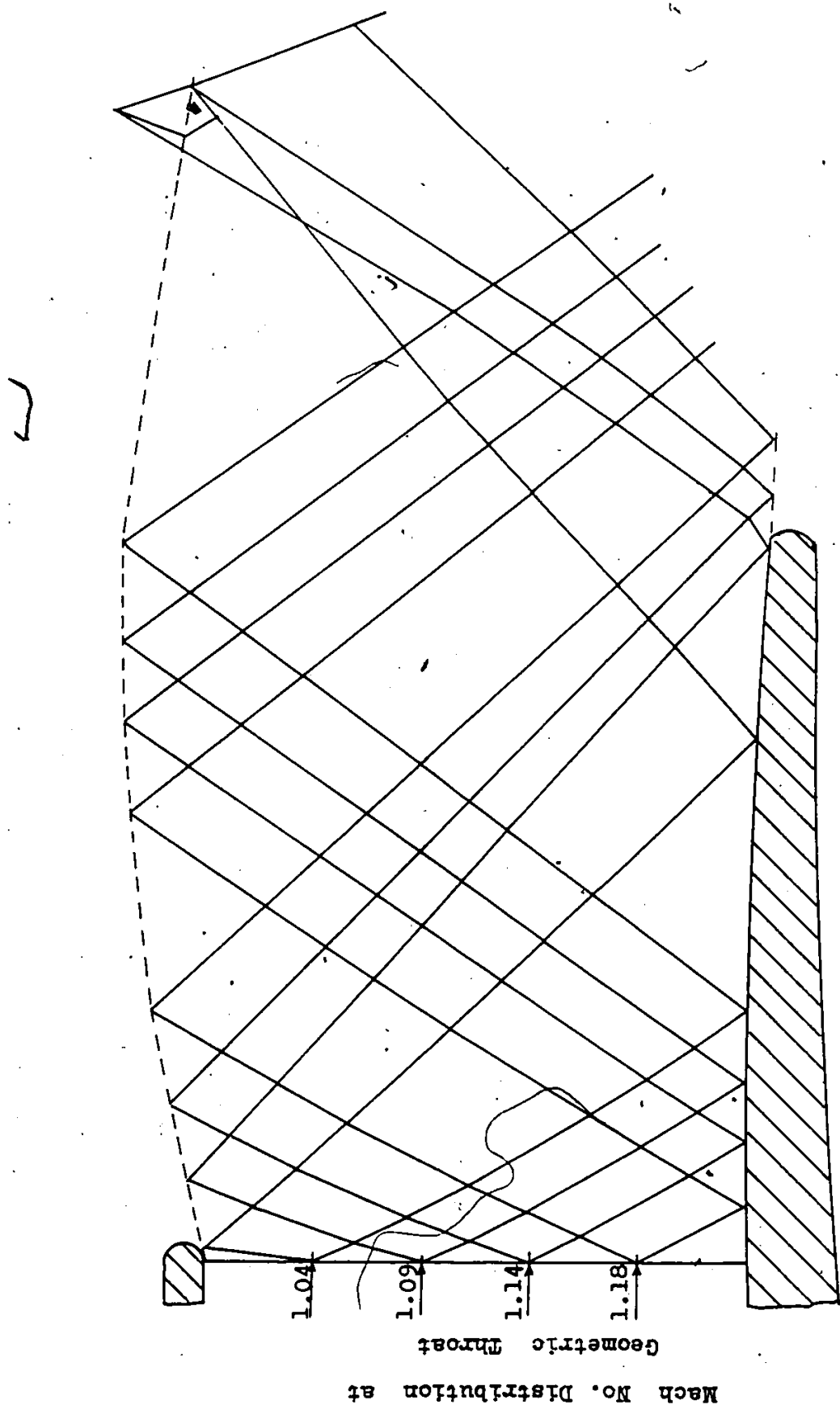


Figure 5.14 Characteristic Lines for Curved Back Turbine Blade  
for Pressure Ratio  $P_0/p = 3.038$

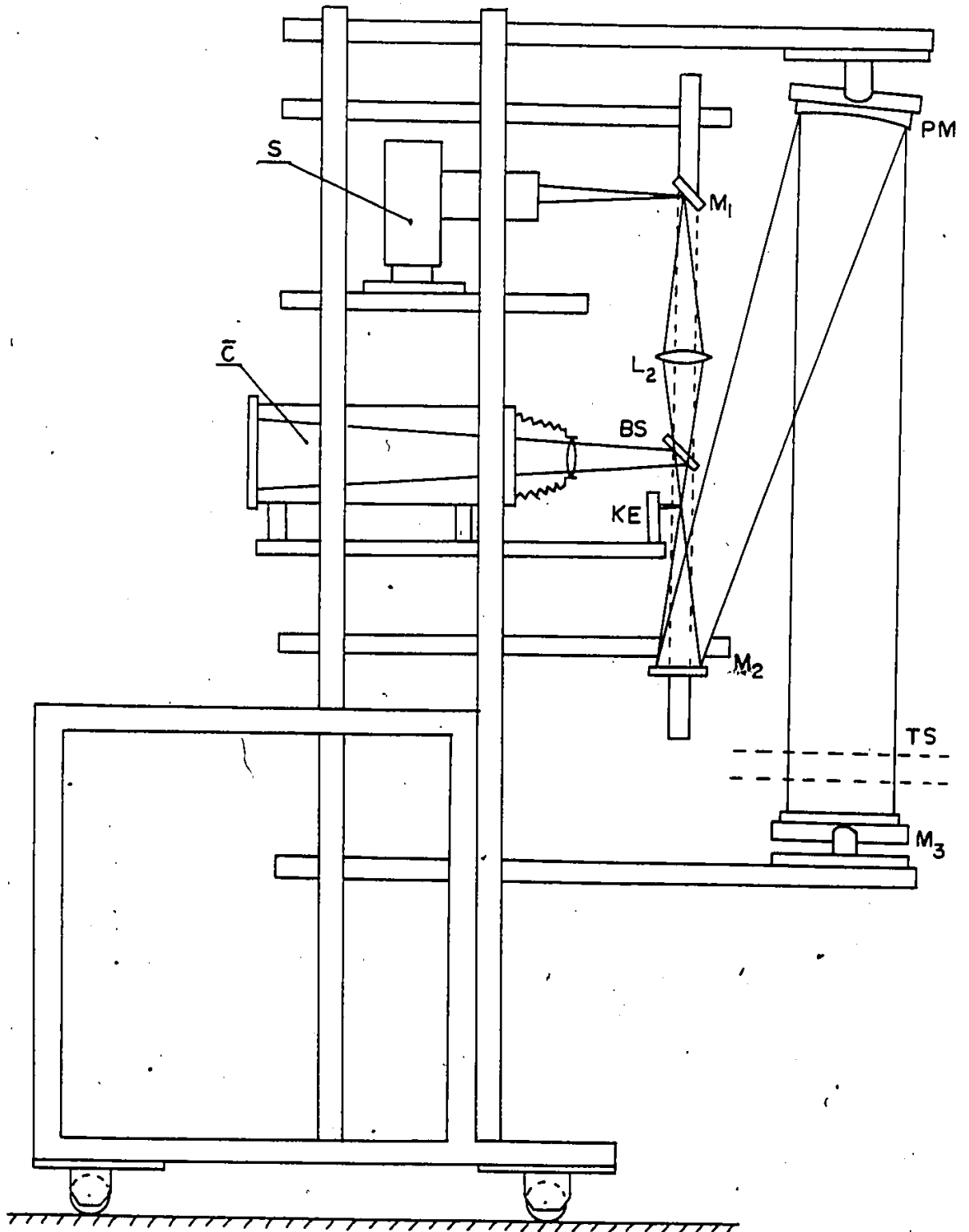


Figure 5.15 Proposed Schlieren System

may be obtained. The light source S is a super pressure mercury lamp, 500 watts (OSRAM, HBO 500 W/2 type lamp). The housing to accommodate the lamp is designed and fabricated as detailed in the specification supplied by the manufacturer of the lamp. An arrangement for the lens and iris diaphragm must be provided to control the size of the light source. The mirror  $M_1$ , the lens  $L_2$ , the beam splitter BS and the mirror  $M_2$  are mounted on a square bar which can be adjusted for suitable position and also all the components on the bar can be separately positioned. The parabolic mirror PM and the mirror  $M_3$ , each can be adjusted for the ease of proper alignment of the light rays. The knife edge KE is to be placed at the focal point of the parabolic mirror PM. The camera C is about 30 inches long for obtaining better image of the flow field.



## CHAPTER 6

### CONCLUSIONS

The present study represents the application of numerical as well as classical methods for solving the two-dimensional supersonic flow fields. For a high turning angle turbine blade, depending on the working pressure ratios, a supersonic flow field appears near the trailing edge of the blade. The numerical method is successfully applied to locate the compression as well as expansion waves after the geometric throat. An increase in the total-to-static pressure ratio gradually moves the shock towards the trailing edge of the blade and for a pressure ratio ( $p_0/p$ ) equal to 3.038, an over-expanded situation occurs. Figures 5.7 and 5.11 describe this effect. This situation gives the maximum area of the pressure distribution along the blade chord. Pressure ratios higher than this critical value may not be useful in increasing the work load of the blade.

For a pressure ratio of  $p_0/p = 2.486$ , both the numerical and the classical (Riemann Invariants) methods give results which agree quite closely, (Figure 5.5 and Figure 5.8).

For curved back blades, the analysis showed that once again the position of shock gradually moved towards the trailing edge with increasing pressure ratios. From the program

developed in Appendix B, static temperature, Mach number, and the flow deflection may be estimated at different coordinate points in the flow field.

## REFERENCES

1. Hawthorne, W. R., Aerodynamics of Turbines and Compressors, Princeton University Press, 1964.
2. Ainley, D. G. and Mathieson, G. C. R., A Method of Performance Estimation for Axial Flow Turbines, Brit. Aero. Council, R & M 2974, 1957.
3. Zweifel, O., The Spacing of Turbomachine Blading, Especially with Large Angular Deflection, Brown Boveri Review, Dec. 1945.
4. Davis, W. R. and Millar, D. J., A Matrix Method applied to the Analysis of the Flow past Turbomachine Blades, Carleton University, ME/A, 72-7.
5. Kumar, V., The Design of Three Related Gas Turbines for an Experimental Investigation of the Effect of Blade Loading on Performance, M.Eng. Thesis, Mech. Eng. Dept., Carleton University, 1968.
6. Malhotra, R. K., The Two-Dimensional Development and Analysis of Blade Profiles Having Large Turning Angles, M.Eng. Thesis, Dept. of Mech. Eng., McMaster University, 1971.
7. Stannard, J. H., The Aerodynamic Design and Testing of High Turning Angle Turbine Blades, Ph.D. Thesis, Dept. of Mech. Eng., McMaster University, 1975.
8. Liepmann, H. W. and Roshko, A., Elements of Gas Dynamics, J. Wiley & Sons, 1956.
9. Stanitz, J. O., Design of Two-Dimensional Channels with Prescribed Velocity Distribution Along the Channel Walls; Part I: Relaxation Solution, NACA Tech. Note 2593, 1952. Part II: Solution by Green's Function, NACA Tech. Note 2595, 1952.
10. Martensen, G., Calculation of Pressure Distribution over Profiles in Cascade in Two-Dimensional Potential Flow by Means of a Fredholm Integral Equation, Archs. Ration. Mech. Analysis, 3, 3, 1959.

11. McDonald, P. W., The Computation of Transonic Flow Through Two-Dimensional Gas Turbine Cascades, ASME, 71-GT-89, 1971.
12. Hilderband, F. B., Introduction to Numerical Analysis, McGraw Hill Book Company, 1956.
13. Shapiro, A. H., The Dynamics and Thermodynamics of Compressible Fluid Flow, Vol. I, Ronald Press Company, 1953.
14. Zucrow, M. J. and Hoffman, J. D., Gas Dynamics, Vol. I and Vol. II, John Wiley & Sons, 1976.
15. Courant, R. and Friedrichs, K. O., Supersonic Flow and Shock Waves, Interscience Publishers, 1948.
16. Holt, Maurice, Numerical Methods in Fluid Dynamics, Springer-Verlog, Berlin Heidelberg, 1977.
17. Todd, K. W., Some Developments in Instrumentation for Air Flow, Proc. I. Mech. Engrs., Vol. 161, 1949.
18. Barnes, N. F. and Bellinger, S. L., Schlieren and Shadowgraph Equipment for Air Flow Analysis, Optical Society of America, Vol. 35, No. 8, 1945.
19. Taylor, H. G. and Waldram, J. M., Improvements in Schlieren Method, J. of Sci. Instruments, Vol. 10, 1933.
20. Brusseeleers, M., Physical and Numerical Aspects of Shock Boundary Layer Interactions, VKI Lecture Series 1980-8, Vol. I.
21. Davidson, I. M., Some Properties of Compression Shock as in Turbine and Compressor Blade Passages, Proc. I. Mech. Engrs., Vol. 158.
22. Todd, K. W., Practical Aspects of Cascade Wind Tunnel Research, Proc. Inst. of Mech. Engrs., Vol. 157, 1947.
23. Hoffman, J. D., Accuracy Studies of the Numerical Method of Characteristics for Axisymmetric, Steady Supersonic Flows, J. of Computational Physics, Vol. 11, No. 2, 1973.
24. Ainley, D. G., Performance of Axial Flow Turbines, Proc. Inst. of Mech. Engrs., 159, (1948).
25. Horlock, J. H., Axial Flow Turbines, Butterworth, 1966.
26. Horlock, J. H., Flow Disturbances due to Blade Thickness, J. Mech. Eng. Sci., Vol. 1, (1969).

27. Hauser, C. H., Flohr, H. W. and Sonder, G., Study of Flow Conditions and Deflection Angle at Exit of Two-Dimensional Cascade of Turbine Rotor Blades at Critical and Supersonic Pressure Ratios, NACA RM E9K25, 1950.
28. Ainley, D. G. and Mathieson, G. C. R., An Examination of the Flow and Pressure Losses in Blade Rows of Axial Flow Turbines, B.A.R.C. R & M 2891, 1955.
29. Houghton, E. L. and Brock, A. E., Tables for the Compressible Flow of Dry Air, Third Edition, Edward Arnold, 1975.
30. Liepmann, H. W., The Interaction Between Boundary Layer and Shock Waves in Transonic Flow, J. of the Aero. Sci., Vol. 13, No. 12, December 1946.
31. Carnahan, B., Luther, H. A. and Wilkes, J. O., Applied Numerical Methods, Wiley, New York, 1969.
32. Conte, S. D. and deBoor, C., Elementary Numerical Analysis, Second Edition, McGraw Hill, New York, 1972.
33. Pearcey, H. H., Some Effects of Shock-Induced Separation of Turbulent Boundary Layers in Transonic Flow Past Aerofoils, Aero. Research Council, R & M No. 3108, 1959.

APPENDIX A  
COMPUTER PROGRAM FOR PRESSURE  
AND MACH NUMBER DISTRIBUTION

APPENDIX A1  
USER'S MANUAL FOR THE PROGRAM

This appendix contains the flow chart and program listing for the program used for finding the pressure and Mach number distribution in a convergent passage. For a particular type of blade the curvatures  $C_p$ ,  $C_s$  and Gauge (length of orthogonal) are specified. The pressure distribution shown in Figure 2.15 confirms the shape of the blade passage with that obtained in the earlier design [7]. At the geometric throat the distribution of Mach number is most important and depending on this distribution the initial value line is constructed for the method of characteristics.

The program starts by reading the inlet flow conditions, then it reads the important constants of the flow field such as gas constant, acceleration due to gravity, specific heat ratio, etc. Next it sets the control variables to pre-assigned values. A mass flow is calculated which is the mass flow required for choking the geometric throat or a mass flow less than the choked mass flow which may be termed as design mass flow somewhere in the channel. For the first quasi-orthogonal line, it reads in the values for the pressure and suction surface curvatures along with the length of the quasi-orthogonal. Using a velocity equation

as developed in Chapter 2, a mass flow value is calculated and compared to the design mass flow value. If the value is within the certain limit of the design value, the program prints out the results and proceeds to the next quasi-orthogonal. When the flow is choked at the throat, the alternative calculation procedure may be employed.

For all orthogonals, the values of static pressure, Mach number distribution, velocities, pressure ratios, static temperatures and densities are calculated for all of the nine stream tubes. The values of Mach numbers of the last quasi-orthogonal that is the geometric throat are utilized for initial value line for the Mach number distribution.

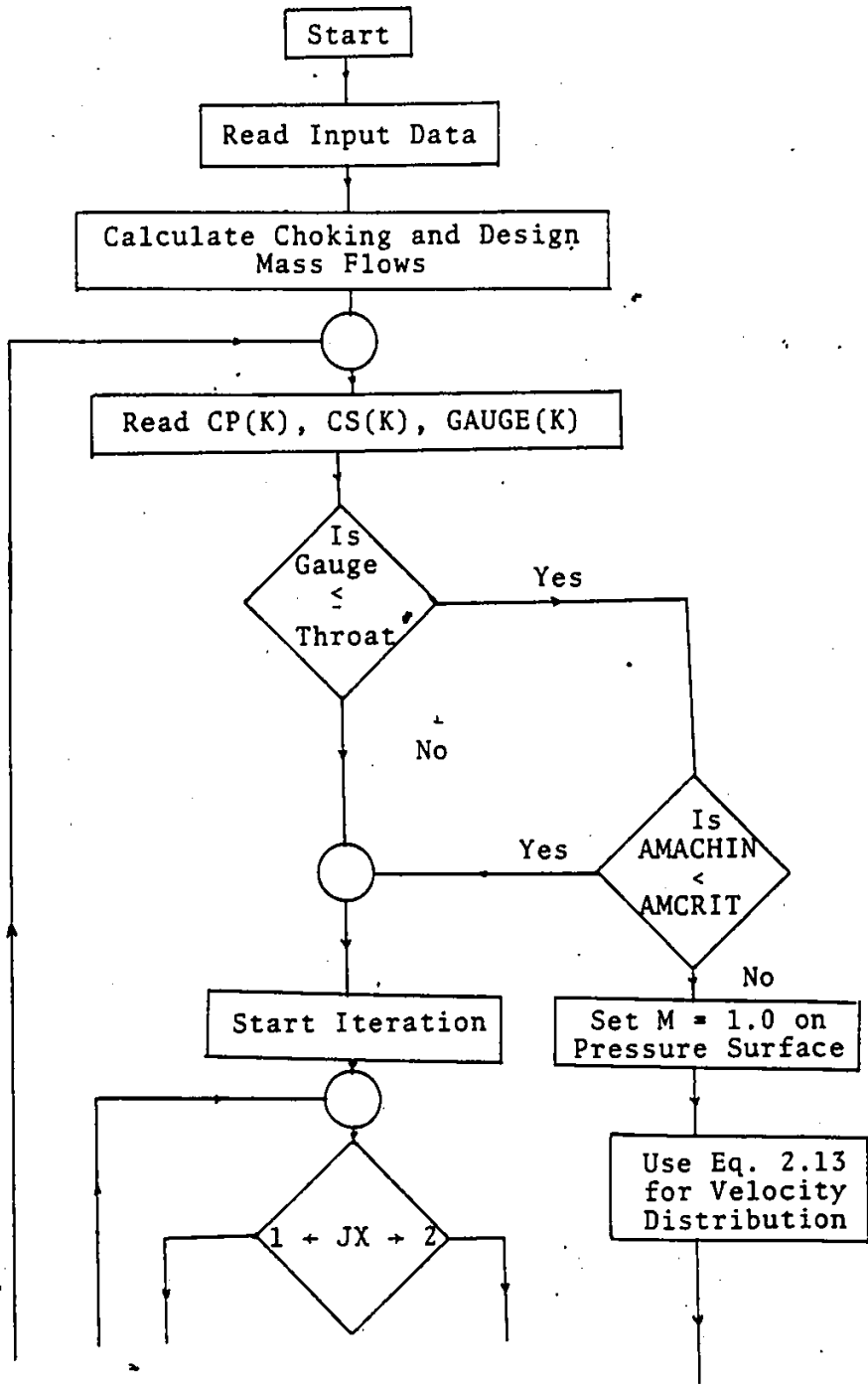
<u>VARIABLE</u>	<u>DESCRIPTION</u>
A(I)	Speed of Sound
ACC	Difference between Design and Calculated Mass Flow
AMACH(I)	Mach Number
AMACHIN	Inlet Mach Number
AMAS	Design Channel Mass Flow
AMCRIT	Critical Inlet Mach Number for Choking the Geometric Throat
AP	Static Pressure
AR	Density
AT	Static Temperature
AV	Resultant Velocity

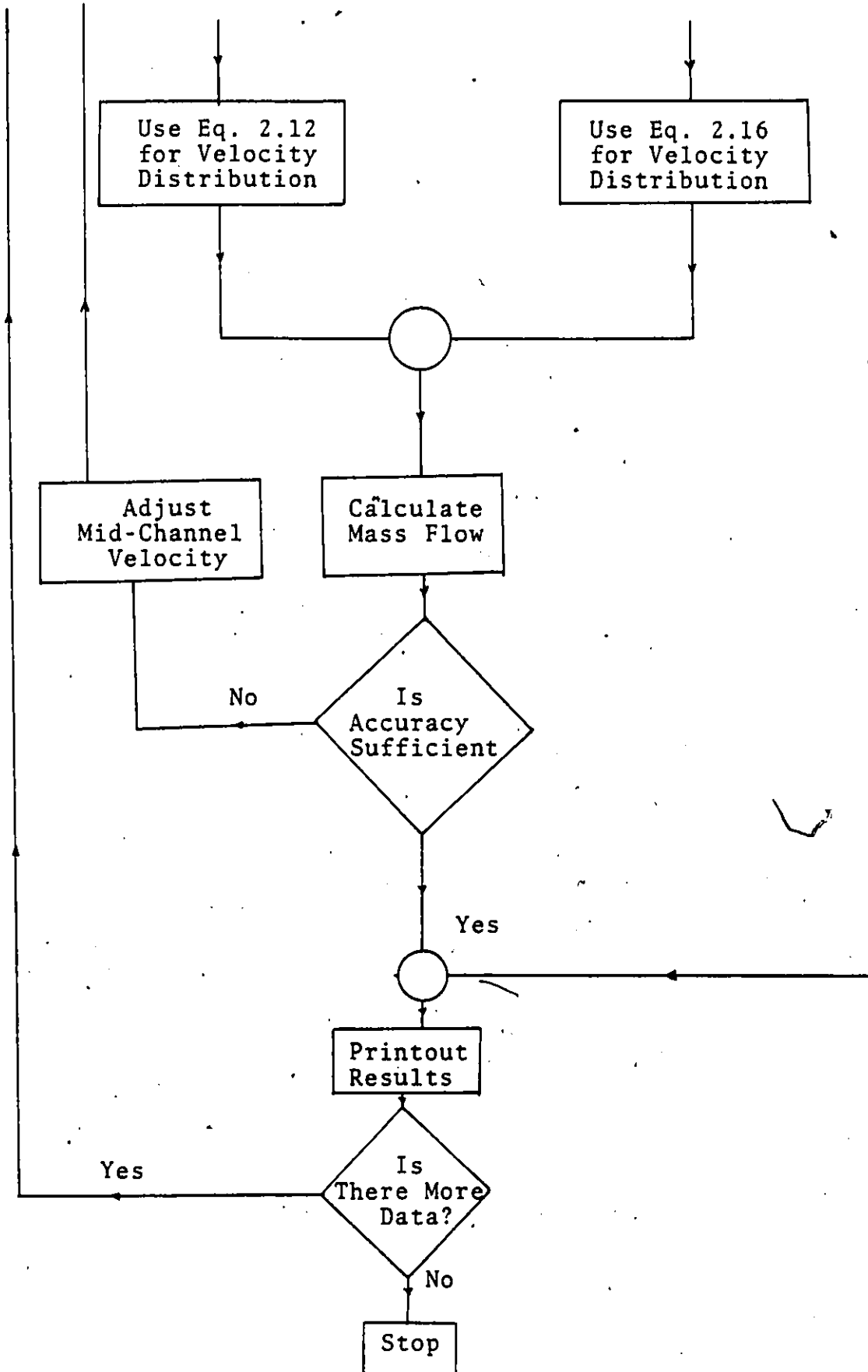


<u>VARIABLE</u>	<u>DESCRIPTION</u>
CMAS	Choking Mass Flow for Geometric Throat
CP(K)	Curvature of Pressure Surface
CS(K)	Curvature of Suction Surface
D	Constants (with suffix) for Easy Calculations Step
DELG	Distance between Two Adjacent Stream Lines
DRPR	Ratio of Static to Total (relative) Pressure
G	Acceleration due to Gravity
GAGE	Width of Flow Passage defined by Inlet Stream Lines. (Pitch X Cosine of Inlet Air Angle)
GAMMA	Ratio of Specific Heats
GASC	Gas Constant for Air
GAUGE(K)	Quasi-orthogonal Length
JX	Control Variable; 1 for Linear Curvature Variation; 2 for Linear Radius of Curvature Variation
NDAATA	Number of Quasi-orthogonals
PEXIT	Static Pressure Downstream of Cascade
POW	Variable to Calculate the Velocity Distribution Expressions
RATIO	Iteration Variable, Given Starting Value Equal to 1
RELTOP	Relative Total Pressure
RELTOPT	Relative Total Pressure at Inlet

<u>VARIABLE</u>	<u>DESCRIPTION</u>
RELTOT	Relative Total Temperature
RO(I)	Density
RPR(I)	Static Pressure
RT(I)	Static Temperature
SPACE	Blade Pitch
THROAT	Geometric Throat Width
TMAS	Calculated Mass Flow in Channel
W(I)	Velocity
Z(I)	Density X Velocity

FLOW CHART





## APPENDIX A2

```

C *****
C * PROGRAM TO CALCULATE THE MACH NUMBER *
C * AND OTHER FLOW PARAMETER DISTRIBUTIONS *
C * IN TURBINE PASSAGES *
C * *
C *****
C
C )
C PROGRAM TST (INPUT, OUTPUT, TAPE5=INPUT, TAPE6=
C OUTPUT)
C
C DIMENSION W(9),RPR(9), Z(9),AMACH(9), DRPR(9)
C
C READ THE FLOW PROPERTIES
C
C READ (5,*) RETOPI,PEXIT,AMACHIN,RELTOT
C
C READ THE CONSTANT VALUES
C
C READ (5,*) GASC,G,GAMMA,SPACE,JX
C
C
C READ THE CONTROL PARAMETER VALUES
C
C READ (5,*) ACC,GAGE,THROAT,RATIO,AMCRIT, NDATA
C
C
C CALCULATE THE USEFUL CONSTANTS
C
C D1=2.0*GAMMA*GASC*G
C D3=GAMMA-1.0
C D2=GAMMA/D3
C D4=GAMMA+1.0
C D5=((GAMMA*G)/(GASC*RELTOT))**0.5
C
C
C CALCULATE THE CHOKING MASS FLOW
C
C CMAS=(D5)*THROAT*RETOPI*12.0/1.728
C WRITE(6,21) CMAS
C WRITE(6,999)
C
C WRITE(6,22) RETOPI,PEXIT,AMACHIN,RELTOT
C WRITE(6,999)
C WRITE(6,23) GASC,G,GAMMA,SPACE,JX
C WRITE(6,999)
C WRITE(6,25) ACC, GAGE,THROAT,RATIO,AMCRIT,NDATA

```

```

WRITE (6,999)
C
C
AT=RELTOT/(1.0+(D3*(AMACHIN**2.0))/2.0)
AP=RETOPI*(AT/RELTOT)**D2
AR=AP/GASC/AT*144.0
AV=AMACHIN*((GAMMA*GASC*G*AT)**0.5)
C
C
C
CALCULATE THE DESIGN MASS FLOW
C
C
AMAS=AR*AV*GAGE/12.0
WRITE (6,24) AMAS
C
C
C
READ THE SURFACE CURVATURES AND
QUASI-ORTHOGONAL LENGTHS
C
C
READ (5,*) CP(K),CS(K),GAUGE(K)
WRITE (6,28)
WRITE (6,241) CP(K),CS(K),GAUGE(K)
C
IF(GAUGE(K)-THROAT) 63,63,62
C
IF(AMCRIT - AMACHIN) 64,64,62
63
C
62
W(5)=AV*GAGE/GAUGE(K)
C
51
IF(((W(5)**2)*D3/D1).LT.(RELTOT)) GO TO 52
W(5)=W(5)/2.0
52
CONTINUE
66
W(5)=W(5)*RATIO
DO 235 I=1,9
C
53
C=I
C
DELG=(C-1.0)*GAUGE(K)/8.0
IF(JX.EQ.2) GO TO 57
56
D6=DELG/GAUGE(K)
D7=CS(K)*(0.375-D6)
D8=0.125*CP(K)-0.5*(CP(K)-CS(K))*(D6**2.0)
POW=GAUGE(K)*(D7+D8)
49
W(I)=W(5)*EXP(POW)
GO TO 60
C
57
IF(CP(K)-CS(K)) 58,59,58
C
58
D9=CP(K)+(CS(K)-CP(K))*DELG/GAUGE(K)
D10=GAUGE(K)*CS(K)*CP(K)/(CP(K)-CS(K))
W(I)=W(5)*(2.0*D9/(CP(K)+CS(K)))**D10
GO TO 60

```

```

59     POW=GAUGE(K)*(0.5-DELG/GAUGE(K))*CS(K)
      GO TO 49
60     RELTOP=RETOPI
      RT(I)=RELTOT-(W(I)**2)*D3/D1
      A(I)=(GAMMA*GASC*G*RT(I))**0.5
      AMACH(I)=W(I)/A(I)
      RPR(I)=RELTOP/(RELTOT/RT(I))**D2
      DRPR(I)=RPR(I)/RELTOP
      RO(I)=144.0*RPR(I)/(GASC*RT(I))
C
235    Z(I)=RO(I)*W(I)
C
54     D11=0.03489*(Z(1)+Z(9))+0.20769*(Z(2)+Z(8))-0.03273*
      $(Z(3)+Z(7))
      D12=0.371023*(Z(4)+Z(6))-0.16014*Z(5)
      TMAS=(D11+D12)*GAUGE(K)/12.0
      RATIO=2.0-(TMAS/AMAS)
      IF(ABS(AMAS-TMAS).LE.ACC) GO TO 61
      GO TO 66
64     DO 245 I=1,9
      RT(9)=RELTOT*2.0/(GAMMA+1.0)
      W(9)=(GAMMA*GASC*G*RT(9))**0.5
C
      C=I
C
      DELG=(C-1.0)/8.0
      D13=CP(K)+CS(K)-2.0*CS(K)*DELG
      D14=(CP(K)-CS(K))*(DELG**2.)
      POW=GAUGE(K)*(D13-D14)
      W(I)=W(9)*EXP(POW)
C
      RELTOP=RETOPI
C
      RT(I)=RELTOT-(W(I)**2.0)*D3/D1
      A(I)=(GAMMA*GASC*G*RT(I))**0.5
      AMACH(I)=W(I)/A(I)
C
      RPR(I)=RELTOP/(RELTOT/RT(I))**D2
      DRPR(I)=RPR(I)/RELTOP
      RO(I)=144.0*RPR(I)/(GASC*RT(I))
245    Z(I)=RO(I)*W(I)
      D11=0.03489*(Z(1)+Z(9))+.20769*(Z(2)+Z(8))-0.03273*(Z(3)+
      $(Z(7))
      D12=0.371023*(Z(4)+Z(6))-0.16014*Z(5)
      TMAS=(D11+D12)*GAUGE(K)/12.0
C
C
61     WRITE (6,27) TMAS
C
C

```

```

WRITE (6,999)
WRITE (6,999)
WRITE (6,999)
C
C
WRITE (6,30)
WRITE (6,999)
DO 26 I=1,9
C
C
21 FORMAT (/,10X,*CHOKING MASS FLOW=*, F10.3)
22 FORMAT (4F8.3)
23 FORMAT (4F8.4,I2)
C
24 FORMAT (/,10X,*DESIGN MASS FLOW=*,F10.3)
C
25 FORMAT (5F8.4,I8)
C
26 WRITE (6,29)RPR(I),AMACH(I),W(I),DRPR(I),RT(I),RO(I)
C
27 FORMAT (/,10X,*CALCULATED MASS FLOW=*,F10.3)
C
28 FORMAT (1H0,20X,*CP(K) CS(K) GAUGE(K)*)
C
29 FORMAT (1H0,5X,F10.3,1X,F10.3,3X,F10.3,1X,F6.3,
$3X,F10.3,3X,F6.3)
C
30 FORMAT (1H0,* RPR(I) AMACH(I) W(I)
$ DRPR(I) RT(I) RO(I)*)
C
241 FORMAT (16X,3F10,4)
C
999 FORMAT (10X,* )
C
900 CONTINUE
STOP
END

```



## APPENDIX A3

## C INPUT DATA FOR McMASTER BLADE

27.800	14.696	.680	530.000		
53.350	32.140	1.400	.650	1	
.0005	.285	.257	1.000	.670	12

CP(K)	CS(K)	GAUGE(K)
.100	3.000	.420
.500	3.250	.425
1.500	3.250	.420
2.000	3.500	.420
2.000	3.500	.380
1.500	4.500	.370
1.000	4.500	.330
.750	4.500	.3000
.250	4.000	.290
.100	2.500	.270
.050	1.000	.260
.020	.600	.257

APPENDIX B  
COMPUTER PROGRAM FOR METHOD  
OF CHARACTERISTICS

## APPENDIX B1

## USER'S MANUAL FOR THE PROGRAM:

This appendix contains the program listing and the program as developed in Chapter 3 for analysing the supersonic flow field at the exit section of the McMaster blade (converging passage). The resultant velocity, flow deflection, pressure and temperature at any point with known coordinate axes can easily be determined with the help of above program.

The Mach number distribution at the geometric throat of a particular blade passage is obtained by using stream-tube method (Appendix A) and a few equispaced points are selected (in this case  $N=4$ ) at the geometric throat. The origin of coordinate system may preferably be chosen as the suction surface of the pair forming the convergent passage. A suitable scale is selected to enlarge (or reduce) the throat section for a better appreciation of the characteristics or Mach lines covering the flow field. The coordinates of all the points including the total length of the throat (upper corner point) section are obtained with the help of a good drafting technique, preferably mechanical, and the Prandtl-Meyer expansion angle  $\nu$  (here THEUC) is provided at the beginning of the program from the isentropic flow tables.

This gives the deviation of the free pressure boundary and the deviation can be linearly distributed at the selected points (here THE(I)). Once all these values are specified, the other input values are mentioned in the beginning have to be supplied as a suitable input statement.

The numbering of the flow field (Figure 4.2 and Figure 5.2) is done in conjunction with the flow field obtained by using Riemann Invariants method and the computer program is suitably applied when the solution point is an interior, wall or free pressure boundary point. The numbering system is shown in Figure 5.2. As seen from the sketch, the points 5, 14, 23, 32, 41, 50, etc. are on the solid wall and points 9, 18, 27, 36, etc. are on the intersection of free pressure boundary and characteristic lines - so these points are termed as boundary point. Other points such as 5, 7, 8, etc. are the interior points. The subroutines are developed to suit the solution of all these three types of points. Subroutine INTPT solves for the points which are interior to the flow i.e. at the points of intersections of both left and right running characteristics. The subroutine wall point (WALPT) and BODPT are for solution of points on the suction surface wall and free pressure boundary of the flow. The subroutine FLOW determines flow velocities at the selected points (4 points in this case) on the initial value line or geometric throat depending on the flow devia-

tions at all these points. Similarly, the subroutine FLOW1 determines the flow velocities at the exit corner of pressure surface of the blade. Subroutine BODPT1 determines the first point (here point 9) on the free pressure boundary line whereas the remainder of the points on the free pressure boundary are determined by using subroutine BODPT. Subroutine THERMO determines sonic velocity, Mach number, static pressure and static temperature at any point in question. The subroutine BOUNDRY determines the contour of the suction surface from the geometric throat to the trailing edge radius. For a curved surface, a quadratic form of the surface such as  $y = Ax^2 + Bx + C$  is used and the coefficients, A, B, and C are determined depending on the initial and final conditions of the blade surface after the throat. For a straight back blade  $y = 0.0$  everywhere is assumed as obvious from the geometry of the blade. For a curved blade the slope  $dy/dx = 2Ax + B$  can be evaluated at the origin of the suction surface and also at the exit of the blade surface. Three equations are formed with three initial conditions to solve the coordinates, A, B, and C and thus the equation of curvature of the suction surface after the throat.

## Program Listing:

<u>VARIABLE</u>	<u>DESCRIPTION</u>
ICOR	Number of applications of the corrector
E1	Convergence tolerance for location, metre
E2	Convergence tolerance for velocity m/sec
ITER	Number of interations desired
THAE	Angle of free pressure boundry line after successive reflected waves cross it
IFIN	Value chosen to generate about 100 points in the flow field
THEUC	Value of Prandtl-Meyer expansion angle in degrees $\nu$ for a definite pressure ratio $P_0/p$
XO	Origin of X-coordinate
YO	Origin of Y-coordinate
XE	Maximum X-coordinate, for curved back blade, m m
YE	Maximum Y-coordinate for curved-back blade, m m
THEO	Slope of suction surface at $x_0, y_0$
THEE	Slope of suction surface at XE, YE
G	Specific heat ratio, 1.4
RG	Gas constant, 287.0 J/Kg-K
TS	Stagnation temperature, K
PS	Stagnation pressure, $N/m^2$

<u>VARIABLE</u>	<u>DESCRIPTION</u>
PA	Ambient pressure, $N/m^2$
TA	Static temperature, K
GC	Gravitational constant $1.0 \text{ m-Kg/N-sec}^2$
M(I)	Mach number
X(I)	X-coordinate of locations, m m
Y(I)	Y-coordinate of locations, m m
U(I)	Velocity along X-axis, m/sec
V(I)	Velocity along Y-axis, m/sec
Q(I)	Resultant velocity, m/sec
THE(I)	Streamline angle with x-axis at different locations in degrees
XUC	X-coordinate of upper corner point
YUC	Y-coordinate of upper corner point
MUC	Mach number of upper corner point
UUC	X-component of velocity at upper corner point
VUC	Y-component of velocity at upper corner point
QUC	Velocity (Resultant) at upper corner point
C	Velocity of sound, m/sec
A	Flow angle, $\theta$ in rad
LM	$m_- = \tan(\theta - \mu)$
LP	$m_+ = \tan(\theta + \mu)$
QM	$Q_- = (u^2 - a^2)m^2/\text{sec}^2$ along $C_-$ characteristics
QP	$Q_+ = (u^2 - a^2)m^2/\text{sec}^2$ along $C_+$ characteristics
RM	$R_- = (2u_v - m Q_-)m^2/\text{sec}^2$ along $C_-$ characteristics

<u>VARIABLE</u>	<u>DESCRIPTION</u>
RP	$R_+ = (2u_+v_+ - m_+ Q_+)m^2/\text{sec}^2$ along $C_+$ characteristics
TM	$T_- = Q_-u + R_-v, m^3/\text{sec}^3$ along $C_-$ characteristics
TP	$T_+ = Q_+u + R_+v, m^3/\text{sec}^3$ along $C_+$ characteristics
LO	$m_0 = v_3/u_3$ , slope of jet boundary 3-4 at point 3
UU	Average value of u
VV	Average value of v
YY	Average value of Y
QQ	Average value of q
DENO	$Q_-R_+ - Q_+R_-$
DD	$Q_+^2 + R_+^2$
XC	Corrected value of X
YC	Corrected value of Y
UC	Corrected value of u
VC	Corrected value of v



## APPENDIX B2

## PROGRAM

C THIS PROGRAM IS USED TO FIND THE CHARACTERISTICS  
C WITH THE HELP OF EULER PREDICTOR-CORRECTOR (MODIFIED)  
C METHOD  
C

PROGRAM GAS (INPUT,OUTPUT)

COMMON/CONTRL/ICOR, E1,E2,PI,COUNT,THAE,YFIN,THEUC

COMMON/PROPT/XO,YO,XE,THEO,THEE

COMMON/PROPTY/G,RG,TS,PS,PA,GC,TA,YUC

REAL M(150),THE(150),Q(150),X(150),Y(150),U(150),V(150)

REAL M1,M2,LP,LM,LE,L12,LO

REAL MUC,XUC,YUC,UUC,VUC,QUC,THEUC,~~MUC~~

C READ ALL THE INPUT DATA

C READ ALL THE CONTROL VARIABLE

READ\*,ICOR,E1,E2,IFIN,N,THAE

C READ THE THERMODYNAMICS PROPERTIES OF THE FLUID

READ\*,G,RG,GC

C READ THE FLOW PROPERTIES OF FLUID

READ \*,TS,TA,PS,PA

C READ THE VARIABLES FOR CURVED BLADES

READ \*,XO,YO,XE,THEO,THEE

C READ THE UPPER CORNER VALUES

READ \*,XUC,YUC,MUC,THEUC

```

C      READ THE VALUES OF M(I),X(I),Y(I) AND THE(I)
      DO 22 I=1,N
      READ *, X(I)
      READ *, Y(I)
      READ *, M(I)
      READ *, THE(I)
22     CONTINUE
      THAE=THEUC/ N
C
C
      CALL FLOW1 (QUC,UUC,VUC,THEUC,MUC)
      PRINT *,"      UPPER CORNER VALUES"
      PRINT *,"      X=",XUC," Y= ", YUC," M= ", MUC
      PRINT *,"      Q=",QUC," U= ", UUC," V= ", VUC
      PRINT *,"      THE= ", THEUC
      PRINT *,"      "
      PRINT *,"      "
      PRINT *,"      INITIAL ", N, " POINTS"
      CALL FLOW (Q,U,V,THE,M,N)
      DO 33 I = 1,N
      PRINT *," X",I, "=", X(I)," Y",I,"=",Y(I),"M",I,
      PRINT *,"=", M(I)
      PRINT *," Q= ", Q(I), "U= ",U(I),"V = ",V(I)
33     CONTINUE
      I = 1

```

```
CALL WALPT(X,Y,U,V,M,I,N)
NN = N-1
DO 17 J= 1,NN
CALL INTPT(X,Y,U,V,M,I,N)
I = I+1
17 CONTINUE
CALL BODPT1(XUC,YUC,UUC,VUC,MUC,I,N,X,Y,U,V,M)
COUNT = 1
DO 18 J = 1,N
I = I+1
CALL INTPT(X,Y,U,V,M,I,N)
18 CONTINUE
DO 12 K=1,IFIN
I = I+2
CALL WALPT(X,Y,U,V,M,I,N)
NN = N-1
DO 13 J = 1,NN
CALL INTPT(X,Y,U,V,M,I,N)
I = I+1
13 CONTINUE
CALL BODPT(X,Y,U,V,M,I,N)
DO 14 J = 1,N
I = I+1
CALL INTPT(X,Y,U,V,M,I,N)
14 CONTINUE
```

```
12 CONTINUE
C
C
C SUBROUTINES USED FOR DRAWING THE CHARACTERISTIC
C LINES
CALL FACTOR(I,X,Y,10.0,7.0,1.0,2.5)
DO 34 J = 1,I
CALL PLTSPT(X(J),Y(J),0.2,1H+,0.0)
34 CONTINUE
I = 1
DO 89 J = 1,IFIN
C DRAW LINES FROM N INTERIOR POINTS BACK
DO 91 K = 1,N
CALL PLTLN(X(I),Y(I),X(I+4),Y(I+4))
CALL PLTLN(X(I),Y(I),X(I+5),Y(I+5))
I = I+1
91 CONTINUE
C DRAW LINES TO FREE SURFACE BOUNDARY
CALL PLTLN(X(I),Y(I),X(I+5),Y(I+5))
I = I+1
NN = N-1
DO 92 K = 1,NN
C
CALL PLTLN(X(I),Y(I),X(I+4),Y(I+4))
CALL PLTLN(X(I),Y(I),X(I+5),Y(I+5))
I = I+1
```

```

92    CONTINUE
      CALL PLTLN(X(I),Y(I),X(I+4),Y(I+4))
      I = I+1
89    CONTINUE
      DO 99 K = 1,NN
      CALL PLTLN(X(I),Y(I),X(I+4), Y(I+4))
      CALL PLTLN(X(I),Y(I),X(I+5),Y(I+5))
      I = I+1
99    CONTINUE
      CALL NEWPEN
      CALL INCHTO(10.0,7.0,XX,YY)
      CALL PLTLN(XUC,YUC,X(2*N+1),Y(2*N+1))
      IFINI = IFIN - 1
      CALL NEWPEN (3)
      DO 93 J = 1,IFINI
      JN = 2*N+1
      CALL PLTLN(X(J*JN),Y(J*JN),X((J+1)*(JN)),Y((J+1)*(JN)))
      KN = 2*N+1
      K = J-1
      CALL PLTLN(X(5+K*KN),Y(5+K*KN),X(5+(K+1)*KN),
$Y(5+(K+1)*KN))
93    CONTINUE
      CALL LETTER(10,.1,0.0,1.0,0.5,10HCHARACTERI)
      CALL LETTER(10,.1,0.0,2.0,0.5,10HSTIC LINES)
      CALL LETTER(10,.1,0.0,3.0,0.5,10H FOR      )

```

CALL LETTER(10,.1,0.0,5.0,0.5,10HTURBINE BL)  
 CALL LETTER(10,.1,0.0,6.0,0.5,10HADE )  
 CALL LETTER(10,.1,0.0,1.5,0.25,10HFOR PRESSU)  
 CALL LETTER(10,.1,0.0,2.5,0.25,10HRE RATIO P)  
 CALL LETTER(4,.1,0.0,3.5,0.25,4H /P= )  
 CALL LETTER(1,.05,0.0,3.5,0.25,1H0)  
 CALL LETTER(2,.1,0.0,0.5,5.0,2HM=)  
 IF (THEE.EQ.0.0) GO TO 118  
 CALL LETTER(10,.1,0.0,3.5,0.5,10H CURVED )  
 CALL LETTER(5,.1,0.0,4.5,0.5,5HBACK )  
 GO TO 119

118

CONTINUE  
 CALL LETTER(10,.1,0.0,3.5,0.5,10HSTRAIGHT B)  
 CALL LETTER(5,.1,0.0,4.5,0.5,5HACK )

119

CONTINUE  
 END

C  
 C  
 C  
 C  
 C  
 C  
 C  
 C  
 C

\*\*\*\*\*  
 \*  
 \* FLOW SUBROUTINE \*  
 \*  
 \*\*\*\*\*

SUBROUTINE FLOW(Q,U,V,THE,M,N)  
 COMMON/PROPTY/G, RG, GC, TS, PS, PA, TA, YUC

```
REAL M(150),THE(150),X(150),Y(150),U(150),V(150),Q(150)
```

```
PI = 4.0*ATAN(1.0)
```

```
DO 30 I = 1,N
```

```
THE(I) = THE(I)*2*PI/360
```

```
C = 20.0*SQRT(TS)
```

```
Q(I) = C*M(I)/SQRT(1.0 + .2*M(I)**2)
```

```
U(I) = Q(I)/(SQRT(1.0+TAN(THE(I))**2))
```

```
V(I) = U(I)*TAN(THE(I))
```

```
30 CONTINUE
```

```
RETURN
```

```
END
```

```
C
```

```
C
```

```
C
```

```
*****
```

```
C
```

```
*
```

```
FLOW1 SUBROUTINE
```

```
*
```

```
C
```

```
*
```

```
*
```

```
C
```

```
*
```

```
*
```

```
C
```

```
*****
```

```
C
```

```
SUBROUTINE FLOW1(QUC,UUC,VUC,THEUC,MUC)
```

```
COMMON/PROPTY/G,RG,GC,TS,PS,TA,PA,YUC
```

```
REAL MUC,THEUC,XUC,YUC,UUC,VUC,QUC
```

```
PI = 4.0*ATAN(1.0)
```

```
THEUC = THEUC*2*PI/360
```

```
C = 20.0*SQRT(TS)
```

```

QUC = C*MUC/SQRT(1.0+0.2*MUC**2)
UUC = QUC/(SQRT(1.0+TAN(THEUC)**2)
VUC = UUC*TAN(THEUC)
RETURN
END

```

C

C

C

\*\*\*\*\*

C

\*

\*

C

\*

SUBROUTINE FOR INTERIOR POINTS

\*

C

\*

\*

C

\*\*\*\*\*

C

SUBROUTINE INTPT(X,Y,U,V,M,I,N)

COMMON/CONTRL/ICOR,E1,E2,PI,COUNT,THAE,YFIN,THEUC

COMMON/PROPTY/G,RG,GC,TS,PS,TA,PA,YUC

REAL M(150),X(150),Y(150),U(150),V(150)

REAL MM,LP,LM,LE,L12,LO

C

X1 = X(I+1)

Y1 = Y(I+1)

U1 = U(I+1)

V1 = V(I+1)

X2 = X(I)

Y2 = Y(I)



```

U2 = U(I)
V2 = V(I)
Q = SQRT(U1**2+V1**2)
A = ATAN(V1/U1)
CALL THERMO(Q,P,R,T,C,MM)
LM = TAN(A-ASIN(1.0/MM))
QM = U1**2-C**2
RM = 2.0*U1*V1-QM*LM
PRINT *, "          "
PRINT *, "          INTERIOR POINT ", I+N+1
Q = SQRT(U2**2 + V2**2)
A = ATAN(V2/U2)
CALL THERMO(Q,P,R,T,C,MM)
LP = TAN(A+ASIN(1.0/MM))
QP = U2**2 - C**2
RP = 2.0*U2*V2 - QP*LP
ITER = 0
C  SOLUTION OF THE FINITE DIFFERENCE EQUATIONS
10 X4 = (Y1-Y2-LM*X1+LP*X2)/(LP - LM)
Y4 = Y1+LM*(X4-X1)
IF (Y4.LT. 0.0) GO TO 30
TM = QM*U1 + RM*V1
TP = QP*U2 + RP*V2
DENO = QM*RP - QP*RM
U4 = (TM*RP - TP*RM)/DENO

```

```

V4 = (QM*TP - QP*TM)/DENO
C CHECK FOR CONVERGENCE OR COMPLETION OF ITERATIONS
IF (ITER.EQ.ICOR) GO TO 30
IF (ITER.EQ.0 ) GO TO 20
IF ((ABS(X4 - XC).GT.E1).OR.(ABS(Y4-YC).GT.E1)) GO TO 20
IF ((ABS(U4-UC).LT.E2*UC).AND.(ABS(V4-VC).LT.E2*VC)
GO TO 30
C CALCULATE THE COEFFICIENTS FOR THE CORRECTOR
20 ITER = ITER + 1
XC = X4
YC = Y4
UC = U4
VC = V4
YY = 0.5*(Y1 + Y4)
UU = 0.5*(U1 + U4)
VV = 0.5*(V1 + V4)
Q = SQRT(UU**2 + VV**2)
A = ATAN(VV/UU)
CALL THERMO(Q,P,R,T,C,MM)
LM = TAN(A - ASIN(1.0/MM))
QM = UU**2 - C**2
RM = 2.0*UU*VV - QM*LM
UU = 0.5*(U2 + U4)
VV = 0.5*(V2 + V4)
A = ATAN(VV/UU)

```

```
- YY = 0.5*(Y2 + Y4)
  Q = SQRT(UU**2 + VV**2)
  CALL THERMO(Q,P,R,T,C,MM)
  LP = TAN(A + ASIN(1.0/MM))
  QP = UU**2 - C**2
  RP = 2.0*UU*VV - QP*LP
  GO TO 10
```

```
30  CONTINUE
```

```
  NI = N+1
```

```
  Y(I+NI) = Y4
```

```
  X(I+NI) = X4
```

```
  U(I+NI) = U4
```

```
  V(I+NI) = V4
```

```
  D = ATAN(V4/U4)
```

```
  PRINT 5, X4,Y4,U4,V4
```

```
5   FORMAT(1X,"      X=",F8.2,5X,"Y=",F8.2,5X,"U=",F8.2,
$5X,"V=",F6.2)
```

```
  PRINT 6,T,P,D
```

```
6   FORMAT(1X,"      T=",F8.2,5X,"P=",F10.2,5X,"D=",F8.3)
```

```
  RETURN
```

```
  END
```

```
C
```

```
C
```

```

C *****
C *
C *          SUBROUTINE FOR BOUNDARY POINTS          *
C *
C *****
C
SUBROUTINE BODPT(X,Y,U,V,M,I,N)
COMMON/CONTRL/ICOR,E1,E2,PI,COUNT,THAE,YFIN,THEUC
COMMON/PROPTY/G,RG,GC,TS,PS,TA,PA,YUC
REAL M(150),X(150),Y(150),U(150),V(150)
REAL MM,LP,LM,LE,L12,LO

X3 = X(I-4)
Y3 = Y(I-4)
U3 = U(I-4)
V3 = V(I-4)

X2 = X(I)
Y2 = Y(I)
U2 = U(I)
V2 = V(I)

PRINT *, "          "

YI = YUC
40 CONTINUE

GK = (G-1.0)/G)
Q4 = SQRT(2.0*G*RG*TS*(1.0-(PA/PS)**GK)/(G-1.0))

```

```

ITER = 0
Q = SQRT(U2**2 + V2**2)
A = ATAN(V2/U2)
CALL THERMO(Q,P,R,T,C,MM)
LP = TAN(A+ASIN(1.0/MM))
LO = V3/U3
19  CONTINUE
QP = U2**2 - C**2
RP = 2.0*U2*V2* - QP*LP
PRINT*,"
PRINT *,"          BOUNDARY POINT      ",I+N+1
C   SOLUTION OF THE FINITE DIFFERENCE EQUATIONS
10  CONTINUE
X4 = (Y3-Y2-LO*X3 + LP*X2)/(LP - LO)
TP = QP*U2 + RP*V2
Y4 = Y3 + LO*(X4 - X3)
DD = QP**2 + RP**2
U4 = (QP*TP - RP*SQRT(Q4**2*DD-TP**2))/DD
V4 = (TP } QP*U4)/RP
C   CHECK FOR CONVERGENCE OR COMPLETION OF ITERATION
IF (ITER.EQ.ICOR) GO TO 30
IF (ITER.EQ.0) GO TO 20
IF ((ABS(X4-XC).GT.E1).OR.(ABS(Y4-YC).GT.E1))
GO TO 20
IF ((ABS(U4-UC).LT.E2*UC).AND.(ABS(V4-VC).LT.E2*VC))

```

```
GO TO 30
C CALCULATE THE COEFFICIENTS FOR CORRECTOR
20 ITER = ITER + 1
   XC = X4
   YC = Y4
   UC = U4
   VC = V4
   UU = 0.5*(U2 + U4)
   VV = 0.5*(V2 + V4)
   A = ATAN(VV/UU)
   YY = 0.5*(Y2 + Y4)
   QQ = SQRT(UU**2 + VV**2)
   CALL THERMO(Q,P,R,T,C,MM)
   LP = TAN(A + ASIN(1.0/MM))
   QP = UU**2 - C**2
   RP = 2.0*UU*VV - QP*LP
   UU = 0.5*(U3 + U4)
   VV = 0.5*(V3 + V4)
   LO = VV/UU
   GO TO 104
30 CONTINUE
   N1 = N+1
   X(I+N1) = X4
   Y(I+N1) = Y4
   U(I+N1) = U4
```

V(I+N1) = V4

D = ATAN(V4/U4)

M(I+N1) = MM

PRINT 5,X4,Y4,U4,V4

5   FORMAT(1X,"       X=",F8.2,5X,"Y=",F8.2,5X,  
\$"U=",F8.2,5X,"V=",F6.2)

PRINT 6,T,P,D

6   FORMAT(1X,"       T=",F8.2,5X,"P=",F10.2,5X,"D=",F8.3)

RETURN

END

C

C

C

C

C

C

C

C

```
*****
*
*       SUBROUTINE FOR BLADE CORNER POINT       *
*
*****
```

SUBROUTINE BODPT1(XUC,YUC,UUC,VUC,MUC,I,N,X,Y,U,V,M)

COMMON/CONTRL/ICOR,E1,E2,PI,COUNT, THAE,YFIN,THEUC

COMMON/PROPTY/G,RG,GC,TS,PS,TA,PA,YUC

REAL MUC,XUC,YUC,UUC,VUC,QUC

REAL M(150),X(150),Y(150),U(150),V(150)

REAL MM,LP,LM,LE,L12,L0

X2 = X(N)

```

Y2 = Y(N)
U2 = U(N)
V2 = V(N)
X3 = XUC
Y3 = YUC
U3 = UUC
V3 = VUC
YI = YUC
40 CONTINUE
GK = (G - 1.0)/G
Q4 = SQRT(2.0*G*RG*TS*(1.0-(PA/PS)**GK))/(G-1.0)
ITER = 0.0
Q = SQRT(U2**2 + V2**2)
A = ATAN(V2/U2)
CALL THERMO(Q,P,R,T,C,MM)
LP = TAN(A + ASIN(1.0/MM))
LO = THEUC*2*PI/360
QP = U2**2 - C**2
RP = 2.0*U2*V2 - QP*LP
PRINT I,"          BOUNDARY POINT  ", I+N+1
C SOLUTION OF THE FINITE DIFFERENCE EQUATIONS
10 CONTINUE
X4 = (Y3-Y2-LO*X3+LP*X2)/(LP-LO)
TP = QP*U2 + RP*V2
Y4 = Y3+LO*(X4-X3)

```



$$DD = QP^{**2} + RP^{**2}$$

$$U4 = (QP*TP) / RP * \sqrt{Q4^{**2}*DD - TP^{**2}} / DD$$

$$V4 = (TP - QP*U4) / RP$$

C CHECK FOR CONVERGENCE OR COMPLETION OF ITERATION

IF (ITER.EQ.ICOR) GO TO 30

IF (ITER.EQ.0 ) GO TO 20

IF ((ABS(X4-XC).GT.E1).OR.(ABS(Y4-YC).GT.E1))

GO TO 20

IF ((ABS(U4-UC).LT.E2\*UC).AND.(ABS(V4-VC).LT.E2\*VC))

GO TO 30

C CALCULATE THE COEFFICIENTS FOR THE CORRECTOR

20 ITER = ITER+1

XC = X4

YC = Y4

UC = U4

VC = V4

UU = 0.5\*(U2 + U4)

VV = 0.5\*(V2 + V4)

A = ATAN(VV/UU)

YY = 0.5\*(Y2 + Y4)

QQ = SQRT(UU\*\*2 + VV\*\*2)

CALL THERMO(Q,P,R,T,C,MM)

LP = TAN(A+ASIN(1.0/MM))

QP = UU\*\*2 - C\*\*2

RP = 2.0\*UU\*VV - QP\*LP

```

UU = 0.5*(U3 + U4)
VV = 0.5*(V3 + V4)
L0 = VV/UU
GO TO 10
30 CONTINUE
N1 = N+1
X(I+N1) = X4
Y(I+N1) = Y4
U(I+N1) = U4
V(I+N1) = V4
D = ATAN(V4/U4)
M(I+N1) = MM
PRINT 5,X4,Y4,U4,V4
5  FORMAT(1X,"      X=",F8.2,5X,"Y=",F8.2,5X,
$ "U=",F8.2,5X,"V=",F6.2)
PRINT 6,T,P,D
6  FORMAT(1X,"      T=",F8.2,5X,"P=",F10.2,5X,"D=",F8.3)
RETURN
END

```

C

C

C

\*\*\*\*\*

C

\*

\*

C

\*

SUBROUTINE FOR CALCULATING WALL POINTS

\*

C

\*

\*

C

\*\*\*\*\*

C

```

SUBROUTINE WALPT(X,Y,U,V,M,I,N)
COMMON/CONTRL/ICOR,E1,E2,PI,COUNT,THAE,YFIN,THEUC
COMMON/PROPTY/G,RG,GC,TS,PS,TA,PA,YUC
REAL M(150),X(150),Y(150),U(150),V(150)
REAL MM,LM,LE,L12,LO
X1 = X(I)
Y1 = Y(I)
U1 = U(I)
V1 = V(I)
PRINT I,"                WALL POINT      ",I+N
Q = SQRT(U1**2 + V1**2)
A = ATAN(V1/U1)
CALL THERMO(Q,P,R,T,C,MM)
LM = TAN(A-ASIN(1.0/MM))
QM = U1**2 - C**2
RM = 2.0*U1*V1 - QM*LM
ITER = 0
C      SOLUTION OF THE FINITE DIFFERENCE EQUATIONS
10     CONTINUE
CALL BOUNDRY(X4,Y4,A4,X1,Y1,LM,XO,YO,XE,THEO,THEE)
TM = QM*U1 + RM*V1
LO = TAN(A4)
U4 = TM/(QM + LO*RM)

```

```

V4 = U4*LO
C   CHECK FOR CONVERGENCE OF COMPLETION OF ITERATIONS
   IF (ITER.EQ.ICOR) GO TO 30
   IF (ITER.EQ.0) GO TO 20
   IF ((ABS(X4-XC).GT.E1).OR. (ABS(Y4-YC).GT.E1))
   GO TO 20
   IF ((ABS(U4-UC).LT.E2*UC).AND. (ABS(V4-VC).LT.E2*VC))
   GO TO 30
C   CALCULATE THE COEFFICIENTS FOR CORRECTOR
20  ITER = ITER + 1
    XC = X4
    YC = Y4
    UC = U4
    VC = V4
    UU = 0.5*(U1 + U4)
    VV = 0.5*(V1 + V4)
    A = ATAN(VV/UU)
    YY = 0.5*(Y1 + Y4)
    Q = SQRT(UU**2 + VV**2)
    CALL THERMO(Q,P,R,T,C,MM)
    LM = TAN(A - ASIN(1.0/MM))
    QM = UU**2 - C**2
    RM = 2.0*UU*VV - QM*LM
    GO TO 10
30  CONTINUE

```

Y(I+N) = Y4

X(I+N) = X4

U(I+N) = U4

V(I+N) = V4

D = ATAN(V4/U4)

PRINT 5, X4, Y4, U4, V4

5 FORMAT(1X, " X=", F8.2, 5X, "Y=", F8.2, 5X,

"U=", F8.2, 5X, "V=", F6.2)

PRINT 6, T, P, D

6 FORMAT(1X, " T=", F8.2, 5X, "P=", F10.2, 5X, "D=", F8.3)

RETURN

END

C

C

C

C

C

C

C

C

\*\*\*\*\*

\*

\* SUBROUTINE FOR CALCULATING FLOW PROPERTIES \*

\*

\*\*\*\*\*

ROUTINE THERMO(Q, P, R, T, C, MM)

MON/PROPTY/G, RG, GC, TS, PS, TA, PA, YUC

REAL MM

C = SQRT(G\*RG\*TS - ((G-1.0)/2.0)\*Q\*\*2)

MM = Q/C



```
10  CONTINUE
    X4 = X1 - Y1/LM
    Y4 = 0.0
    A4 = ATAN(0.0)
    RETURN
    END
```